Université de Montréal

ELECTROSPINNING AND CHARACTERIZATION OF SELF-ASSEMBLED INCLUSION COMPLEXES

par
Yang Liu

Département de chimie
Faculté des arts et des sciences

Thèse présentée à la Faculté des études supérieures et postdoctorales
en vue de l'obtention du grade de Philosophiae Doctor (Ph.D)
en chimie

Août 2009

Université de Montréal

Faculté des études supérieures et postdoctorales

Cette thèse intitulée :

ELECTROSPINNING AND CHARACTERIZATION OF SELF-ASSEMBLED INCLUSION COMPLEXES

présentée par :

Yang Liu

a été évaluée par un jury composé des personnes suivantes :

Professeur	Robert E. Prud'homme	président-rapporteur, Université de Montréal
Professeur	Christian Pellerin	directeur de recherche, Université de Montréal
Professeur	Françoise Winnik	membre du jury, Université de Montréal
Professeur	Abdellah Ajji	examinateur externe, École Polytechnique de Montréal
Professeur	Patrice Hildgen	représentant du doyen de la FES, Faculté de Pharmacie, Université de Montréal

Résumé

L'électrofilage est une technique permettant de fabriquer des fibres polymériques dont le diamètre varie entre quelques nanomètres et quelques microns. Ces fibres ont donc un rapport surface/volume très élevé. Les fibres électrofilées pourraient trouver des applications dans le relargage de médicaments et le génie tissulaire, comme membranes et capteurs chimiques, ou dans les nanocomposites et dispositifs électroniques. L'électrofilage était initialement utilisé pour préparer des toiles de fibres désordonnées, mais il est maintenant possible d'aligner les fibres par l'usage de collecteurs spéciaux. Cependant, il est important de contrôler non seulement l'alignement macroscopique des fibres mais aussi leur orientation au niveau moléculaire puisque l'orientation influence les propriétés mécaniques, optiques et électriques des polymères. Les complexes moléculaires apparaissent comme une cible de choix pour produire des nanofibres fortement orientées.

Dans les complexes d'inclusion d'urée, les chaînes polymères sont empilées dans des canaux unidimensionnels construits à partir d'un réseau tridimensionnel de molécules d'urée liées par des ponts hydrogène. Ainsi, les chaînes polymère sonts très allongées à l'échelle moléculaire. Des nanofibres du complexe PEO-urée ont été préparées pour la première fois par électrofilage de suspensions et de solutions. Tel qu'attendu, une orientation moléculaire inhabituellement élevée a été observée dans ces fibres. De tels complexes orientés pourraient être utilisés à la fois dans des études fondamentales et dans la préparation de matériaux hiérarchiquement structurés.

La méthode d'électrofilage peut parfois aussi être utilisée pour préparer des matériaux polymériques métastables qui ne peuvent pas être préparés par des méthodes conventionnelles. Ici, l'électrofilage a été utilisé pour préparer des fibres des complexes stables (α) et "métastables" (β) entre le PEO et l'urée. La caractérisation du complexe β, qui était mal connu, révèle un rapport PEO:urée de 12:8 appartenant au système orthorhombique avec a = 1.907 nm, b = 0.862 nm et c = 0.773 nm. Les chaînes de PEO sont orientées selon l'axe de la fibre. Leur conformation est significativement affectée

par les ponts hydrogène. Une structure en couches a été suggérée pour la forme β, plutôt que la structure conventionnelle en canaux adoptée par la forme α.

Nos résultats indiquent que le complexe β est thermodynamiquement stable avant sa fonte et peut se transformer en forme α et en PEO liquide par un processus de fonte et recristallisation à 89 ºC. Ceci va dans le sens contraire aux observations faites avec le complexe β obtenu par trempe du complexe α fondu. En effet, le complexe β ainsi obtenu est métastable et contient des cristaux d'urée. Il peut subir une transition de phases cinétique solide-solide pour produire du complexe α dans une vaste gamme de températures. Cette transition est induite par un changement de conformation du PEO et par la formation de ponts hydrogène intermoléculaires entre l'urée et le PEO. Le diagramme de phases du système PEO-urée a été tracé sur toute la gamme de compositions, ce qui a permis d'interpréter la formation de plusieurs mélanges qui ne sont pas à l'équilibre mais qui sont été observés expérimentalement.

La structure et le diagramme de phases du complexe PEO-thiourée, qui est aussi un complexe très mal connu, ont été étudiés en détail. Un rapport molaire PEO :thiourée de 3:2 a été déduit pour le complexe, et une cellule monoclinique avec a = 0.915 nm, b = 1.888 nm, c = 0.825 nm et β = 92.35º a été déterminée. Comme pour le complexe PEO-urée de forme β, une structure en couches a été suggérée pour le complexe PEO-thiourée, dans laquelle les molécules de thiourée seraient disposées en rubans intercalés entre deux couches de PEO. Cette structure en couches pourrait expliquer la température de fusion beaucoup plus faible des complexes PEO-thiourée (110 ºC) et PEO-urée de forme β (89 ºC) en comparaison aux structures en canaux du complexe PEO-urée de forme α (143 ºC).

Mots clés : Electrofilage, nanofibres, auto-assemblage, orientation, complexes, structure en couches, diagramme de phases, diffraction des rayons X, spectroscopie infrarouge.

Abstract

Electrospinning is a technique that allows production of polymeric fibers with diameters ranging from nanometers to a few microns, and thus with an inherent high surface-to-volume ratio. Electrospun fibers are finding potential applications in drug delivery and tissue engineering, as membranes and chemical sensors, and in nanocomposites and electronic devices. Electrospinning was initially used to prepare disordered, non-woven mats, but it is now possible to produce highly aligned fibers by using different target collectors. However, it is of great interest to not only control the macroscopic alignment of the fibers but also their orientation at the molecular level since it influences the mechanical, optical and electrical properties of polymers. Molecular complexes were targeted as a means of increasing molecular orientation in electrospun fibers.

In the host-guest urea inclusion complexes (ICs), polymer chains are packed in one-dimensional channels constructed from an essentially infinite three-dimensional network of hydrogen-bonded urea molecules. The polymer chains are thus highly extended at the molecular scale. PEO-urea complex nanofibers have been prepared for the first time by electrospinning of suspension and solutions. As predicted, an unusually large molecular orientation in the fibers was achieved. Such highly ordered IC fibers could find use both for fundamental studies of the inclusion complexes and for the preparation of hierarchically structured materials.

Electrospinning can also sometimes be used to prepare metastable polymeric materials that cannot be prepared by the conventional methods. Here, solution electrospinning was used to prepare fibers of both the stable (α) and "metastable" (β) complexes between PEO and urea. Detailed characterization of the ill-studied β complex reveals that it possesses a 12:8 PEO:urea stoichiometry and belongs to the orthorhombic system with a = 1.907 nm, b = 0.862 nm, and c = 0.773 nm. The PEO chains are oriented along the fiber axis and present a conformation significantly affected by strong

hydrogen bonding with urea as compared to the pure polymer and the stable α complex. A layered structure, rather than the conventional channel structure, is suggested.

In contrast with previous suggestions based on melt-quenched PEO-urea α complex, our results further indicate that the β complex is thermodynamically stable before melting and can phase-transfer to the α complex and liquid PEO through a thermodynamic melt-recrystallization process at 89 ºC. In contrast, the β complex obtained by melt-quenching the α complex is mixed with urea crystal and is metastable. It can experience a kinetic solid-solid phase transition process to produce α complex within a large temperature range. This transition is induced by a PEO conformation change and by the formation of intermolecular hydrogen bonds between urea and PEO. The phase diagram of the PEO/urea system was drawn over the complete composition range, which allowed interpreting the formation of various out-of-equilibrium mixtures observed experimentally.

The structure and phase diagram of the PEO/thiourea complex, another poorly understood system, was also studied in detail. An EO:thiourea molar ratio of 3:2 was deduced for the complex, and a monoclinic unit cell with a = 0.915 nm, b = 1.888 nm, c = 0.825 nm and β = 92.35º was determined. Just as for the PEO-urea β complex, a layered structure was suggested for the PEO-thiourea complex, in which the thiourea molecules would be arranged into a ribbon-like structure intercalated between two PEO layers. This layered structure could explain the much lower melting temperature of the PEO-thiourea (110 ºC) and PEO-urea β complexes (89 ºC) as compared to the well known channel-structured PEO-urea α complex (143 ºC).

Keywords : Electrospinning, nanofibers, self-assembly, orientation, complexes, layer-structure, phase diagram, X-ray diffraction, infrared spectroscopy.

Table of Contents

Résumé I
Abstract III
Table of contents V
List of tables X
List of schemes XI
List of figures XII
List of abbreviations XVIII
Acknowledgements XXI

Chapter 1: Introduction

1.1 Inclusion compound 1
1.1.1 Urea and thiourea inclusion compounds 1
1.1.2 Cyclodextrin inclusion compounds 7
1.1.3 Application of urea, thiourea and cyclodextrin Ics 10
1.1.4 PEO inclusion compound 11
1.2 Electrospinning 19
1.2.1 History and set up 19
1.2.2 Parameters influencing electrospinning process 23
1.2.2.1 Applied voltage 23
1.2.2.2 Viscosity, concentration and molecular weight 25
1.2.3 Alignment of electrospinning nanofibers 30
1.2.4 Orientation and structure in electrospun fibers 32
1.3 Objectives and content of this work 34

1.4 References 35

Chapter 2: Experimental and characterization methods

2.1 Sample preparation 44
2.1.1 Preparation of PEO urea and thiourea complexes 44
2.1.2 Preparation of electrospun fibers 44
2.1.2.1 Working and counter electrodes 44
2.1.2.2 Electrospinning of PEO and urea/thiourea solutions 46
2.1.2.3 Electrospinning of PEO and urea/thiourea precipitate 46
2.1.3 Preparation of PEG-thiourea complexes 47
2.1.4 Preparation of PEO-cyclodextrin complexes 47
2.2 Characterization methods 48
2.2.1 Wide angle X-ray diffraction (WAXD) 48
2.2.1.1 Unit cell determination by powder diffraction 49
2.2.1.2 Orientation measurement 54
2.2.2 Fourier transform infrared (FT-IR) 58
2.2.2.1 Orientation measurement 59
2.2.2.2 Conformation analysis 61
2.2.2.3 PEO and urea/thiourea chain orientation direction in complexes 63
2.2.3 Microscopy 64
2.2.4 Thermal analysis 66
2.3 References 70

Chapter 3: Highly oriented electrospun fibers of self-assembled inclusion complexes of poly(ethylene oxide) and urea

3.1 Résumé 72
3.2 Abstract 72

3.3 Introduction 73
3.4 Results and discussion 74
3.5 Acknowledgement 80
3.6 Supporting information 80
3.6.1 Sample preparation 80
3.6.2 Characterization 81
3.6.3 Thermogravimetric analysis 82
3.6.4 Infrared spectroscopy 83
3.7 References 84

Chapter 4: Characterization of the stable and metastable poly(ethylene oxide)-urea complexes in electrospun fibers

4.1 Résumé 86
4.2 Abstract 87
4.3 Introduction 87
4.4 Experimental section 89
4.5 Results and discussion 90
4.5.1 Solution electrospinning of the PEO-urea complexes 90
4.5.2 Structure of the form β PEO-urea complex 99
4.6 Conclusions 107
4.7 Acknowledgement 108
4.8 References 109

Chapter 5: Stability and phase behavior of the poly(ethylene oxide)-urea complexes prepared by electrospinning

5.1 Résumé 111
5.2 Abstract 112
5.3 Introduction 112
5.4 Experimental section 114
5.4.1 Sample preparation 114
5.4.2 Sample characterization 115
5.5 Results and discussion 115
5.5.1 Phase transitions of the α and melt-quenched complexes 115
5.5.2 Phase transitions of the pure β complex 119
5.5.3 β – α transition and stability of the pure β complex 121
5.5.4 Phase diagram of the PEO-urea system 125
5.6 Conclusions 128
5.7 Acknowledgement 129
5.8 References 129

Chapter 6: Structure and phase behavior of the poly(ethylene oxide)-thiourea complex prepared by electrospinning

6.1 Résumé 132
6.2 Abstract 133
6.3 Introduction 133
6.4 Experimental section 135
6.5 Results and discussion 136
6.5.1 Composition and phase diagram of the PEO-thiourea complex 136
6.5.2 Structure of the PEO-thiourea complex 142
6.6 Conclusions 149
6.7 Acknowledgement 150

6.8 References 151

Chapter 7: Conclusions and perspectives

7.1 Conclusions 153
7.2 Perspectives of the future 158
7.3 References 165

List of Tables

Table 1.1 The crystal structures and lattice parameters of the complexes formed with urea and thiourea host molecules 5

Table 1.2 The conformation of PEO chains and the crystalline structures of host-guest complexes formed between PEO and some small molecules 16

Table 2.1 Unit cells of the seven crystal systems and the fourteen space lattices 49

Table 2.2 Absorption frequencies and assignment of the main bands of electrospun PEO and PEO-urea form α complex. The type of dominant dichroism for the crystalline samples is also indicated.....60

Table 3.1 WAXD characterization of the degree of orientation for PEO-urea inclusion complex electrospun fibers.....79

Table 4.1 Assignment and dichroism of the main infrared absorption bands for pure PEO and the form α and β PEO-urea complexes 94

Table 4.2 Crystal plane attribution for the form β PEO-urea complex based on an orthorhombic unit cell with a = 1.907 nm, b = 0.862 nm and c = 0.773 nm. σ is the calculated angle between the normal of an hkl plane and the c axis, while φ_{max} is the measured maximum of the azimuthal angle 101

Table 6.1 Crystal plane attribution for the PEO-thiourea complex based on a monoclinic unit cell with *a* = 9.15 Å, *b* = 18.88 Å, *c* = 8.25 Å and β=92.4º 144

Table 7.1 Infrared absorption frequencies of PEO, the assignments of each peak and the type of dominant conformation or dichroism in amorphous and crystalline PEO and in its complexes with urea. 155

List of Schemes

Scheme 4.1 Two possible structural models for the orthorhombic PEO-urea β complex 106

List of Figures

Figure 1.1 Friedrich Wöhler (1800-1882) and Wöhler synthesis of urea 2

Figure 1.2 Representation with van der Waals radii showing nine complete tunnels of the host structure in (a) conventional urea and (b) conventional thiourea inclusion compounds, viewed along the tunnel axis. Note that, in the real inclusion compounds, the tunnels of these host structure are filled with a dense packing of guest molecules (not shown). 3

Figure 1.3 The layer-structured supramolecular compound of A) $NC(CH_2)_5CN$ with urea[60] and B) 1,4-diazabicyclo[2.2.2] octane with thiourea 7

Figure 1.4 Schematic drawing of cyclodextrins (CDs). 8

Figure 1.5 An isolated chain containing (a)10 oxyethylene units (PEG10) and (b)polyrotaxanes containing 10 oxyethylene units and 4 α-cyclodextrins (represented by toruses) oriented head-to-tail or (c)head-to-head and tail-to-tail. All PEG are end-capped by 2,4-dinitrophenylamine groups 10

Figure 1.6 Structure of the poly (ethylene oxide)-urea inclusion complex: (a) the channel structure formed by the hydrogen bonded urea molecules and (b) the association of PEO and urea molecules inside the channel.....13

Figure 1.7 Side and top view of the structures of the four model systems. On the side of the polymeric chains, a line indicates the dimension of the repeating units of each conformation along the chain length direction 18

Figure 1.8 William Gilbert (left), Georg Matthias Bose (middle) and Lord Rayleigh (John William Strutt) (right).....20

Figure 1.9 Basic setup of electrospinning (left) and real-time image of electrospinning process (right) 22

Figure 1.10 Physical representation of the three solution regimes, (a) dilute, (b) semidilute unentangled and (c) semidilute entangled. R_g is the radius of gyration 26

Figure 1.11 Plot of the calculated entanglement number $(n_e)_{soln}$ as a function of concentration for PS/THF system 28

Figure 1.12 Schematic setup of the knife-edged rotating disk (left) and two separated conductive substrates (right) used for obtaining aligned fibers 30

Figure 2.1 Photographs of two types of counter electrodes: rotating cylinder collector with a metal disk in the middle (left) and two separate electrodes (right). 46

Figure 2.2 Two-dimensional X-ray patterns of PEO-urea α complex melt at 160 ºC (left) and the melt-quenched sample at 25 ºC (right) 48

Figure 2.3 Diagram of a plane having the Miller indices of (211) 51

Figure 2.4 WAXD results for PEO, PEO-urea α and β complexes and the melting-cooling of β complexes 54

Figure 2.5 Definition of the coordinate system OXYZ with the unit cell system Oxyz and Euler angles θ, φ, and ψ 55

Figure 2.6 Polarized infrared spectra of PEO fibers prepared by electrospinning. Solid and broken lines represent the spectra measured with the radiation polarized parallel and perpendicular to the fiber direction, respectively 59

Figure 2.7 FT-IR spectra of bulk PEO and electrospun PEO nanofibers (NFs) 62

Figure 2.8 SEM image of PEO-urea IC α form (top) and cross-polarized optical microscopy of PEO fibers (bottom) 64

Figure 2.9 Spin-coated PEO-urea α complex (left), PEO-urea β complex (middle), and β complex after melting and cooling to 25 ºC (right).....66

Figure 2.10 Thermogravimetric analysis plots of pure PEO, α-CD, urea, PEO-urea complex form α and PEO-α-CD complexes with various mass ratios.....67

Figure 2.11 Temperature-composition phase diagram of PEO/urea system.....69

Figure 3.1 Crossed-polarized optical micrograph of electrospun fibers of the PEO-urea inclusion complex.....74

Figure 3.2 DSC thermograms of the bulk PEO, urea and inclusion complex (IC), as well as those of the pure PEO and PEO-urea IC electrospun fibers.....75

Figure 3.3 a) Wide-angle X-ray diffraction 2θ diagrams for the bulk and electrospun fibers of the PEO-urea inclusion complex (IC) and two-dimensional diffraction patterns of bulk IC (left inset) and electrospun fibers (right inset). b) Azimuthal profile of the WAXD pattern for electrospun PEO-urea IC at 2θ=21.6º. 77

Figure S3.1 Thermogravimetric analysis plots of pure PEO and urea, and of the bulk and fibers of the PEO-urea inclusion complex (IC).....82

Figure S3.2 Infrared spectra of pure PEO and urea, and of the bulk and fibers of the PEO-urea inclusion complex (IC).....83

Figure 4.1 Representative crossed-polarized optical micrographs of fibers prepared by electrospinning solutions with A) 4:9 and B) 3:2 PEO:urea molar ratios.....91

Figure 4.2 Wide-angle X-ray diffraction patterns of electrospun fibers with different PEO:urea mass ratios.....92

Figure 4.3 Infrared spectra of electrospun fibers with different PEO:urea mass ratios.....93

Figure 4.4 DSC thermograms recorded for pure PEO and urea, and for the electrospun fibers of the form β and form α PEO-urea complexes.....95

Figure 4.5 Infrared spectra of the form β PEO-urea complex recorded at 25 and 90 ºC, and of pure PEO in the melt state.....96

Figure 4.6 Two-dimensional WAXD patterns of the A) form α and B) form β PEO-urea complexes, and C) azimuthal profiles recorded for the form α (2 θ = 21.2º) and form β (2 θ = 21.6º) fibers prepared by electrospinning of suspensions and solutions. 98

Figure 4.7 Higher resolution WAXD pattern of the form β PEO-urea complex. 100

Figure 4.8 Polarized infrared spectra of the form α and form β PEO-urea complex fibers in the N-H stretching region. Solid and broken lines represent spectra measured with the radiation polarized parallel and perpendicular to the fiber direction, respectively.....103

Figure 4.9 Polarized infrared spectra of the form β PEO-urea complex fibers prepared by electrospinning. Solid and broken lines represent the spectra measured with the radiation polarized parallel and perpendicular to the fiber direction, respectively.....104

Figure 5.1 DSC thermograms recorded for the PEO-urea α complex.....116

Figure 5.2 WAXD patterns of the PEO-urea α complex recorded at 25 °C (top curve), after heating to the liquid state (160 °C), cooling to 75, 65, 50 and 25 °C, and finally after a second heating to 95 °C (bottom trace).....117

Figure 5.3 FT-IR spectra of the PEO-urea α complex recorded at 25 °C (top curve), after heating to the liquid state (160 °C), cooling to 90, 75, 65 and 25 °C, and finally after a second heating to 95 °C (bottom trace).....118

Figure 5.4 DSC thermograms recorded for the pure PEO-urea β complex.....120

Figure 5.5 WAXD patterns of the pure PEO-urea β complex recorded at 25 °C (top curve), after heating slightly above the phase transition temperature (90 °C) and in the melt state (160 °C), after cooling to 75 and 25 °C (middle curves), and finally after a second heating scan to 70 °C (bottom trace) 121

Figure 5.6 A) FT-IR spectra and B) WAXD profiles of the melt-quenched β mixture recorded as a function of time during an annealing at 60 °C 122

Figure 5.7 A) FT-IR spectra of the pure β complex recorded as a function of time during an annealing at 60 °C; B) Time evolution of the normalized absorbance of the 1308 cm^{-1} β complex band during annealings at 70, 75 and 80 °C for the pure β complex and at 60 °C for the melt-quenched β mixture 124

Figure 5.8 Phase diagram of PEO-urea binary system. The open symbols represent the melting events due to kinetic products and the dashed lines the expected behavior under thermodynamic conditions 126

Figure 6.1 DSC thermograms recorded for cocrystallized PEO-thiourea complexes with PEO M_w of 400, 1000 and 400,000 g/mol 137

Figure 6.2 WAXD profiles of the PEO-thiourea complex at 25, 125, 170 ºC compared with those of pure PEO and thiourea at 25 ºC.....138

Figure 6.3 A) DSC thermograms and B) melting enthalpy of the PEO-thiourea complex as a function of the thiourea molar fraction 140

Figure 6.4 WAXD profiles of electrospun fibers prepared with various thiourea molar fractions 141

Figure 6.5 Phase diagram of the PEO-thiourea binary system.....142

Figure 6.6 High resolution WAXD pattern of the PEO-thiourea complex 143

Figure 6.7 Two-dimensional WAXD pattern of the electrospun PEO-thiourea complex fibers (inset) and azimuthal profiles for the peaks at 2θ = 19.9 and 21.1º.....145

Figure 6.8 Infrared spectra of pure PEO and thiourea, and of the PEO-thiourea and PEO-urea β complexes. 146

Figure 6.9 Polarized Raman spectra of the PEO-thiourea complex fibers prepared by electrospinning. The spectra with solid and broken lines were measured with the incident and scattered radiation polarized parallel and perpendicular to the fiber direction, respectively 148

Figure 7.1 Scheme of block-complexes composed of PEO chains and CD and urea guest molecules. 163

List of Abbreviations

2MB:	2-methoxybenzamide
2MRES:	2-methylresorcinol
$A_{//}$:	Absorbance parallel to the reference direction
$A_{\perp}$:	Absorbance perpendicular to the reference direction
ATR:	Attenuated total reflection
c:	Concentration
B_e:	Berry number
c*:	Critical overlap concentration
c_e:	Entanglement concentration
CD(s):	Cyclodextrin(s)
D:	Dichroic ratio
DABCO:	1,4-diazabicyclo[2.2.2] octane
DCM:	dichloromethane
DMF:	dimethylformamide
EO :	Ethylene oxide repeat unit
FT-IR:	Fourier transform infrared
FWHH:	Full width at half height
G(g):	Gauche
θ:	Half of the angle of the diffracted rays from the incident x-rays
η:	Viscosity of the solution
η_r:	Relative viscosity
η_s:	Viscosity of the solvent
η_{sp}:	Specific viscosity
$[\eta]$:	Intrinsic viscosity
H:	Distance between the capillary end and the target
(hkl):	Miller indices of a crystal plane
HYD:	Hydroquinone

IC(s):	Inclusion compound(s) or inclusion complex(es)
K_f:	Force constant of a bond
k_H:	Huggins coefficient
L:	Length of the capillary
λ:	Wavelength
Δn_{ij}:	Birefringence
M_e:	Entanglement molecular weight
M_i:	Mass of the atom
M_w:	Molecular weight
MWNT:	Multiwalled nanotubes
n:	Refractive index
N_b:	Bond order
n_e:	Number of entanglement per chain
$(n_e)_{solution}$:	Solution entanglement number
ν:	Wavenumbers
NMR:	Nuclear magnetic resonance
ODF:	The orientation distribution function
OM:	Optical microscopy
$<P_2(cos\varphi)>$:	Second order moment of the orientation distribution function
$\langle P_2 \rangle_c$:	Second order moment of the orientation distribution function along the c axis
P_{lmn}:	Associated Legendre polynomials
PAN:	Polyacrylonitrile
PCL:	Poly(ε-caprolactone)
PDX:	P-dihalogenobenzenes
PDLA:	Poly(D-lactic acid)
PE:	Polyethylene
PEG:	Poly(ethylene glycol)
PEO:	Poly(ethylene oxide)
PET:	Poly(ethylene terephthalate)

PHTP: Perhydrotriphenylene

PLLA: Poly(L-lactic acid)

PMMA: Poly(methyl methacrylate)

PNP: P-nitrophenol

PP: Polypropylene

PPO: Poly(propylene oxide)

PS: Polystyrene

PTA: Poly(trimethylene adipate)

PTG: Poly(trimethylene glutarate)

PTHF: Poly(tetrahydrofuran)

PVAc: Poly(vinyl acetate)

PVC: Poly(vinyl chloride)

PVME: Poly(vinyl methyl ether)

R: Radius

R_g: Radius of gyration

γ: Surface tension

RES: Resorcinol

SEM: Scanning electron microscopy

σ: Angle between the normal to the (hkl) plane and the c axis

T: Trans

TGA: Thermogravimetric analysis

V_c: Critical voltage

w_a: Weight of samples measured in air

WAXD: Wide angle X-ray diffraction

w_s: Weight of samples measured in solvent

φ: Azimuthal angle

X,Y,Z: Laboratory frame coordinate axes

x,y,z: Sample frame coordinate axes

X_i: Electronegativity of atoms i

XRD: X-ray diffraction

Acknowledgment

I would like to express my sincere thanks and gratitude to my supervisor, Prof. Christian Pellerin for his support, advice and encouragement in the course of my Ph. D studies. Prof. Pellerin always provided me with motivation and guidance in my research. His broad knowledge and creative ideas were crucial for the completeness of this dissertation. Without his patience and guidance, I could not complete this dissertation. My appreciation is also extended to the other jury members.

I am grateful to Dr. Thierry Maris, Dr Damien Maillard and Dr. Thierry Lefèvre for their help with the high resolution XRD experiments, the polarized optical microscopy measurements and the Raman spectra measurements, respectively. I would like to thank Ms. Huguette Dinel for her help in the density measurements.

Many thanks to my current and previous colleagues and friends in University of Montreal, a special acknowledgement belongs to Dr. Yongri Liang for extensive discussions about my research project and Mr. Damien Mauran for his help in taking the FT-IR spectra. Next I would like to thank Ms. Hélène Antaya for her help in preparing some specimens and the translation of the French abstract. I also acknowledge the dedication of the technicians, Mr. Sylvain Essiembre, Ms. Julie Boivin, Mr. Julien Del Testa, Mr. Martin Lambert, Mr. Louis Beaumount and Mr. Yves Teasdale, who were always available to help with my experiments and with the building up of the equipments.

I would like to thank all the other Chinese graduate students and all the other labmates in the Pavillon J. A. Bombardier for sharing the great lunch time, playing badminton, table tennis and basketball in the spare time.

Finally, I would like to express my very deep gratitude to my parents and my spouse for their support and love.

Chapter 1 : Introduction

1.1 Inclusion Compounds

Inclusion compounds (IC), or inclusion complexes, can be defined as systems in which one species (the "guest") is spatially confined within another species (the "host").[1,2] It is convenient to subdivide inclusion compounds into two classes based on the difference of host molecules. In one class, the host molecules possess an appropriate cavity or binding site for inclusion of guest molecules. For such molecular hosts, the host-guest complexes can exist in either solid or dispersed state (e.g. in solution), and the host structure can remain stable when the guest components are removed. Examples of this type of hosts are crown ethers, cyclodextrins, cryptands, rotaxanes and catenanes.[1-5] In the second class of inclusion compounds, guest molecules are located within the architecture or crystalline framework of solid host materials. For such molecular hosts, the host-guest association is a solid state phenomenon and the host structure undergoes substantial reorganization when the guest molecules are removed. Such solid hosts include a wide range of inorganic materials, for example, inorganic salts (e.g. H_gCl_2,[6,7] $LiCF_3SO_3$,[8,9] LiI,[10] NaSCN,[11] LiV_3O_8,[12] $CdPS_3$ preintercalated with hydrated alkali cations[13]), aluminosilicates (including zeolitic and clay minerals), aluminophosphates, graphite, layered metal chalcogenides and layered metal phosphonates,[1,2,14] as well as crystalline organic hosts, such as urea,[14-16] thiourea, [14,17,18] p-dihalogenobenzenes (PDX),[19,20] perhydrotriphenylene (PHTP),[21] p-nitrophenol (PNP),[22,23] resorcinol (RES),[24] 2-methylresorcinol (2MRES),[25] and hydroquinone (HYD).[26,27] In this thesis, we researched both types of host molecules, focusing on the crystalline organic hosts, especially on urea, thiourea and cyclodextrin (CD) inclusion compounds.

1.1.1 Urea and thiourea inclusion compounds

Urea, also known as carbamide, was first isolated from urine by Rouelle in 1773. Then in 1828, it was synthesized by Wöhler and became the first organic substance synthesized from inorganic compounds in the laboratory.[28] Wohler's historic preparation of "artificial" urea demonstrated to the scientific world that an organic compound could be synthesized, not only by a living organism, but by the chemist. For many, then, Wöhler is considered the father of organic chemistry. In 1940, while studying the effects of urea on proteins in pasteurized milk, Bengen accidentally found that 1-octanol forms crystalline adducts with urea.[29] Following that, it was reported that other linear aliphatic compounds, including carboxylic acids, higher alcohols and paraffins with six or more carbon atoms, could also form adducts with urea molecules in which the ratio of urea to guest molecules was nonstoichiometric.[14,30] Smith conducted an investigation of the crystalline structure of the hexadecane-urea inclusion compound and provided the structure found for most urea ICs.[31] In this structure, the urea molecules are connected by hydrogen bonds to form a hexagonal array of linear channels that contain the guest molecules. The Van der Waals diameters of urea channels are 5.5-5.8 Å.[1,2,14] Within this range, only linear n-alkane chains or analogous guest molecules with minimal branching, such as α,ω-dihalogenoalkanes, could be fitted in.

$$Pb(NCO)_2 + 2NH_3 + 2H_2O \rightarrow Pb(OH)_2 + 2NH_4NCO$$

$$NH_4NCO \rightarrow NH_3 + HNCO \rightleftarrows (NH_2)_2CO$$

Figure 1.1. Friedrich Wöhler (1800-1882) and the synthesis of urea.[28]

In addition to urea ICs, another adduct host, thiourea, has been found independently by Angla and Fetterly[32,33] to form crystalline inclusion compounds with

guests that are somewhat larger and differently shaped than those included within the channels of urea. Lenne and Schlenk et al. demonstrated that the thiourea and urea tunnels have similar structures, but that the thiourea tunnel has a larger cross-section.[34-36] As shown in Figure 1.2, George and Harris[37] calculated the tunnel diameter of urea and thiourea inclusion compounds, which fluctuates between ca. 5.5 and 5.8 Å for the conventional urea inclusion compounds ($a = b = 8.23$ Å, $c = 11.02$ Å) and ranges from 5.8 to 7.1 Å for the conventional thiourea inclusion compounds ($a = b = 15.97$ Å, $c = 12.48$ Å). Consequently, the types of guest molecules that form inclusion compounds with urea and thiourea are generally different, and thiourea accommodates a greater diversity of guest molecules than urea.

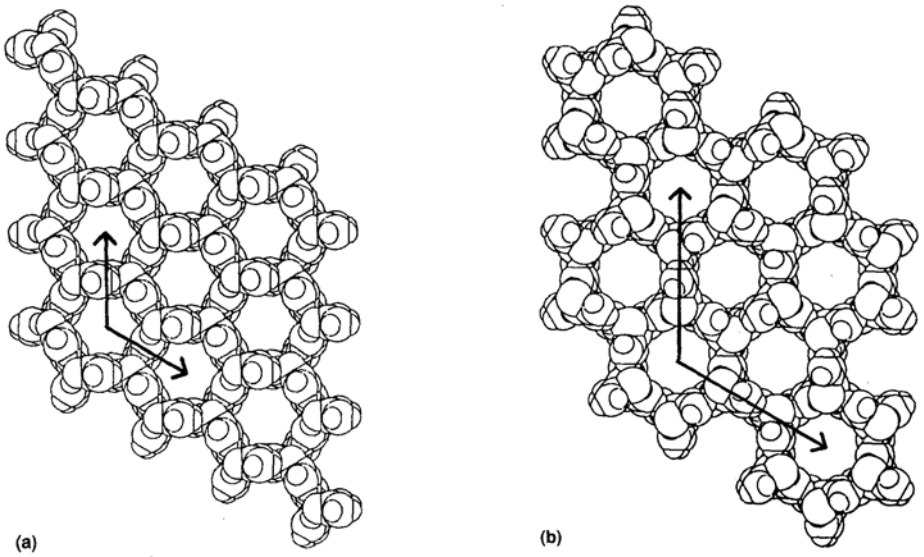

Figure 1.2. Representation with Van der Waals radii showing nine complete tunnels of the host structure in (a) conventional urea and (b) conventional thiourea inclusion compounds, viewed along the tunnel axis. Note that, in the real inclusion compounds, the tunnels of these host structures are filled with a dense packing of guest molecules (not shown).[37]

Brown and White screened over 175 compounds for adduct formation and found that thiourea complexes can be grouped into five classes: 1) polymethylated, polychlorinated, or polybrominated alkanes and their derivatives; 2) derivatives of cyclopentane or its heterocyclic analogs; 3) derivatives of cyclohexane or its heterocyclic analogs; 4) miscellaneous cyclic and bicyclic compounds; 5) small flat molecules.[38] Later, it was found that thiourea channel structures can also include ferrocene, organometallics and compounds containing aromatic rings.[14] Schiessler and Flitter made the generalization that most molecules which are capable of complex formation with thiourea have cross-sectional areas of approximately 5.8 x 6.8 Å.[39] The exception are the small flat molecules in the last group, which are not lined up end to end in the channel as the other classes of compounds, but are packed in some sort of overlapping arrangement as in stacks of coins.[38]

In addition to the short chain molecules, polymers have been found to form inclusion compounds with urea and thiourea by co-crystallization (see Table 1.1).[14-18,40-47] The conformational properties of alkane guest molecules within urea ICs have been widely investigated and many authors propose that the main portion of the alkane molecules exists essentially in the all-trans conformation. Therefore, it was proposed that the alkane-urea inclusion compounds could be used as model systems for the characterization of alkanes in all-trans conformation.[14,48] As for the long chain polymers, molecular modeling has shown that polyethylene (PE), poly(trimethylene adipate) (PTA), poly(trimethylene glutarate (PTG) and poly(tetrahydrofuran) (PTHF) assume an all-trans, planar zigzag conformation.[40,41,49] Poly(ε-caprolactone) (PCL), poly(L-lactic acid) (PLLA) and nylon-6 prefer extended, nearly planar zigzag all-trans and kink ($g^{\pm}tg^{\pm}$) conformations.[49-51] On the whole, the guest molecules within the urea channels are more extended and exist essentially in the all-trans conformations.

The narrow channels which exist in urea and thioura inclusion compounds have been chosen as templates to carry out polymerization reactions. Presumably, monomers polymerizing in urea or thiourea channels are subjected to a spatial control that may produce long, regular, unbranched, and even stereospecific polymer molecules. The

reactions studied were the polymerization of various olefins, dienes and epoxides. For example, poly(vinyl chloride) (PVC) thus obtained was found to be more syndiotactic than usual, polyacrylonitrile (PAN) was more stereoregular, and the polymerization of butadiene, 2,3-dichlorobutadiene and 2,3-dimethylbutadiene were reported to produce extremely regular 1,4-trans polymers.[38,52-56]

Table 1.1. Crystal structures and lattice parameters of the complexes formed with urea and thiourea host molecules.

Host Molecules	**Guest Molecules**	**Crystal system and lattice constant**	**Ref.**
Urea	N/A	Tetragonal, $a = b = 5.66$ Å , $c = 4.71$Å	57
Urea	Poly (ethylene oxide)	Trigonal, $a = b = 10.43$Å, $c = 9.12$Å	16,42
Urea	Poly (ethylene glycol)	Tetragonal, $a = b = 7.3$ Å , $c = 19.51$Å	58
Urea	Poly (trimethylene adipate)	Hexagonal, $a = b = 8.22$Å, $c = 11.00$Å	41
Urea	Poly (trimethylene glutarate)	Hexagonal, $a = b = 8.19$Å, $c = 11.04$Å	41
Urea	Poly (tetrahydrofuran)	Hexagonal, $a = b = 8.20$Å, $c = 11.03$Å	40
Urea	Poly ethylene	Hexagonal, $a = b = 8.23$Å, $c = 11.01$Å	31,59
Urea	Poly (ε-caprolactone)	Hexagonal, $a = b = 8.23$Å, $c = 11.01$Å	31,45
Urea	Poly (L-lactic acid)	Hexagonal, $a = b = 8.23$Å, $c = 11.01$Å	31,44
Urea	Poly (1,3-butadiene)	Hexagonal, $a = b = 8.22$Å, $c = 11.01$Å	54
Urea	Polyacrylonitrile	Pseudo-hexagonal, $a = b = 8.90$Å, $c = 11.88$Å	56
Urea	α,ω-dinitriles $(NC(CH_2)_3CN)$ $(NC(CH_2)_4CN)$ $(NC(CH_2)_5CN)$	Monoclinic, $a = 7.20$Å, $b = 4.58$Å, $c = 15.97$Å, β= 98.77º Monoclinic, $a = 8.89$Å, $b = 4.58$Å, $c = 11.45$Å, β= 96.48º Orthorhombic, $a = 6.50$Å, $b = 13.71$Å, $c = 4.57$Å	60

Thiourea	N/A	Orthorhombic, a = 7.66Å, b = 8.56Å, c = 5.49Å	61-63
Thiourea	Cycloheptane	Hexagonal, $a = b$ = 16.01Å, c = 12.45Å	64
Thiourea	Cyclohexane	Phase I: Hexagonal, $a = b$ = 15.84Å, c = 12.46Å Phase II: Monoclinic, a = 9.99Å, b = 15.58Å, c = 12.43Å, β= 114.64º Phase III: Monoclinic, a = 10.21Å, b = 14.98Å, c = 12.41Å, β= 115.18º	63
Thiourea	1,5-cyclooctadiene	Monoclinic, a = 12.24Å, b = 16.05Å, c = 9.63Å, β= 110.73º	65
Thiourea	Carbon tetrachloride	Trigonal, $a = b$ = 15.54Å, c = 12.53Å	66
Thiourea	Adamantane	Trigonal, $a = b$ = 16.19Å, c = 12.58Å	67
Thiourea	2,6-diethylnaphthalene	Monoclinic, a = 12.57Å, b = 9.28Å, c = 14.63Å, β= 92.1º	68
Thiourea	2-methoxybenzamide	Orthorhombic, a = 10.04Å, b = 10.88Å, c = 20.40Å	69
Thiourea	Ethenzamide	Orthorhombic, a = 10.66Å, b = 10.99Å, c = 20.68Å	70
Thiourea	1,4-diazabicyclo octane	Monoclinic, a = 9.68Å, b = 7.87Å, c = 18.25Å, β= 95.27º	71
Thiourea	Poly(2,3-dichlorobutadiene)	Monoclinic, a = 9.87Å, b = 15.83Å, c = 12.53Å, β=114.1º	53
Thiourea	Poly(2,3-dimethylbutadiene)	Monoclinic, a = 9.52Å, b = 15.4Å, c = 12.55Å, β=114º	53,72

Urea and thiourea inclusion complexes with such channel structure are usually prepared by cocrystallization from a solution in which the host and guest molecules are dissolved. The urea and thiourea inclusion complexes show either commensurate or

incommensurate structural properties and temperature-dependent phase properties. For example, the thiourea - cyclohexane inclusion complex is known to exist in three phases (phases I, II and III). The stable phase I experiences a second-order phase transition to phase II at ca. 148 K, and phase II undergoes a first-order transition to phase III at ca. 127 K.[63]

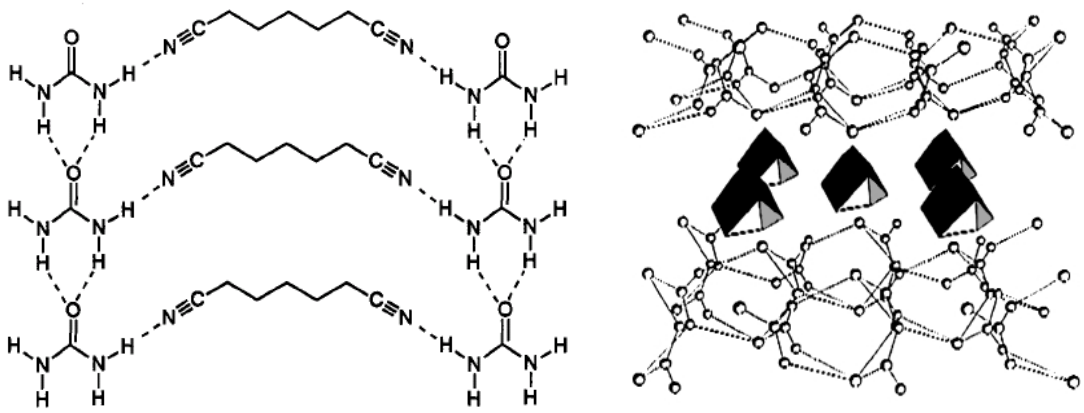

(A) (B)

Figure 1.3. The layer-structured supramolecular compound of A) $NC(CH_2)_5CN$ with urea[60] and B) 1,4-diazabicyclo octane with thiourea.[71]

In addition to the conventional channel-structured inclusion complexes, both urea and thiourea have been found to form layer-structured complexes and most of these complexes are commensurate.[59,20,60,68-71] For instance, $NC(CH_2)_nCN$-urea crystals with n = 6, 8, 10 are conventional channel inclusion compounds, while the others, with n = 3, 4, 5 are novel layered complexes that consist of sheets of hydrogen-bonded molecules in which linear arrays of urea molecules similar to the packing in tetragonal urea are separated by dinitriles and the adjacent layers are held together by dipolar and van der Waals forces (Figure 1.3A).[60] As illustrated in Figure 1.3B, the 1,4-diazabicyclo[2.2.2] octane (DABCO)-thiourea complex may be described as a pillar structure, in which the thiourea molecules are forming solid layers among which the DABCO molecules are

interacting and the thiourea networks are held together by DABCO bridges through hydrogen bonds.[71]

1.1.2 Cyclodextrin inclusion compounds

Cyclodextrins (CDs), sometimes called cycloamyloses, are α-1,4-linked cyclic oligomers of anhydroglucopyranose. The CDs consisting of six, seven, or eight glucose entities are called α-, β- and γ-CDs, respectively. Villiers discovered α- and β-CDs by digesting starch with bacillus amylobacter in 1891.[73] More than fifty years later, γ-CD had been discovered and the structures of α, β, and γ CDs were elucidated by Schardinger, Pringsheim and Szejtli.[74,75] As shown in Figure 1.4, CDs assume a toroidal shape with the primary hydroxyl groups at the narrow side (tail) and the secondary hydroxyl groups at the wide side (head).[5] Therefore, the two rims (head and tail) made of hydroxyl groups are hydrophilic and the cavity of the toroid tunnel is hydrophobic.

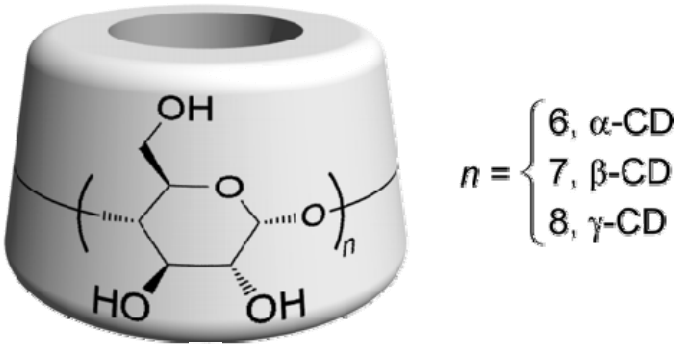

Figure 1.4. Schematic drawing of cyclodextrins (CDs). [5]

One of the most remarkable features of CDs is their ability to form inclusion complexes with small molecules and polymers. Since the appearance of the first inclusion complex formed between CDs and organic compound in 1928, a large number of inclusion compounds with low molecular weight compounds have been prepared and characterized.[5] The inclusion complex formation of CDs with polymers was not reported until Harada et al. prepared crystalline complexes with poly(ethylene oxide) in 1990.[76-78]

Since then, a lot of polymers, such as poly(propylene oxide) (PPO), polyolefins, polyamides, polyurethanes, polyamines, poly(vinyl methyl ether) (PVME), poly(ethylene terephthalate) (PET), poly(ε-caprolactone) (PCL), poly(L-lactic acid) (PLLA), poly(vinyl acetate) (PVAc), poly(methyl methacrylate) (PMMA), and polystyrene (PS) have been found to form ICs with CDs.[5,79]

The inclusion of a polymer chain into the CDs cavity is entropically unfavorable, but this threading process is promoted by intermolecular hydrogen bonds between neighboring CDs and noncovalent attractive interactions, such as Van der Waals and hydrophobic interactions, between polymer chains and CDs. Since a CD has two different hydroxyl groups on the two ends of its cavity, a primary (tail) and two secondary hydroxyl groups (head) (Figure 1.5), CD can have three assemblies, namely, head-to-head (secondary-to-secondary), tail-to-tail (primary-to-primary) and head-to-tail (secondary-to-primary). Pozuelo et al. simulated the hydrogen bonds interactions of the CDs in the ICs, and found that the strength of the intermolecular hydrogen bonds (per CD unit) is almost the same for the head to head or head to tail arrangements, but there are more intermolecular hydrogen bonds between CDs with head to head arrangement than head to tail ones. (Figure 1.4)[80] This simulation is consistent with the observation made by Harada's group and it indicates that the CDs assemble in a head-to-head, tail-to-tail sequence rather than head-to-tail one.[77]

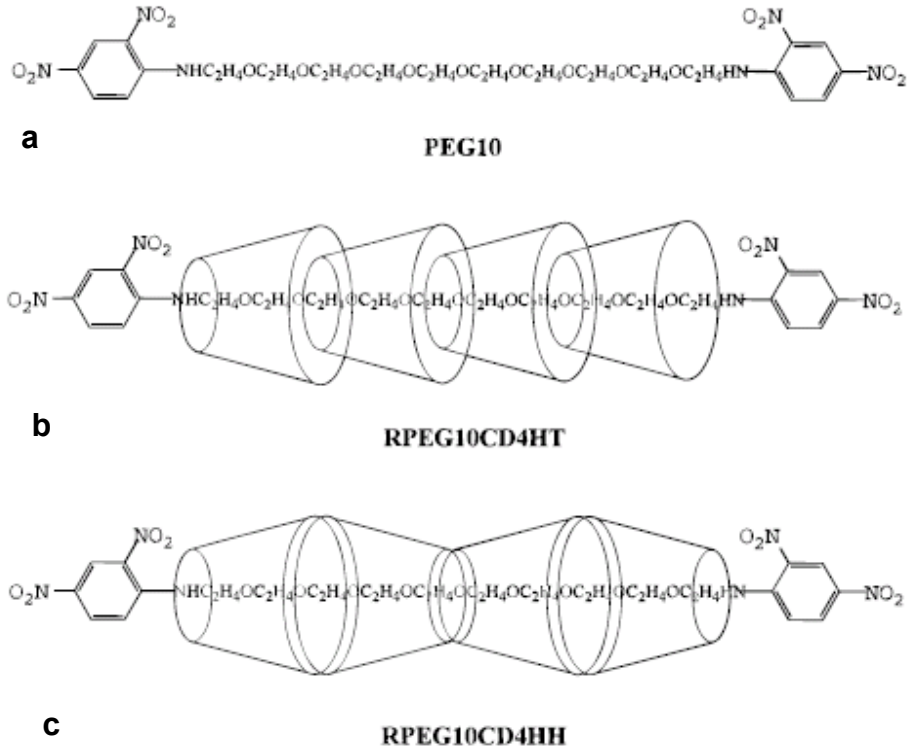

Figure 1.5. An isolated chain containing (a) 10 oxyethylene units (PEG10) and (b) polyrotaxanes containing 10 oxyethylene units and 4 α-cyclodextrins (represented by toruses) oriented head-to-tail or (c)head-to-head and tail-to-tail. All PEG are end-capped by 2,4-dinitrophenylamine groups.[80]

The threading process of ICs formed with CDs and polymer is more complex than the formation of urea or thiourea ICs, which could be divided into five different steps: 1) diffusion of the two reactants in the solvent, 2) initial threading of polymer chain ends into CD cavities, 3) sliding of CD over the polymer chain, 4) dethreading of CD from the polymer chain, 5) precipitation of the final aggregate. [81] Urea or thiourea ICs are commonly prepared by the co-crystallization method and can only exist in the solid state. Once dissolved they will separate into host (urea, thiourea) and guest molecules. In contrast, cyclodextrin ICs are not only stable in the solid state but can also easily dissolve in water and maintain a dynamic equilibrium in solution (threading and

dethreading). Moreover, the columnar cavity structure of CDs can be maintained without the involvement of guest molecules.[82]

The formation of ICs with α-, β-, or γ-CDs is mainly governed by the size of the guest molecules compared with the internal diameter of the CDs. The tail/head diameters of the cavity are 4.7/5.3, 6.0/6.5, 7.5/8.3 Å for α-, β-, and γ-CDs respectively.[74] Thus, the diameter of urea channel is close to that of α-CD and thiourea is close to that of β-CD. The γ –CD cavity is larger than the others. As a result, we can hypothesize that the guest polymers that can form ICs with urea could also form ICs with α-CD, and that the ones that can form ICs with thiourea could also form ICs with β-CD, while γ-CD could only include larger guest molecules.

As in urea and thiourea ICs, polymer chains included in CD ICs are both highly extended and isolated from neighboring polymer chains. Because of the head-to-head, tail-to-tail arrangement of CD channels, the ICs channels and polymer chains are found to be oriented by themselves.[82] Tonelli suggested that polymer chains that coalesce from CD ICs might be significantly different from those normally produced from solutions or melts.[79] For example, PET coalesces from γ-CD ICs crystallized quickly, achieves ca. 40% crystallinity and shows no glass transition or cold crystallization in the differential scanning colorimetry (DSC) scans. This is completely different from the conventional PET and is attributed to the different kink conformations of the non-crystalline regions, as existed in the initial γ-CD ICs.[83]

1.1.3 Application of urea, thiourea and cyclodextrin ICs

Due to the capability of urea, thiourea and CDs to isolate guest molecules inside their stacked channels, the ICs provide unique solid state environments for guest molecules, and can yield information regarding the dynamics of guest motions and other properties originating from the inherent behavior of individual guest chains. Among those properties, the conformation and orientation of guest chains inside the urea, thiourea or cyclodextrin channels are the main research contents. These two properties

are associated with the one-dimensional channel structure, which will orient and isolate guest molecules and limit their conformations so that they might be widely used.

The practical applications of urea, thiourea and cyclodextrin ICs include inclusion polymerization to prepare less-branched and stereoselective polymers,[38,52-55,84-86] molecular separation to isolate linear compounds from multi-branched ones or to separate low molecular weight compounds from high molecular weight ones,[14,87-90] and the separation of enantiomers by chiral recognition.[91-95] Finally, they can allow the preparation of new materials with unusual properties, such as the urea, thiourea ICs containing appropriate organic or organometallic guests that exhibit second harmonic generation (SHG) (doubling of the frequency of light as it passes through a material),[96-98] which originates from molecular orientation and dipole moment alignment of guest molecules within the inclusion compound channels.[14,98]

1.1.4 PEO inclusion compounds

Linear polymers are usually found to form ICs with urea and α-CD. In contrast, polymers with multiple side chains or substituted functional groups are found to form ICs with thiourea, β-, or γ- CD. For example, PEO was the first polymer found to form an IC with urea and α-CD, and it is also able to form a stable complex with γ-CD, but not with β-CD in aqueous solution.[76,77] On the other hand PPO is able to form ICs with β- and γ-CD, but not with α-CD. This is consistent with the host diameters of α-, β- and γ- CD, which are around 4.7-5.3, 6.0-6.5 and 7.5-8.3 Å, respectively. The diameters of the α-CD and γ-CD channels are large enough to include one and two PEO chains, respectively, while β- CD is large enough for PPO chains but is too large to form a stable IC with PEO. Just as for CDs, the polymers that can form ICs with urea and thiourea are generally different. Linear polymers, such as polyethylene, PCL and PLLA will form ICs with urea, while substituted polymers, such as PVC and poly(2,3-dimethylbutadiene), prefer forming ICs with thiourea.

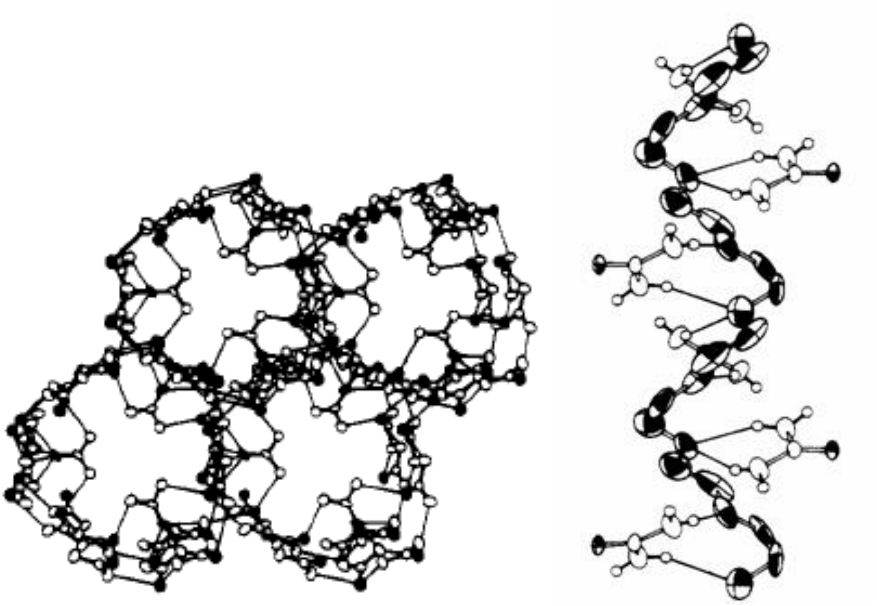

A B

Figure 1.6. Structure of the poly (ethylene oxide)-urea inclusion complex: (a) the channel structure formed by the hydrogen bonded urea molecules and (b) the association of PEO and urea molecules inside the channel.[16]

Perhaps the most interesting of the polymer-urea ICs is that with PEO. Barker and Ranauto first achieved complex formation of PEO and its derivatives with urea.[15,99] The crystalline structure of the PEO-urea complex was determined to be trigonal ($a = b$ = 10.43 Å, c = 9.12 Å) with a stoichiometry of $(EO)_4(urea)_9$ by Tadokoro et al. and by Chenite and Brisse.[16,42] This structure is different from that of conventional urea ICs (hexagonal, a = b = 8.23 Å, c = 11.01 Å).[31] In this unusual inclusion complex structure, the PEO chains form an approximate 4_1 helix in which each pair of adjacent ether oxygen is hydrogen bonded to a urea molecule that is located inside the channels formed by urea molecules. Therefore, two types of urea molecules exist within the unit cell: two thirds of the urea molecules (6 urea) form the channels (Figure 1.6A) and one third (3 urea) are embedded inside the channels and associate with PEO chains (Figure 1.6B). As a result, the channel diameter of the PEO-urea IC is larger and the repeat length of the channel is less than in the ordinary urea channels. For polyethers $[(CH_2)_mO]_n$ with m>3,

the urea ICs are the same as those formed with n-alkanes, and the polymers take trans (zig-zag) conformations.[16,40,41] Tonelli simulated the PEO conformations assuming the conventional hexagonal channel structure, and results showed that the all-trans (TTT) (O-C-C-O) conformation could be included but that the most common TGT (O-C-C-O) 7_2 helical conformation of PEO cannot be included inside the urea channels.[49] This could be further confirmed by the complex formed between PEO and α-CD, in which PEO chains are thought to take all-trans conformation to thread through the α-CD channels.

In addition to the trigonal PEO-urea IC, named Form α here on, two other modifications are reported for low molecular weight PEG (M_w = 400) and for samples resulting from the melt-quenching of Form α. The low molecular weight PEG-urea complex was reported to be tetragonal (*a* = 7.3 Å, *b* = 19.51 Å) with a 1:1 EO:urea composition.[58] After melt-quenching of Form α, a mixture of tetragonal urea and a second complex of PEO-urea, named Form β here on, is formed. This β complex was reported to be metastable and to phase transfer to Form α after annealing at 90 ºC.[100-104] As to the crystalline structure of Form β, it is assigned to either the hexagonal structure by Tonelli et al.[105] or to the low molecular weight PEG-urea complex by Bogdanov.[100-104] and Ye et al. [104,106] However, Form β does not seem to fit completely with either, indicating that a new unknown crystalline structure exists. As shown in Table 1.2, the formation of two different crystalline structures between PEO and some small host molecules is not uncommon. For instance, both resorcinol and 2-methyl resorcinol (MRES) can form two different complexes with urea. The Form β is generally metastable and will undergo a transformation to the stable Form α within a few minutes at room temperature.[107] Because of the metastability of these β forms, the composition and crystalline structure of these β complexes have not been obtained yet.

Compared with the complex formed with urea, the PEO-thiourea complex is less well researched. In fact, its composition as well as its crystal structure are not well determined yet. PEO-thiourea complex was first obtained by Parrod and Kohler,[15,108] then further researched by Bailey,[17,109] Tarnrutskii[110] and more recently by Campo et

al.[18] The PEO:thiourea molar ratio is considered as 1:2, 1:0.7 and 1:4 by these three groups, respectively. As mentioned above, the diameter of thiourea channels is close to that of β-CD, therefore, a single PEO chain seems too small and two PEO chains seem too large to fit in one thiourea channel. In other words, the channel-structured PEO-thiourea complex might be as unstable as PEO with β-CD and should collapse into uncomplexed thiourea rather than forming the channel structure[18] Therefore, it is worth further studies to confirm the composition and crystalline structure of the PEO-thiourea complex and the "metastable" PEO-urea β complex.

In addition to the complexes formed with urea and thiourea, PEG/PEO has also been found to form complexes with other organic molecules, such as p-nitrophenol(PNP), resorcinol, 2-methyl resorcinol (MRES), hydroquinone (HYD) and some inorganic salts, such as mercuric chloride, sodium thiocyanate (NaSCN) and sodium iodide (NaI) (Table 1.2). Different conformations have been observed for the bond sequence O-C-C-O in PEO chains, and the most popular ones are TTT, TGT, TGG(TG^-G^-) and TGG^-. The dihedral angle is 180º for trans and 60º and 270º (-60 º) for G and G^-, respectively. The most commonly observed PEO form is the 7_2 helical conformation with trans-gauche-trans TGT sequences.[111] Another less observed form is the triclinic planar zigzag conformation with all-trans (TTT) sequences that can be obtained by stretching to two folds[112] or by freeze-drying dilute solutions.[113]

The introduction of small host molecules in the PEO unit cell has different effects on the conformation and the crystal structure of PEO chains. For weak Van der Waals interactions, such as PEO-p-dihalogenobenzene complexes, the conformation of PEO molecules is nearly identical to that found for pure PEO.[19] However, stronger electrostatic interactions, such as in the PEO-$HgCl_2$ complex, induce dramatic modification of the chain conformation. Two more models of PEO chain with H_gCl_2 complex were proposed by Tadokoro et al.[6,7] One is the zigzag form I with a TTTTGT conformation and the other is the zigzag form II with a $TGGTG^-G^-$ conformation (Figure 1.7). The population of TGT and TGG conformation of PEO was observed to increase and that of the TTT, TGG^- conformations to decrease upon complexation with LiI.[10] The

zigzag form I TTTTGT has been considered as the main conformation of PEO in the complex with LiV_3O_8[12] and $CdPS_3$ preintercalated with hydrated alkali cations.[13] As to the complex with $LiCF_3SO_3$, [8,9] PEO may still take a TGT conformation but the gauche torsional angle of the C-C bond decreases from 79º in bulk PEO to 47º in the complex. When hydrogen bonds are formed between the oxygen ether of PEO chains and the O-H or N-H group of guest molecules, such as with PEO-p-nitrophenol, the PEO chains adopt a glide-type conformation TGTTGTTTT stabilized by hydrogen bonds and this conformation is not helical as in pure PEO.[114]

Table 1.2. The conformation of PEO chains and the crystalline structures of host-guest complexes formed between PEO and some small molecules.

Host molecules	PEO conformations	Crystalline structrue	Ref.
Pure PEO	7_2 helix, TGT	Monoclinic, a = 8.05Å, b = 13.04Å, c = 19.48Å, β= 125.4º	111,115
Urea	7_2 helix, TGT 4_1 helix (assumption)	Trigonal, $a = b$ = 10.43Å, c = 9.12Å Tetragonal, $a = b$= 7.3 Å , c = 19.51Å	16,42 58
p-nitrophenol (PNP)	TGTTGTTTT	α form: Triclinic, a = 11.72Å, b = 5.55Å, c = 15.57Å, α = 90.7º, β = 87.1º, γ = 104.0º β form: metastable	22
Resorcinol	7_2 helix, TGT	α form: Orthorhombic, a = 10.5Å, b = 10.13Å, c = 9.776Å β form: metastable	24
2-methyl resorcinol (MRES)	7_2 helix, TGT	α form: orthorhombic, a = 10.4Å, b = 15.9Å, c = 18.5Å; β form: orthorhombic, a = 11.1Å,	25

	4_1 helical	b = 18.6Å, c = 10.6Å	
Hydroquinone (HYD)	7_2 helical, TGT	Triclinic, *a* = 11.7Å, *b* = 12.0Å, *c* = 10.6Å, α = 78º, β = 64º, γ = 115º	26
Mercuric chloride	TTTTGT TGGTG$^-$G$^-$	Zigzag form I: Orthorhombic, *a* = 13.55Å, *b* = 8.58Å, *c* = 11.75Å, Zigzag form II: Orthorhombic, *a* = 7.75Å, *b* = 12.09Å, *c* = 5.88Å,	6,7
sodium thiocyanate (NaSCN)	2_1 helix, TGTTGTTG$^-$T TGGTG$^-$G$^-$	Form I: Monoclinic, *a* = 16.83Å, *b* = 10.64Å, *c* = 7.19Å, β = 125.5º Form II: Monoclinic, *a* = 7.55Å, *b* = 12.10Å, *c* = 5.83Å, β = 97.5º	11
Sodium iodide (NaI)	2_1 helix, TGTTGTTG$^-$T	Monoclinic, *a* = 18.15Å, *b* = 8.41Å, *c* = 7.98Å, β = 122.3º	116
Lithium Iodide (LiI)	TGT,TGG	N/A	10
p-$C_6H_4Cl_2$ p-$C_6H_4Br_2$	7_2 helix, TGT 7_2 helix, TGT	Orthorhombic, *a* = 16.48Å, *b* = 9.51Å, *c* = 27.86Å Orthorhombic, *a* = 16.74Å, *b* = 9.68Å, *c* = 27.98Å	19,20
LiV_3O_8	TTT, TGT	N/A	12
$LiCF_3SO_3$	TGT	N/A	8,9

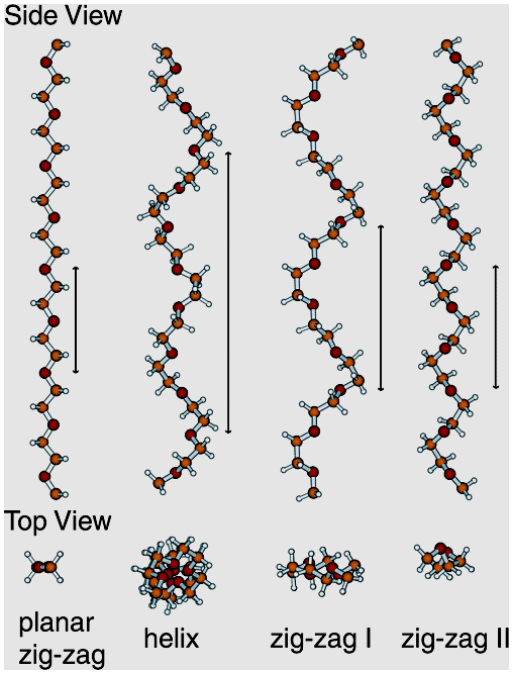

Figure 1.7. Side and top view of the structures of the four model conformations of PEO. On the side of the polymeric chains, a line indicates the dimension of the repeating units of each conformation along the chain length direction.[6,7,111,115,117]

It is reported[118] that the TTT conformation is the lowest in energy, while the TGT and TGG conformers are only 0.1- 0.2 kcal/mol higher in energy in the model compound 1,2-dimethoxyethane (DME). Of the three conformers, TGG is more popular in the gas state with strong 1,5 CH---O hydrogen-bond interactions[119] and TGT is stabilized by polar interactions in the liquid or solid states,[118] while the nonpolar TTT conformer is most stable in an argon matrix at 34K.[120] In the melt state or in an aqueous solution, the molecular dynamics simulations[121-127] have revealed that the conformation of DME and PEO depends strongly upon temperature and solution composition. In general, the conformations of TGT and TGG are more favorable than TTT and TGG^- when the solution is more dilute, thus Smith et al. classified the former as hydrophilic and the later as hydrophobic.[123] The solution stabilization energy is about 1.7 kcal/mol. Therefore, the population of TGT and TGG conformation is much more than TTT and

TGG^- in aqueous solution. Simulation also showed that PEO chains in the melt are more extended than the phantom chains which represent the unperturbed chains in θ solution and TGT, TTT conformations are more favorable in the totally amorphous state.

1.2 Electrospinning

1.2.1 History and set-up

In the urea, thiourea and cyclodextrin inclusion complexes, guest polymers are packed in one-dimensional, narrow channels or tubular structures constructed from either an essentially infinite three-dimensional hydrogen-bonded network of urea molecules or from covalent-bonded oligomers of anhydroglucopyranose. The guest polymer chains are thus highly extended and oriented at the molecular scale inside the channel. However, the polymer and the inclusion complexes themselves are not aligned at the larger macroscopic level. To optimize the orientation of channel-structured urea, thiourea and cyclodextrin complexes, it is necessary to find a way to align the channels at the macroscopic level. Here we use the electrospinning method.

Electrospinning, also known as electrostatic spinning, is a highly versatile method to produce continuous fibers with diameters ranging from several nanometers to several micrometers. It is applicable to most soluble or fusible polymers, polymer blends, nanoparticles or drug-impregnated polymers and ceramic precursors. The simplicity of the setup and the possibility of large scale productions make this technique attractive for academic research and industry as well. Electrospinning relies on theoretical principles developed in the early studies on the application of electric potentials to liquid drops. In 1600, Gilbert first demonstrated that a drop of water on a smooth surface can be extended into a cone if a piece of rubbed amber is held at a suitable distance from it.[128] In 1745, Bose described the process of applying a high electric field on liquid drops to produce electrohydrodynamic spraying of fluids.[129] In 1882, Lord Rayleigh researched the electric field needed to overcome the surface tension of a liquid drop and the stability criterion of thin liquid jets in electric field.[130] The most

important patent describing the electrospinning of polymers was issued to Formhals[131] in 1934. He successfully electrospun cellulose acetate fibers in an acetone/alcohol solution and used a movable thread-collecting device to collect aligned and stretched fibers. In several following patents, Formhals achieved simultaneous electrospinning of a number of fibers by using multiple nozzles from the same polymer solution to increase the productivity and generate composite fibers on a moving base.[132-135] Following the work of Formhals, Taylor researched the jet forming process and found that the pendant droplet developed into a cone (now called Taylor cone) when the surface tension was balanced by electrostatic forces and the fiber jet was emitted from the apex of the cone, which is one of the reasons why electrospinning can generate small diameter fibers.[136]

(1544-1603) (1710-1761) (1842-1919)

Figure 1.8. William Gilbert (left), Georg Matthias Bose (center) and Lord Rayleigh (John William Strutt) (right).

Baumgarten studied the relationships between the processing parameters, such as solution viscosity, flow rate and applied voltage, and the structural properties of electrospun fibers by using a high-speed camera. He discovered that fiber diameters decreased with decreasing solution viscosity but did not have a proportional decrease with increased applied voltage.[137] Then Larrondo and St. John Manley demonstrated that continuous filaments of rapidly crystallizing polymers, such as polyethylene (PE) and polypropylene (PP), can be electrospun from the melt using an electric field as the only

driving force. The electrospun fibers prepared from a melt had relatively larger diameters than fibers spun from a solution, but these diameters are still much smaller than those of textile fibers prepared by conventional melt-spinning or solution-spinning.[138-140]

Despite these early discoveries and research, electrospinning did not attract much attention until several research groups, especially Reneker,[141,142] revived interest in this technique in the 1990s to prepare nano or micro fibers from a wide range of polymers. One reason for this fascination is the interest in the field of nanoscience and nanotechnology. Another reason is its combination of fundamental and applied research from different science and engineering disciplines. There are several methods of producing nanofibers, such as nanolithography,[143] melt-blowing,[144] island-in-sea,[145] gas jet technique[146] and self-assembly of multicomponents.[144,147,148] But these methods are limited by their restricted material ranges, cost and production rate. Electrospinning is a technique that allows the production of continuous polymeric fibers with diameters ranging from nanometers to a few microns, and thus with an inherent high surface-to-volume ratio. This method can be applied on a wide range of soluble or molten polymers with sufficiently high moleclular weight, including bulk polymers, polymer blends and polymers loaded with nanoparticles, metals and ceramics. It also allows making fibers with complex architectures, such as porous, beaded, ribbon, core-shell, or hollow fibers.[149-158]

To produce electrospun nanofibers, a concentrated polymer solution is forced through a syringe and subjected to a large electric field applied between a metallic needle and a collection target. When the potential difference is large enough, charge repulsion overcomes the surface tension of the viscous solution and a charged jet is expulsed at high speed towards the grounded (or oppositely charged) target (Figure 1.9). This jet travels with a whipping motion while the solvent rapidly evaporates, leading to the formation of a highly extended polymer fiber with a much reduced diameter. The behavior of electrically driven jets, the shape of the jet originating surface and the jet instability are three important areas that need to be understood for controlling the

electrospinning process. Taylor showed that a conical shaped surface with an angle of 49.3º is formed when a critical potential is reached to disturb the equilibrium of the droplet, which will initiate the electrospinning process by jetting when the potential further increases.[136] The jet ejected from the apex of the cone continues to narrow down along the path to the collector and undergoes a chaotic motion or bending instability.[159] The bending instability was originally thought to be occurring by a single jet splitting into multiple thin fibers due to the repulsive forces of the charged ions within the electrospinning jet, resulting in smaller diameter fibers.[141] However, viewed with high-speed photography by decreasing exposure times down to 1 ms, it was confirmed that the unstable region of the jet is in reality a single rapidly whipping jet and that it was the whipping instability that causes the stretching and bending of the jet into a smaller fiber. The whipping instability is dominant with high charge density in the jet and can occur through either: (1) small lateral fluctuations in the centerline of the jet, resulting in the induction of a dipolar charge distribution which will interact with the external electric field to further bend the jet, or (2) the mutual repulsion of surface charges carried by the jet, causing the centerline to bend.[160,161] Reneker et al. have contributed significantly to understanding the instability behavior and have mathematically modeled the jet path, trajectory, velocity of jet, area reduction ratio and the longitudinal strain of the jets.[161]

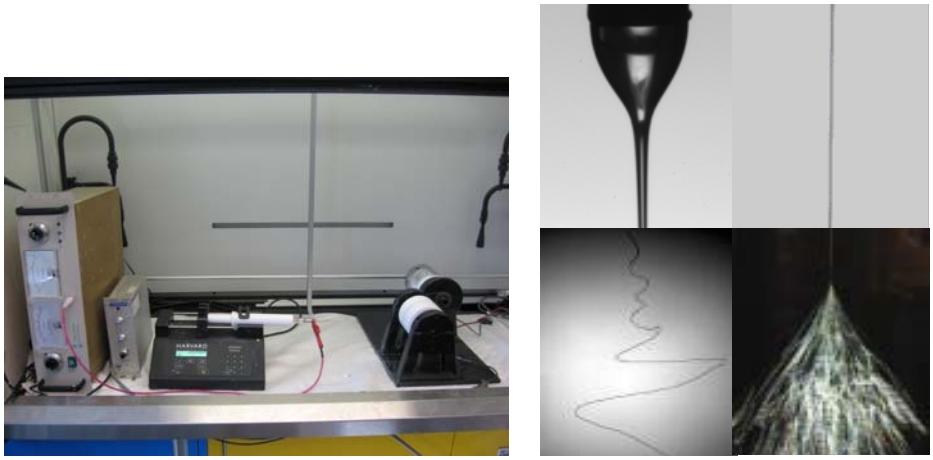

Figure 1.9. Basic setup of electrospinning (left) and real-time images of the electrospinning process (right).[162]

1.2.2 Parameters influencing electrospinning process

For the formation of electrospun fibers, a high voltage is applied to the polymer solution or molten polymer to provide a stretching force. When a sufficiently high voltage is generated to overcome the surface tension of the polymer fluid, a jet of polymer fluid erupts. If the molecular weight and concentration of polymer is high enough to form polymer chain entanglements and to prevent the electrospinning jet from breaking up, an electrospun fiber is formed when the solvent evaporates. In principle, nearly all soluble or fusible polymers can be processed to get electrospun fibers, provided that both intrinsic properties of polymer molecules (such as viscosity, concentration, molecular weight, surface tension, electrical conductivity and entanglement) and the process parameters (such as applied electric field, capillary-collector distance, polymer flow rate, and capillary diameter) are correctly adjusted. Grouped in order of relative impact on the electrospinning process, these parameters will be discussed separately.

1.2.2.1 Applied voltage

As shown in Figure 1.9, a spherical droplet is formed on the polymer solution pumped at the end of the needle. To eject fibers out of the droplet, a critical voltage is needed to overcome the surface tension of the droplet. Surface tension is a property of the surface of a liquid. It results from an imbalance of molecular forces in a liquid. In the bulk of the liquid each molecule is pulled equally in all directions, resulting in a net force of zero. At the surface of the liquid, such as in the air, the molecules are pulled inward by other molecules inside the liquid and are not attracted as intensely as by the molecules in the neighboring medium. As a result, a net force inwards is produced on the surface, which will diminish the surface area until it has the lowest surface area possible. In 1969, Taylor[163] derived the equation (equation 1.1) for the critical electric potential needed to transform a droplet of liquid into a cone (thereafter named Taylor cone).

$$V_c^2 = 4\frac{H^2}{L^2}(\ln\frac{2L}{R} - \frac{3}{2})(0.117\gamma R) \quad (1.1)$$

where V_c is the critical voltage, H the distance between the capillary end and the target, L the length of the capillary with radius R, and γ the surface tension of the liquid. Generally, both high negative or positive voltages of more than 6 kV are able to convert the droplet into the shape of Taylor cone. The high voltage initiates the electrospinning process by inducing necessary charges on the polymer fluids. Taylor began with the observation of a droplet in equilibrium at the end of the capillary and observed its deflection under applied fields. In most cases, a higher voltage leads to greater stretching of the polymer fluids due to the greater coulombic forces in the jet and the stronger electric field.

Based on equation 1.1, several parameters can alter the critical applied voltage. First, it is obvious that the applied voltage depends on the capillary-collector distance. Varying the distance influences both the electric field strength and the flight time. As a result, when the distance decreases, the electric field strength and the acceleration of the jet increase. At the same time, the flight time decreases so that the solvent might not evaporate completely. This in turn influences the morphology of the electrospun fibers. For example, if finer fibers are needed, a longer distance might be favorable, because it will reduce the electric field and the acceleration of the jet so that longer flight time of the jet might favor the formation of finer fibers. Secondly, any effects that could change the surface tension of the polymer liquid, such as a different solvent system, alter the critical voltage needed. Therefore, by choosing a solvent with a lower surface tension or by adding a surfactant to decrease the surface tension, the critical voltage is decreased dramatically. Third, the increase of the conductivity of the polymer fluid produces more charges at its surface and, accordingly, lowers the critical voltage needed for electrospinning to occur. The increase of conductivity could be achieved by using different solvents or by adding a small amount of salt or polyelectrolyte. Another effect of the increased conductivity of the polymer solution is that it results in a greater

bending instability, as discussed in Chapter 1, which is mainly attributed to greater repulsive interactions of the charges on the jet surface during the electrospinning process. As a result, the flight area of the fibers will increase and the diameter of the electrospun fibers will decrease.

1.2.2.2 Viscosity, concentration and molecular weight

When the charged jet is ejected from the polymer fluid droplet, its route is controlled by the electric field. As discussed in section 1.2.1, the charged jet exhibits bending instabilities caused by the interaction of repulsive forces between charges carried with the jet and it will be further bent by the external electric field. As a result, a spiralling loop is formed and the jet grows longer and thinner. During this process, it is the entanglements of the polymer chains that prevent the charged jet from breaking up into droplets, thus maintaining a continuous jet. On the other hand, if the viscosity of the polymer fluid is too low, electrospraying may occur to form polymer particles or droplets rather than fibers. Therefore, factors that affect the viscosity of the polymer fluid will also affect the electrospinning process and the resultant fibers.

Viscosity is a measure of the resistance of a fluid to flow. For a homogeneous solution of a linear polymer, the well known Huggins equation describes the solution viscosity as:[164]

$$\eta_{sp} = \eta_r - 1 = \frac{\eta - \eta_s}{\eta_s} = [\eta]c + k_H([\eta]c)^2 + \cdots \qquad (1.2)$$

where η_{sp} is the specific viscosity, η_r the relative viscosity, η and η_s the viscosity of the solution and the solvent, respectively, $[\eta]$ the intrinsic viscosity, c the polymer concentration and k_H the Huggins coefficient. From equation 1.2, $[\eta]$ can be obtained from the plot of η_{sp} vs. c, and $[\eta]$ is the initial slope. The dimensionless product of the

intrinsic viscosity and the concentration, $[\eta]c$, is named the Berry number (B_e). B_e <1 when there is no chain overlap, while B_e >1 if there is polymer chain overlap. The critical chain overlap concentration, c*, is defined as

$$c^* = \frac{1}{[\eta]} \tag{1.3}$$

Physically, the critical chain overlap concentration c* is the point where the concentration inside a single macromolecular chain equals the solution concentration.

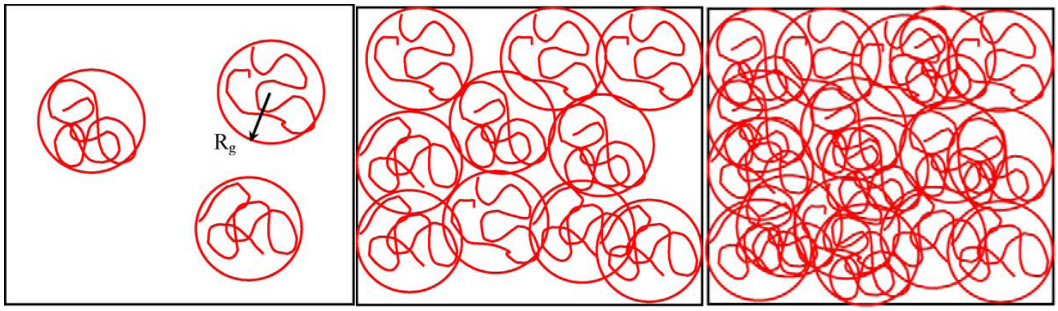

(a) $c < c^*$ (b) $c^* < c < c_e$ (c) $c > c_e$

Figure 1.10. Physical representation of the three solution regimes, (a) dilute, (b) semidilute unentangled and (c) semidilute entangled. R_g is the radius of gyration.[165]

As shown in Figure 1.10, when the polymer concentration c is less than c*, there is no overlap of polymer chains. As a result, only small droplets or microbeads are generated. When the polymer concentration is larger than c*, but less than the critical entanglement concentration of polymer solution (c_e), chain overlap is initiated but there are no significant entanglements. Therefore, a mixture of fibers and beads might be produced within this concentration range. Only when the concentration is further increased to c_e, the critical concentration from the semidilute unentangled to semidilute entangled regime, the topological constraints will introduce large chain

entanglements.[164,165] The increased chain entanglements can serve to stabilize the electrospinning jet by inhibiting jet breakup. Thus, c_e is an important parameter for the electrospinning process. Uniform electrospun fibers can be formed only when the polymer concentration is larger than c_e. Gupta et al. found that the c_e is 3c* for PMMA.[165] Beaded fibers were obtained when the concentration was larger than 3c* and uniform fibers only formed if the concentration was $6c^*$ or larger.

In addition to the polymer concentration, $[\eta]$ is related with the molecular weight (M_w) by the Mark-Houwink-Sakurada equation.

$$[\eta] = KM_w^{\alpha} \tag{1.4}$$

where the constant K is characteristic of the polymer and solvent, and the exponential α is a function of the shape of the polymer coil in solution.[166] The value of α is around 0.5-0.8 for flexible chains in good solvents and exceeds 1 for rigid chains. In the Flory theta solution, the flexible chain has α = 0.5. Generally, the higher the molecular weight, the higher the intrinsic viscosity. Considering equation 1.3, the c* and c_e become smaller with larger polymer molecular weight. Thus, one necessary condition for the formation of electrospun fibers is that the polymer used must have high enough molecular weight so that the polymer fluids can be sufficiently viscous to be entangled.

In a polymer melt, the critical molecular weight (M_c) for forming an entangled network is approximately twice the entanglement molecular weight (M_e). For most polymers, experimental observations suggest that the ratio of M_c/M_e, corresponding to the number of entanglements (n_e), is between 1.7 and 3.[167] Although molten polymers can be electrospun,[138-140] it is more common to electrospin polymer solutions, especially in academic labs. The solubility of polymers is more complicated than that of small molecule due to their long chains and high molecular weight. Generally, a polymer with higher molecular weight is less soluble than one with a lower molecular weight because

of a reduced mixing entropy. In addition, the intermolecular interactions between long chain polymers are stronger than for short-chain ones, so that it takes a longer time to dissolve. In a polymer solution, both concentration or polymer volume fraction (ϕ_p) and molecular weight affect the number of chain entanglements. The solution entanglement number $(n_e)_{soln}$ is defined as the ratio of the polymer molecular weight to its solution entanglement molecular weight $(M_e)_{soln}$ (equation 1.5).

$$(n_e)_{soln} = \frac{M_w}{(M_e)_{soln}} = \frac{\phi_p M_w}{M_e} \qquad (1.5)$$

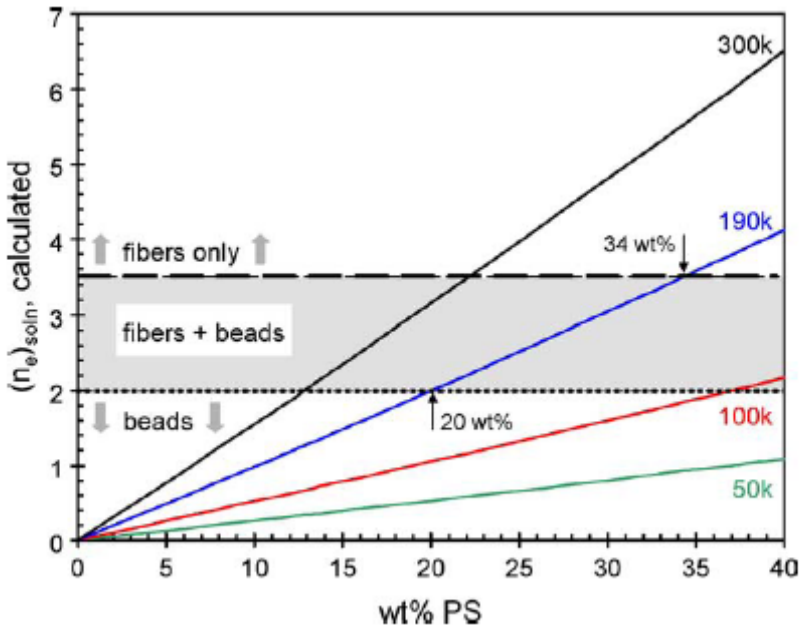

Figure 1.11. Plot of the calculated entanglement number $(n_e)_{soln}$ as a function of concentration for PS/THF system.[167]

Utilizing entanglement molecular weight (M_e) and weight-average molecular weight (M_w), the requisite polymer concentration for fiber formation can be determined by calculation, avoiding the trial-and-error methodology typically used to produce electrospun fibers. Shenoy et al.[167] analyzed the data obtained from PS/THF, PDLA/dimethylformamide (DMF), PLLA/dichloromethane (DCM), PEO/H_2O and

PVP/ethanol systems and concluded that electrospun fibers with beads are formed at one entanglement per chain, while complete, stable fibers are formed at 2.5 entanglements per chain, corresponding to $(n_e)_{soln}$ equals to 2.5 and 3.5, respectively. As shown in Figure 1.11, the concentration needed to generate uniform fibers is different for various M_w of PS. The higher the M_w, the lower concentration required. Similar to the effect of molecular weight, an increase in the concentration of the polymer solution will result in greater polymer chain entanglements. As a result, to maintain the continuity of the jet during electrospinning, both molecular weight and concentration must be high enough to satisfy the requirement of polymer chain entanglement.

In the case of less viscous polymer solutions or in solutions with short or rigid polymer chains, a second polymer is often added to increase the viscosity and create entanglements, so that it is possible to produce electrospun fibers. Since the M_e of PEO is small, ca. 2100 g/mol, it is often used to improve spinnability by imparting greater elasticity to the solution.[166,167] The added polymer might form network of entanglements. However, as pointed by Yu et al., the presence of entanglements is a sufficient but not a necessary condition for the polymer solution to demonstrate strong elastic properties; the elastic property could also be achieved at lower polymer concentration if the relaxation time of the solution is longer than the time of extensional deformation.[168]

Up to now, all the electrospinning processes are run with either polymer solutions or molten polymers. Before running our electrospinning experiments, the viscosities of PEO/methanol solutions with 1, 5 and 7.5 % PEO (M_w= 400,000 g/mol) concentrations were measured. As shown in Figure 1.12, the viscosity increases dramatically with the PEO concentration. It was found that the 1 % PEO cannot produce continuous electrospun fibers, but that the 5 % and 7.5 % PEO solutions could. However, since the PEO-urea complex formed by co-crystallization method is a precipitate, could it still be electrospinnable? Compared with the PEO solutions, the suspension obtained by mixing 5% PEO with an appropriate mass of urea in 20 ml methanol solution has a similar viscosity as the 5 % PEO solution. We then attempted to

use the insoluble PEO-urea IC suspension to prepare electrospun fibers and it proved successful, as will be discussed in Chapter 3. Therefore, we think complete solubility of polymers might not be a necessary condition for the formation of electrospun fibers. As long as the viscosity is high enough for the entanglement network to be formed, electrospun fibers could be produced. Here it should be pointed that the usual measurement of shear flow viscosity is not sufficient to characterize the deformation behaviour of a fluid. In the process of electrospinning, it is the elongation rather than shear viscosity that is the most dominant mode of deformation.

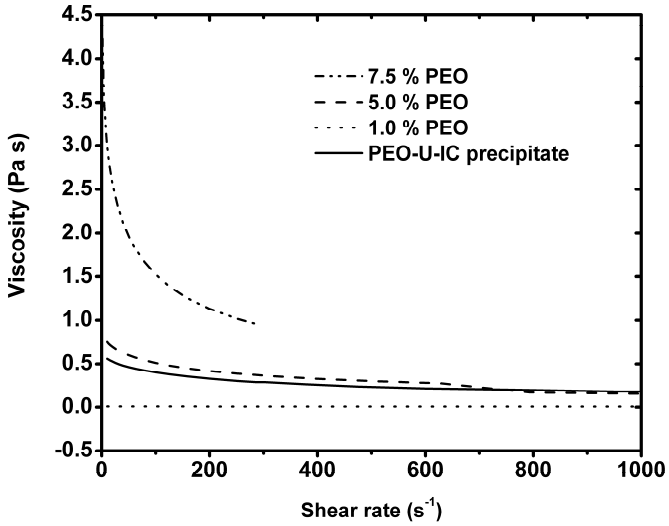

Figure 1.12. Plot of viscosity as a function of shear rates for various PEO solutions and the PEO-urea-IC suspension.

1.2.3 Alignment of electrospun nanofibers

Because of the bending instability associated with the spinning jet, electrospinning was initially used to prepare randomly aligned non-woven mats, which can be used in filtration, tissue scaffolds and wound dressing. But for many other applications, it is necessary to control the alignment of the fibers to obtain better mechanical, electronic and optical properties.[169] In the past several years, a number of

target collectors, which can modify the jet movement by controlling of the electric field, have been designed and used to produce highly aligned fibers. These target collectors include knife-edged rotating disk,[170] rotating drums,[171-173] metal frames,[174,175] and two separated conductive substrates.[176] The schematic set-ups of rotating disk and separated electrodes are shown in Figure 1.12.

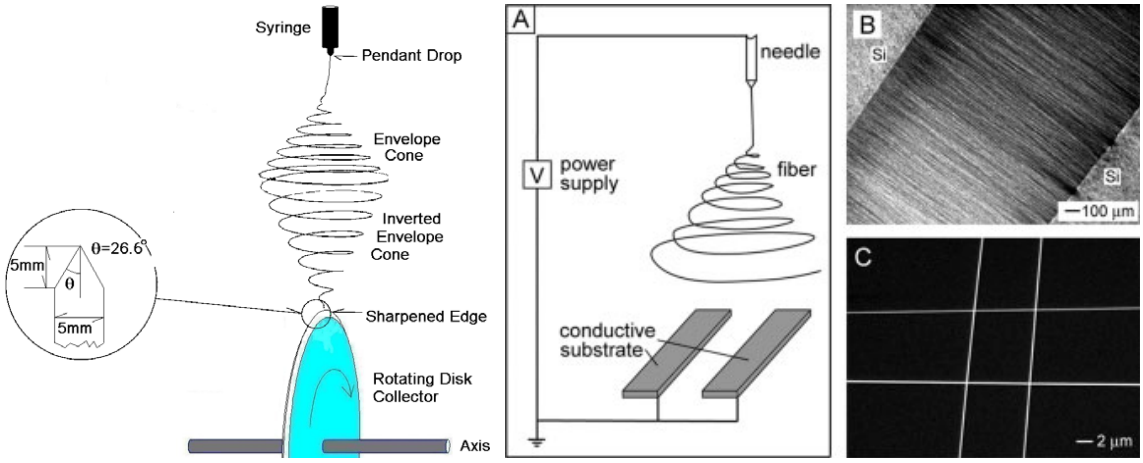

Figure 1.12. Schematic setup of the knife-edged rotating disk (left)[170] and two separated conductive substrates (right) used for obtaining aligned fibers.[176]

Winding a single fiber on a rotating drum is the ordinary textile technology to produce fibers. This winding process can be achieved easily because the spinlines are straight in these cases. However, as explained in section 1.2.1, the jet path during electrospinning is a complicated three-dimensional loop, which is the main reason why an aligned nanofiber seems difficult to be achieved by the conventional winding method. Nevertheless, since electrospinning process needs a high electrostatic field, it is possible to control the jet path by manipulating the auxiliary electrostatic field. As shown in Figure 1.12, although the electrospun jet is three-dimensional looped, when it approaches the sharp end of a rotating counter electrode, the loop begins to shrink and

ultimately forms an inverted cone with its apex on the sharp edge. In the end, all fibers are pulled toward the tip of the rotating disk and are assembled in a parallel array.[170]

As to the mechanism for the alignment of electrospun fibers on the two separate electrodes, it could be attributed to the electrostatic forces exerted by the strong external field, the collector and any adjacent charged fibers.[176,177] When a continuous conductive plate is used as the collector, there will be no preferential direction for the electrostatic forces, therefore, only randomly aligned fibers are collected. In contrast, when an insulating gap is kept between two separate electrodes, the external electrostatic field is changed. As a result, the direction of the electrostatic force on the fibers across the gap will be changed also. It is reported that the electrostatic forces will simultaneously pull the fibers towards the edges of the two electrodes and that the residual charges on the fibers will repel the neighboring fibers to achieve uniaxial alignment across the gap.[176,177]

1.2.4 Orientation and structure in electrospun fibers

It is of great interest to not only control the macroscopic alignment of the fibers but also their orientation at the molecular level, because it strongly influences most mechanical, optical, and electrical properties. Aligned polymeric fibers[175,178,179] and nanocomposite fibers containing highly oriented carbon nanotubes[171,180,181] or a one-dimensional array of nanoparticles[182,183] have recently been prepared. Polymer chains present different molecular orientation in electrospun fibers. For instance, Dersch et al.[175] found that polylactide does not show any molecular orientation while polyamide-6 shows relatively large orientation. But it is not homogenous along the fiber axis, with both low and high orientation regions occurring along the individual fibers. Bellan and Craighead[178] quantified the order parameter $\langle P_2 \rangle$ of a single electrospun nylon-6 fiber at different positions using Raman spectroscopy. The $\langle P_2 \rangle$ values they obtained varied from 0.59 to 1.1, a maximum $\langle P_2 \rangle$ value over 1 is physically meaningless. Fennessey and Farris reported a maximum orientation parameter of 0.23 in electrospun polyacrylonitrile (PAN), and measurements of the nitrile stretching vibration showed an

increase in the molecular orientation with the take-up speed of the rotating drum.[179] In contrast, extended structures such as carbon nanotubes develop a higher level of anisotropy when electrospinning composite nanofibers.[181] For example, the full width at half-maximum (fwhm) of the azimuthal angle obtained by integration of a specific X-ray diffraction crystal plane is 25º and 52º for the multiwalled nanotubes (MWNTs) and electrospun PAN nanofibers respectively, which correspond to an orientation factor of ca. 0.90 and 0.62 for MWNTs and PAN respectively.[181] As a result of the anisotropic orientation, the composite nanofibers of PAN/MWNT possess enhanced electrical conductivity, mechanical properties, thermal deformation temperature, thermal stability and dimensional stability.

In addition, electrospinning often produces fibers in which the polymers are in unusual or metastable crystalline forms because of the rapid solvent evaporation and the strong electric field and elongational forces involved in the process. For instance, nylon-6 fibers with the metastable γ form[184-187] and poly(1-butene) fibers with metastable form I and thermodynamically stable form II crystals[188,189] could be obtained by electrospinning instead of their usual stable structures obtained from solvent cast film, which is α form for nylon-6 or form III crystal for poly(1-butene), respectively. What is more, the metastable nylon-6 γ form can convert back to the α structure by solvent casting a film from the electrospun membrane.[185] Rabolt et al.[188] also found that the metastable poly(1-butene) form II obtained by electrospinning gradually transformed into the stable form I either at room temperature over the span of several days or with a more rapid rate at an increased temperature. This transformation is retarded by the addition of poly(4-methyl-1-pentene), which is due to stabilization of the metastable form II of poly(1-butene) in the blend.[189] Most recently, the electrospun syndiotactic polypropylene (sPP) fibrous membrane was found to exhibit a mixture of stable form I and metastable form III crystals, with form I being the dominant crystal structure, whereas a solvent cast film only exhibit the stable form I crystal.[190]

1.3 Objectives and content of this work

As described in section 1.1, an independent method for preparing highly structured self-assembled materials is the formation of inclusion complexes (IC) of polymeric guests inside a small molecule host matrix. In their urea inclusion complexes, guest polymers are packed in one-dimensional narrow channels constructed from an essentially infinite three-dimensional network of hydrogen-bonded urea molecules. The guest polymer chains are thus highly extended and oriented at the molecular scale. However, the polymer and the inclusion complexes themselves are not aligned at the macroscopic level. Therefore, there is an opportunity in combining electrospinning and self-assembled inclusion complex formation to prepare fibers that are aligned on a macroscopic scale and highly oriented at the molecular level. This work in presented in chapter 3 and was published in Macromolecules.[191]

Considering the potential of electrospinning to produce unusual polymer structures, we attempted to use it for preparing fibers of the pure stable (α form) and "metastable" forms (β form) of the PEO-urea complex in order to characterize their fiber and solid-state structures. The experimental difficulty of preparing pure samples of the PEO-urea β complex has left open the question of whether it is really stable or metastable by itself, therefore preventing the drawing of a complete phase diagram for the PEO-urea binary system. As a result, we want to obtain a series of PEO-urea complexes with various PEO:urea molar ratio by electrospinning method and, if it is possible, to suggest the crystalline structure and stoichiometry of PEO-urea β form. This work is presented in chapter 4 and was published in J. Polym. Sci. Polym. Phys.[192] Our research further about the phase transitional phenomena between α form and β form can be found in chapter 5 and was published in Polymer.[193] In addition, we want to use the same procedure to solve the composition and crystalline structure of the PEO-thiourea complexes because of the confusing data reported up to now. This work is presented in chapter 6 and has been published in J. Phys. Chem. B.[194]

1.4 References

1. Harris, K. D. M. *Chem. Soc. Rev.* **1997**, 26, 279.
2. Harris, K. D. M. *J. Mol. Struct.* **1996**, 374, 241.
3. Nepogodiev, S. A.; Stoddart, J. F. *Chem. Rev.* **1998**, 98, 1959.
4. Harada, A. *J. Polym. Sci. Part A: Polym. Chem.* **2006**, 44, 5113.
5. Wenz, G.; Han, B.-H.; Mueller, A. *Chem. Rev.* **2006**, 106, 782.
6. Iwamoto, R.; Saito, Y.; Ishihara, H.; Tadokoro, H. *J. Polym. Sci. Part A-2* **1968**, 6, 1509.
7. Yokoyama, M.; Ishihara, H.; Iwamoto, R.; Tadokoro, H. *Macromolecules* **1969**, 2, 184.
8. Dissanayake, M. A. K. L.; Frech, R. *Macromolecules* **1995**, 28, 5312.
9. French, R.; Huang, W. *Macromolecules* **1995**, 28, 1246.
10. Borodin, O.; Smith, G. D. *Macromolecules* **1998**, 31, 8396.
11. Chatani, Y.; Fujii, Y.; Takayanagi, T.; Homma, A. *Polymer* **1990**, 31, 2238.
12. Yang, G.; Hou, W.; Sun, Z.; Yan, Q. *J. Mater. Chem.* **2005**, 15, 1369.
13. Jeevanandam, P.; Vasudevan, S. *Chem. Mater.* **1998**, 10, 1276.
14. Hollingsworth, M. D.; Harris, K. D. M., *Comprehensive Supramolecular Chemistry*. Elsevier Science Ltd.: Oxford, 1996; Vol. 6, p 177.
15. Tadokoro, H. *Macromol. Rev.* **1967**, 1, 119.
16. Chenite, A.; Brisse, F. *Macromolecules* **1991**, 24, 2221.
17. Bailey, F. E., Jr.; France, H. G. *J. Polym. Sci.* **1961**, 49, 397.
18. Campo, A.; Fretti, J.; Vasanthan, N. *Polymer* **2008**, 49, 374.
19. Point, J. J.; Jasse, B.; Dosiere, M. *J. Phys. Chem.* **1986**, 90, 3273.
20. Point, J. J.; Damman, P. *Macromolecules* **1991**, 24, 2019.
21. Sozzani, P.; Bovey, F. A.; Schilling, F. C. *Macromolecules* **1991**, 24, 6764.
22. Point, J. J.; Damman, P. *Macromolecules* **1992**, 25, 1184.
23. Damman, P.; Point, J. J. *Macromolecules* **1993**, 26, 1722.
24. Delaite, E.; Point, J. J.; Damman, P.; Dosière, M. *Macromolecules* **1992**, 25, 4768.

25. Paternostre, L.; Damman, P.; Dosière, M. *Macromolecules* **1999**, 32, 153.
26. Paternostre, L.; Damman, P.; Dosière, M. *J. Polym. Sci. Part B: Polym. Phys.* **1999**, 37, 1197.
27. Paternostre, L.; Damman, P.; Dosière, M. *Polymer* **1998**, 39, 4579.
28. http://en.wikipedia.org/wiki/Urea
29. Bengen, M. F. *Ger. Pat. Appl.* **1940**, OZ 123438.
30. Bengen, M. F. *Angew. Chem.* **1951**, 63, 207.
31. Smith, A. E. *Acta Crystallogr.* **1952**, 5, 224.
32. Angla, B. *Compt. rend.* **1947**, 224, 1166.
33. Fetterly, L. C. *US Pat.* **1950**, 2499820.
34. Hermann, C.; Lenne, H. U. *Naturwissenschaften* **1952**, 39, 234.
35. Lenne, H. U. *Acta Crystallogr.* **1954**, 7, 1.
36. Schlenk, W. *Justus Liebigs Ann. Chem.* **1949**, 565, 204.
37. George, A. R.; Harris, K. D. M. *J. Mol. Graphics* **1995**, 13, 138.
38. Brown, J. F.; White, D. M. *J. Am. Chem. Soc.* **1960**, 82, 5671.
39. Schiessler, R. W.; Flitter, D. *J. Am. Chem. Soc.* **1952**, 71, 1720.
40. Chenite, A.; Brisse, F. *Macromolecules* **1992**, 25, 776.
41. Chenite, A.; Brisse, F. *Macromolecules* **1993**, 26, 3055.
42. Tadokoro, H.; Yoshihara, T.; Chatani, Y.; Murahashi, S. *J. Polym. Sci. B* **1964**, 2, 363.
43. Parrod, J.; Kohler, A.; Hild, G. *Makromol. Chem.* **1964**, 75, 52.
44. Howe, C.; Vasanthan, N.; MacClamrock, C.; Sankar, S.; Shin, I. D.; Simonsen, I. K.; Tonelli, A. E. *Macromolecules* **1994**, 27, 7433.
45. Choi, C.; Davis, D. D.; Tonelli, A. E. *Macromolecules* **1993**, 26, 1468.
46. Eaton, P.; Vasanthan, N.; Shin, I. D.; Tonelli, A. E. *Macromolecules* **1996**, 29, 2531.
47. Vasanthan, N.; Shin, I. D.; Huang, L.; Nojima, S.; Tonelli, A. E. *Macromolecules* **1997**, 30, 3014.
48. Casal, H. L. *J. Phys. Chem.* **1990**, 94, 2232.
49. Tonelli, A. E. *Macromolecules* **1990**, 23, 3134.
50. Tonelli, A. E. *Macromolecules* **1991**, 24, 1275.

51. Tonelli, A. E. *Macromolecules* **1992**, 25, 3581.
52. White, D. M. *J. Am. Chem. Soc.* **1960**, 82, 5678.
53. Chatani, Y.; Nakatani, S. *Macromolecules* **1972**, 5, 597
54. Chatani, Y.; Kuwata, S. *Macromolecules* **1975**, 8, 12.
55. Chatani, Y.; Nakatani, S.; Tadokoro, H. *Macromolecules* **1970**, 3, 481.
56. Minagawa, M.; Yamada, H.; Yamaguchi, K.; Yoshii, F. *Macromolecules* **1992**, 25, 503.
57. Vaughan, P.; Donohue, J. *Acta Crystallogr.* **1952**, 5, 530.
58. Suehiro, K.; Nagano, Y. *Makromol. Chem.* **1983**, 184, 669.
59. Monobe, K.; Yokoyama, F. *J. Macromol. Sci. Phys.* **1973**, B8, 277.
60. Hollingsworth, M. D.; Santarsiero, B. D.; Oumar-Mahamat, H.; Nichols, C. J. *Chem. Mater.* **1991**, 3, 23.
61. Kunchur, N. R.; Truter, M. R. *J. Chem. Soc.* **1958**, 517, 2551.
62. Truter, M. R. *Acta Crystallogr.* **1967**, 22, 556.
63. Pan, Z.; Desmedt, A.; J., E.; MacLean, F. G.; Harris, K. D. M. *J. Phys. Chem. C* **2008**, 112, 839.
64. Maris, T.; Henson, M. J.; Heyes, S. J.; Prout, K. *Chem. Mater.* **2001**, 13, 2483.
65. Garneau, I.; Raymond, S.; Brisse, F. *Acta Crystallogr. Sect. C* **1995**, 51, 538.
66. Fait, J. F.; Fitzgerald, A.; Caughlan, C. N.; McCandless, F. P. *Acta Crystallogr. Sect. C* **1991**, 47, 332.
67. Gopai, R.; Robertson, B. E.; Rutherford, J. S. *Acta Crystallogr. Sect. C* **1989**, 45, 257.
68. Shindo, T.; Shindo, M.; Ohnuma, H.; Kabuto, C. *Bull. Chem. Soc. Jpn.* **1993**, 66, 1914.
69. Moribe, K.; Tsuchiya, M.; Tozuka, Y.; Yamaguchi, K.; Oguchi, T.; Yamamoto, K. *J. Incl. Phenom. Macro.* **2006**, 54, 9.
70. Moribe, K.; Tsuchiya, M.; Tozuka, Y.; Yamaguchi, K.; Oguchi, T.; Yamamoto, K. *Chem. Pharm. Bull.* **2004**, 52, 524.
71. Yutronic, N.; Manriquez, V.; Jara, P.; Witke, O.; Merchan, J.; Gonzalez, G. *J. Chem. Soc., Perkin Trans.* **2000**, 2, 1757.
72. Chatani, Y.; Nakatani, S. *Z. Kristallogr.* **1977**, 144, 175.

73. Villiers, A. *Compt. rend.* **1891**, 112, 536.
74. Szejtli, J. *Chem. Rev.* **1998**, 98, 1743.
75. Freudenberg, K.; Cramer, F. *Z. Naturforsch.* **1948**, 3b, 464.
76. Harada, A.; Kamachi, M. *Macromolecules* **1990**, 23, 2821.
77. Harada, A.; Li, J.; Kamachi, M. *Nature* **1992**, 356, 325.
78. Harada, A.; Li, J.; Kamachi, M. *Macromolecules* **1993**, 26, 5698.
79. Tonelli, A. E. *Polymer* **2008**, 49, 1725.
80. Pozuelo, J.; Mendicuti, F.; Mattice, W. L. *Macromolecules* **1997**, 30, 3685.
81. Ceccato, M.; Nostro, P. L.; Baglioni, P. *Langmuir* **1997**, 13, 2436.
82. Topchieva, I. N.; Tonelli, A. E.; Panova, I. G.; Matuchina, E. V.; Kalashnikov, F. A.; Gerasimov, V. I.; Rusa, C. C.; Rusa, M.; Hunt, M. A. *Langmuir* **2004**, 20, 9036.
83. Wei, M.; Bullions, T. A.; Rusa, C. C.; Wang, X.; Tonelli, A. E. *J. Polym. Sci. Part B: Polym. Phys.* **2003**, 42, 386.
84. Ogata, N.; Sanui, K.; Wada, J. *J. Polym. Sci. Polym. Lett. Ed.* **1976**, 14, 459.
85. Maciejewski, M. *J. Macromol. Sci. Part A* **1979**, 13, 77.
86. Steinbrunn, M. B.; Wenz, G. *Angew. Chem. Int. Ed.* **1996**, 35, 2139.
87. Harada, A. *Supramol. Sci.* **1996**, 3, 19.
88. Harada, A.; Li, J.; Suzuki, S.; Kamachi, M. *Macromolecules* **1993**, 26, 5267.
89. Harada, A.; Takahashi, S. *Chem. Lett.* **1984**, 2089.
90. Rusa, C. C.; Tonelli, A. E. *Macromolecules* **2000**, 33, 1813.
91. Mertzman, M. D.; Foley, J. P. *Electrophoresis* **2004**, 25, 1188.
92. Hinze, W. L.; Riehl, T. E.; Armstrong, D. W.; DeMond, W.; Alak, A.; Ward, T. *Anal. Chem.* **1985**, 57, 237.
93. Miyauchi, M.; Takashima, Y.; Yamaguchi, H.; Harada, A. *J. Am. Chem. Soc.* **2005**, 127, 2984.
94. Rekharsky, M.; Inoue, Y. *J. Am. Chem. Soc.* **2000**, 122, 4418.
95. Ohya, Y.; Takamido, S.; Nagahama, K.; Ouchi, T.; Ooya, T.; Katoono, R.; Yui, N. *Macromolecules* **2007**, 40, 6441.
96. Tam, W.; Eaton, D. F.; Calabrese, J. C.; Williams, I. D.; Wang, Y.; Anderson, A. G. *Chem. Mater.* **1989**, 1, 128.

97. Eaton, D. F.; Anderson, A. G.; Tam, W.; Wang, Y. *J. Am. Chem. Soc.* **1987**, 109, 1886.

98. Shang, Q.-Y.; Dou, X.; Hudson, B. S. *Nature* **1991**, 352, 703.

99. Barker, G. E.; Ranauto, H. J. *J. Am. Oil Chemists' Soc.* **1955**, 32, 249.

100. Bogdanov, B.; Uzov, C.; Gavrailova, G. *Acta Polym.* **1994**, 45, 381.

101. Bogdanov, B.; Mikhailov, M.; Uzov, K.; Gavrailova, G. *Angew. Makromol. Chem.* **1992**, 195, 165.

102. Bogdanov, B.; Mikhailov, M.; Uzov, K.; Gavrailova, G. *J. Polym. Sci. Part B: Polym. Phys.* **1994**, 32, 387.

103. Bogdanov, B.; Michailov, M.; Uzov, C.; Gavrailova, G. *Makromol. Chem.* **1994**, 195, 2227.

104. Bogdanov, B. G., Molecular complexes [poly(ethylene oxide) and urea]. In *Polymeric Materials Encyclopedia*, Salamone, J. C., Ed. 1996; Vol. 6, pp 4418.

105. Vasanthan, N.; Shin, I. D.; Tonelli, A. E. *Macromolecules* **1996**, 29, 263.

106. Ye, H. M.; Peng, M.; Xu, J.; Guo, B. H.; Chen, Q.; Yun, T. L.; Ma, H. *Polymer* **2007**, 48, 7364.

107. Damman, P.; Point, J. J. *Macromolecules* **1995**, 28, 2050.

108. Parrod, J.; Kohler, A. *Compt. Rend.* **1958**, 246, 1046.

109. Bailey, F. E., Jr.; France, H. G. *Am. Chem. Soc. Div. Polym. Chem. Preprints* **1960**, 1, 194.

110. Tarnrutskii, M. M.; Shkol'nikova, L. S.; Lorei, A. K.; Dindoin, V. I.; Zykova, L. I. *Vysokomolekulyarnye Soedineniya, Seriya B: Kratkie Soobshcheniya* **1975**, 17, 817.

111. Tadokoro, H.; Yoshihara, T.; Tahara, S.; Murahashi, S. *Makromol. Chem.* **1964**, 73, 109.

112. Takahashi, Y.; Sumita, I.; Tadokoro, H. *J. Polym. Sci. Polym. Phy. Ed.* **1973**, 11, 2113.

113. Gu, F.; Bu, H.; Zhang, Z. *Polymer* **2000**, 41, 7605.

114. Damman, P.; Point, J. J. *Macromolecules* **1994**, 27, 3919.

115. Takahashi, Y.; Sumita, I.; Tadokoro, H. *J. Polym. Sci. Polym. Phys. Ed.* **1973**, 11, 2113.

116. Chatani, Y.; Okamura, S. *Polymer* **1987**, 28, 1815.
117. Brena, B.; Zhuang, G. V.; Augustsson, A.; Liu, G.; Nordgren, J.; Guo, J.-H.; Ross, P. N.; Luo, Y. *J. Phys. Chem. B* **2005**, 109, 7907.
118. Smith, G. D.; Jaffe, R. L.; Yoon, D. Y. *J. Am. Chem. Soc.* **1995**, 117, 530.
119. Jaffe, R. L.; Smith, G. D.; Yoon, D. Y. *J. Phys. Chem.* **1993**, 97, 12745.
120. Yoshida, H.; Kaneko, I.; Matsuura, H.; Ogawa, Y.; Tasumi, M. *Chem. Phys. Lett.* **1992**, 196, 601.
121. Bedrov, D.; Pekny, M.; Smith, G. D. *J. Phys. Chem. B.* **1998**, 102, 996.
122. Smith, G. D.; Yoon, D. Y.; Jaffe, R. L.; Colby, R. H.; Krishnamoorti, R.; Fetters, L. J. *Macromolecules* **1996**, 29, 3462.
123. Smith, G. D.; Bedrov, D.; Borodin, O. *J. Am. Chem. Soc.* **2000**, 122, 9548.
124. Smith, G. D.; Bedrov, D. *J. Phys. Chem. A* **2001**, 105, 1283.
125. Smith, G. D.; Bedrov, D. *Macromolecules* **2002**, 35, 5712.
126. Borodin, O.; Smith, G. D. *J. Phys. Chem.B* **2003**, 107, 6801.
127. Annis, B. K.; Kim, M.-H.; Wignall, G. D.; Borodin, O.; Smith, G. D. *Macromolecules* **2000**, 33, 7544.
128. Gilbert, W., *De Magnete, Magneticisque Corporibus, et de Magno Magnete Tellure*. 1600.
129. G. M. Bose, *Recherches sur la cause et sur la véritable théorie de l'électricité*. Wittenberg: 1745.
130. Rayleigh, L. *Philos. Mag.* **1882**, 14, 184.
131. Formhals, A. US Patent No. 1,975,504, 1934.
132. Formhals, A. US patent No. 2,169,962, 1939.
133. Formhals, A. US Patent No. 2,187,306, 1940.
134. Formhals, A. US Patent No. 2,323,025, 1943.
135. Formhals, A. US Patent No. 2,349,950, 1944.
136. Taylor, G. *Proc. Natl. Acad. Sci. USA.* **1969**, A313, 453.
137. Baumgarten, P. *J. Colloid Interface Sci.* **1971**, 36, 71.
138. Larrondo, L.; St. John Manley, R. *J. Polym. Sci. Polym. Phy. Ed.* **1981**, 19, 909.
139. Larrondo, L.; St. John Manley, R. *J. Polym. Sci. Polym. Phy. Ed.* **1981**, 19, 921.
140. Larrondo, L.; St. John Manley, R. *J. Polym. Sci. Polym. Phy. Ed.* **1981**, 19, 933.

141. Doshi, J.; Reneker, D. H. *J. Electrost.* **1995**, 35, 151.
142. Reneker, D. H.; Chun, I. *Nanotechnology* **1996**, 7, 216.
143. Wouters, D.; Schubert, U. S. *Angew. Chem. Int. Ed.* **2004**, 43, 2480.
144. Hagewood, J.; Wilkie, A. *Nonwovens World* **2003**, 12, 69.
145. Pike, R. D. US Patent No. 5,935,883, 1999.
146. Reneker, D. H. US Patent No. 6,382,526, 2002.
147. Faul, C. F. J.; Antonietti, M. *Adv. Mater.* **2003**, 15, 673.
148. Whitesides, G. M.; Boncheva, M. *Proc. Natl. Acad. Sci. USA.* **2002**, 99, 4769.
149. Huang, Z.-M.; Zhang, Y.-Z.; Kotaki, M.; Ramakrishna, S. *Comp. Sci. & Tech.* **2003**, 63, 2223.
150. Frenot, A.; Chronakis, I. S. *Curr. Opin. Colloid Interface Sci.* **2003**, 8, 64.
151. Li, D.; Xia, Y. *Adv. Mater.* **2004**, 16, 1151.
152. Subbiah, T.; Bhat, G. S.; Tock, R. W.; Parameswaran, S.; Ramkumar, S. S. *J. Appl. Polym. Sci.* **2005**, 96, 557.
153. Chronakis, I. S. *J. Mater. Proc. Tech.* **2005**, 167, 283.
154. Lyons, J.; Ko, F. *Polymer News* **2005**, 30, 1.
155. Teo, W.; Ramakrishna, S. *Nanotechnology* **2006**, 17, R89.
156. Ramakrishna, S.; Fujihara, K.; Teo, W.-E.; Yong, T.; Ma, Z.; Ramaseshan, R. *Mater Today* **2006**, 9, 40.
157. Greiner, A.; Wendorff, J. H. *Angew. Chem. Int. Ed.* **2007**, 46, 5670.
158. Sill, T. J.; von Recum, H. A. *Biomaterials* **2008**, 29, 1989.
159. Yarin, A. L.; Koombhongse, S.; Reneker, D. H. *J. Appl. Phys.* **2001**, 89, 3018.
160. Shin, Y. M.; Hohman, M. M.; Brenner, M. P.; Rutledge, G. C. *Appl. Phys. Lett.* **2001**, 78, 1149.
161. Reneker, D. H.; Yarin, A. L.; Fong, H.; Koombhongse, S. *J. Appl. Phys.* **2000**, 87, 4531.
162. Yan, X.; Gevelber, M., The Fiber Society 2008 Fall Meeting and Technical Conference, Boucherville, Québec, Canada, 2008.
163. Taylor, G. *Proceedings of the Royal Society of London A: Mathematical, Physical & Engineering Sciences* **1969**, 313, 453.

164. Teraoka, I., *Polymer Solutions: An Introduction to Physical Properties*. John Wiley & Sons, Inc.,: New York, 2002.
165. Gupta, P.; Elkins, C.; Long, T. E.; Wilkes, G. L. *Polymer* **2005**, 46, 4799.
166. Ramakrishna, S.; Fujihara, K.; Teo, W.-E.; Lim, T.-C.; Ma, Z., *An Introduction to Electrospinning and Nanofibers*. World Scientific Publishing Co.: Singapore, 2005.
167. Shenoy, S. L.; Bates, W. D.; Frisch, H. L.; Wnek, G. E. *Polymer* **2005**, 46, 3372.
168. Yu, J. H.; Fridrikh, S. V.; Rutledge, G. C. *Polymer* **2006**, 47, 4789.
169. Ward, I. M., *Structure and Properties of Oriented Polymers*. 2nd ed.; Chapman & Hall: London, 1997.
170. Theron, A.; Zussman, E.; Yarin, A. L. *Nanotechnology* **2001**, 12, 384.
171. Ko, F.; Gogotsi, Y.; Ali, A.; Naguib, N.; Ye, H.; Yang, G.; Li, C.; Willis, P. *Adv. Mater.* **2003**, 15, 1161.
172. Katta, P.; Alessandro, M.; Ramsier, R. D.; Chase, G. G. *Nano Lett.* **2004**, 4, 2215.
173. Teo, W. E.; Kotaki, M.; Mo, X. M.; Ramakrishna, S. *Nanotechnology* **2005**, 16, 918.
174. Kameoka, J.; Craighead, H. G. *Appl. Phys. Lett.* **2003**, 83, 371.
175. Dersch, R.; Liu, T.; Schaper, A. K.; Greiner, A.; Wendorff, J. H. *J. Polym. Sci. Part A: Polym. Chem.* **2003**, 41, 545.
176. Li, D.; Wang, Y.; Xia, Y. *Adv. Mater.* **2004**, 16, 361.
177. Li, D.; Wang, Y.; Xia, Y. *Nano Letters* **2003**, 3, 1167.
178. Bellan, L. M.; Craighead, H. G. *Polymer* **2008**, 49, 3125.
179. Fennessey, S. F.; Farris, R. J. *Polymer* **2004**, 45, 4217.
180. Dror, Y.; Salalha, W.; Khalfin, R. L.; Cohen, Y.; Yarin, A. L.; Zussman, E. *Langmuir* **2003**, 19, 7012.
181. Ge, J. J.; Hou, H.; Li, Q.; Graham, M. J.; Greiner, A.; Reneker, D. H.; Harris, F. W.; Cheng, S. Z. D. *J. Am. Chem. Soc.* **2004**, 126, 15754.
182. Kim, G.-M.; Wutzler, A.; Radusch, H.-J.; Michler, G. H.; Simon, P.; Sperling, R. A.; Parak, W. J. *Chem. Mater.* **2005**, 17, 4949.

183. Song, T.; Zhang, Y.; Zhou, T.; Lim, C. T.; Ramakrishna, S.; Liu, B. *Chem. Phys. Lett.* **2005**, 415, 317.

184. Liu, Y.; Cui, L.; Guan, F.; Gao, Y.; Hedin, N. E.; Zhu, L.; Fong, H. *Macromolecules* **2007**, 40, 6283.

185. Stephens, J. S.; Chase, D. B.; Rabolt, J. F. *Macromolecules* **2004**, 37, 877.

186. Fong, H.; Liu, W.; Wang, C.-S.; Vaia, R. A. *Polymer* **2002**, 43, 775.

187. Lee, K.-H.; Kim, K.-W.; Pesapane, A.; Kim, H.-Y.; Rabolt, J. F. *Macromolecules* **2008**, 41, 1494.

188. Lee, K.-H.; Snively, C. M.; Givens, S.; Chase, D. B.; Rabolt, J. F. *Macromolecules* **2007**, 40, 2590.

189. Lee, K.-H.; Givens, S. R.; Snively, C. M.; Chase, B.; Rabolt, J. F. *Macromolecules* **2008**, 41, 3144.

190. Lee, K.-H.; Ohsawa, O.; Watanabe, K.; Kim, I.-S.; Givens, S. R.; Chase, B.; Rabolt, J. F. *Macromolecules* **2009**, 42, 5215.

191. Liu, Y.; Pellerin, C. *Macromolecules* **2006**, 39, 8886.

192. Liu, Y.; Antaya, H.; Pellerin, C. *J. Polym. Sci. Part B: Polym. Phys.* **2008**, 46, 1903.

193. Liu, Y.; Pellerin, C. *Polymer* **2009**, 50, 2601.

194. Liu, Y.; Antaya, H.; Pellerin, C. J. Phys. Chem. B **2010**, DOI:10.1021/jp9103867

Chapter 2 : Experimental and Characterization Methods

2.1 Sample preparation

2.1.1 Preparation of PEO-urea/thiourea complexes

There are several methods for preparation of PEO-urea inclusion complexes. The first method is a solid-solution method. Tadokoro et al.[1] obtained an oriented PEO-urea complex by immersing a piece of oriented bulk PEO film in a methanol solution of urea at room temperature for about 100 hours. If this PEO-urea complex sample is immersed in pure methanol for about 24 hours, an oriented PEO sample similar to the original one is obtained again. This indicates that the orientation direction of the PEO molecule is not distorted by the formation of the PEO-urea complex and is parallel to the *c* axis of the complex crystal. The second preparation method is the co-crystallization or co-precipitation method. Both PEO and urea (or thiourea) are dissolved in methanol and then mixed together under stirring, a white precipitate then forms after one day. After filtration and washing several times with methanol, crystallized PEO-urea or PEO-thiourea complexes are obtained.[2] Single crystal sometimes could be obtained with this method.[3] The third approach is the melt-crystallization method: an appropriate ratio of PEO and urea is mixed, and the temperature is increased above the melting temperatures of PEO and urea; crystallized PEO-urea complex is then formed upon taking the sample back to room temperature.[4]

2.1.2 Preparation of electrospun fibers

2.1.2.1 Working and counter electrodes

To set up the electric field, there must be a working electrode and a counter electrode between the pumped solution and the final product. In practice, the working electrode is inserted into the polymer solution, or the metallic needle at the end of the syringe is used directly (see Figure 1.9). The flow rate of the polymer solution determines the amount of fluid available for electrospinning. It is controlled by a syringe pump and typical rates range from 0.01 ml/min to 0.1 ml/min. A low flow rate is desirable because the solvent then has more time to evaporate. On the other hand, higher flow rates produce electrospun fibers with larger diameters as a greater volume is taken from the needle tip. The diameter of the needles varies from 0.21 mm to more than 1 mm to fit for different systems. Decreasing the internal diameter of the needle was found to cause a reduction in the diameter of the electrospun fibers, but it requires much force to cause the jet initiation for the increase of surface tension at the same time.

To collect the produced electrospun fibers, a counter electrode is either electrically grounded to the earth or connected to a power supply with an opposite charge from that applied on the polymer solution. A piece of aluminum foil can be used as the counter electrode to obtain random mats. As mentioned in Chapter 1, to obtain highly aligned electrospun fibers, two types of counter electrodes are used in our laboratory. One is a rotating cylinder collector made of Teflon with a sharp-edged metal disk in the middle, and another is composed of two separate electrodes (Figure 2.1). The rotation rate can vary from 0 to 1000 rpm. In electrospinning, the charged jet is travelling at a high speed, thus to align the fibers around the rotating cylinder collector. It is necessary that the rotating rate of the cylinder collector, in fact the linear speed of its surface, to be high enough to take up the fibers. It is reported in the literature that higher rotation rates induce higher alignment and orientation on the electrospun fibers because of stretching. As more fibers are collected on the rotating cylinder, accumulated charges may repel the incoming fibers, resulting in a decreased alignment of the fibers. Another type of counter electrode is made of two separate electrodes (Figure 2.1). It is reported that it achieves the best alignment when the distance between the separated electrodes is 3 cm.[5] The aligned fibers are then transferred to and kept on a paper frame for further characterization.

Figure 2.1. Photographs of two types of counter electrodes: rotating cylinder collector with a metal disk in the middle (left) and two separate electrodes (right).

2.1.2.2 Electrospinning of PEO and urea/thiourea solutions

As described in Chapter 1, the composition and the crystalline structure of the second PEO-urea complex (β form) is poorly researched. To determine the composition of PEO-urea β form, a series of PEO-urea solutions were prepared by dissolving 0.5 g of PEO (M_w = 400 000 g/mol) in 10 ml H_2O or methanol, then adding an appropriate amount of urea to obtain mixtures with various PEO:urea molar ratios. The mixed solutions were introduced in a syringe equipped with a 0.41mm diameter flat-end needle in order to prepare PEO-urea complexes fibers by electrospinning. The same method was used to obtain a series of PEO-thiourea complexes to determine its stoichiometry.

2.1.2.3 Electrospinning of PEO-urea/thiourea precipitate

A stable PEO-urea inclusion complex is first prepared via the co-crystallization method. Four grams of PEO (M_w = 400 000 g/mol) are dissolved in 100 ml of methanol saturated with 20 grams of urea at 65 ºC. After complete dissolution, the solution is cooled to room temperature and a white precipitate is formed gradually during one day. After filtration and washing several times with methanol to eliminate uncomplexed urea

and PEO, the precipitate is divided into two parts: the first one is dried under vacuum to produce a bulk PEO-urea inclusion complex, and the second is injected in a syringe to prepare PEO-urea IC fibers by electrospinning. A similar process was used to prepare the PEO-thiourea complexes.

2.1.3 Preparation of PEG-thiourea complexes

0.5 g of PEG with M_w of 400 and 1000 g/mol, respectively, was dissolved in methanol, ethanol or isopropanol solutions saturated with thiourea. It was found that no precipitate formed at room temperature. When the temperature was decreased to 5 ºC, PEG-1000 formed a precipitate in all solutions. When the temperature was decreased to -5 ºC, PEG-400 formed a precipitate in all solutions. The crystals formed in these different solvents have the same crystalline structure as those prepared from high molecular weight PEO. This suggests that the solvent does not take part in the formation of PEO-thiourea complexes.

2.1.4 Preparation of PEO-cyclodextrin complexes

To obtain PEO-α-CD and PEO-γ-CD columnar structures, 1 g of PEG/PEO (M_w= 400, 1000, 35000 or 400000 g/mol) was dissolved in 20 ml of distilled water. Corresponding α-CD or γ-CD was dissolved in distilled water to prepare saturated solutions with continuous stirring at 50° C for 1 hour. The PEO solution was then mixed with the α-CD or γ-CD solutions at various mass ratios at 50° C. Upon continuous stirring and decreasing temperature to room temperature, the low molecular weight PEG (M_w= 400 and 1000 g/mol) formed a white precipitate immediately, and relatively high molecular weight PEO (M_w= 35000 and 400000 g/mol) took one day to form a gel. The products were washed several times with water to get rid of uncomplexed PEG/PEO and CDs.

2.2 Characterization methods

2.2.1 Wide angle X-ray diffraction (WAXD)

The usefulness of X-ray diffraction in the study of substances lies in its ability to separate ordered states from disordered ones. Compared with small molecules, the long chain polymers often include both ordered crystalline and disordered amorphous structures. As a result, their X-ray patterns contain both relatively sharp crystalline peaks and one or more amorphous halos (Figure 2.2, right and left, respectively). Single crystal X-ray diffraction is probably the most powerful approach for the determination of structural information at the atomic level. But, unfortunately, many crystalline solids, especially long-chain polymers, can be prepared only as microcrystalline powders rather than as single crystals. As a result, we have to rely on powder X-ray diffraction data to determine the polymer crystal structures, and this is substantially more challenging and difficult than structure determination from single crystal diffraction data. Sometimes, we have to use the information obtained from other techniques, such as infrared spectroscopy, nuclear magnetic resonance, etc., to justify the assignment of unit cell parameters.

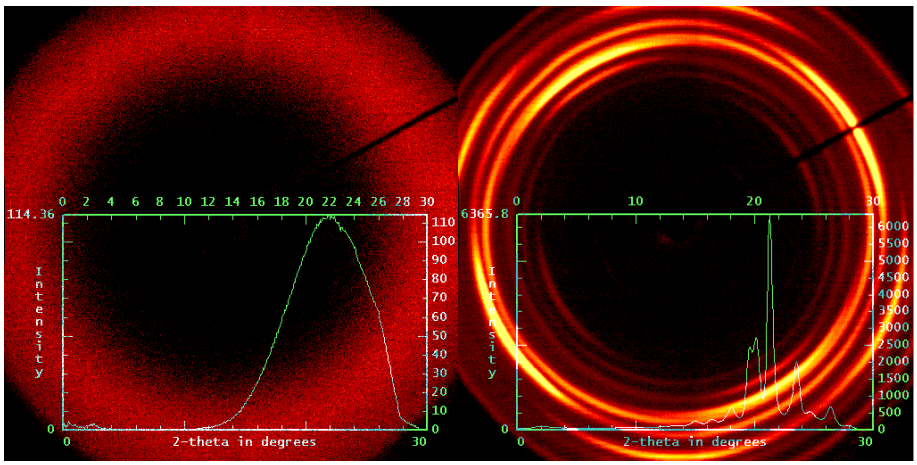

Figure 2.2 Two-dimensional X-ray patterns of PEO-urea α complex melt at 160 ºC (left) and the melt-quenched sample at 25 ºC (right).

2.2.1.1 Unit cell determination by powder diffraction

Table 2.1. Unit cells of the seven crystal systems and the fourteen space lattices.[6,7]

Crystal systems	Bravais lattices			
	Primitive (P)	Body centered(I)	Face centered (F)	Basecentered(C)
Triclinic $a \neq b \neq c$ $\alpha \neq \beta \neq \gamma \neq 90°$	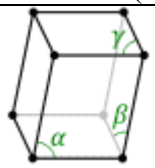			
Monoclinic $a \neq b \neq c$ $\beta \neq 90°$ $\alpha = \gamma = 90°$	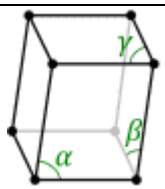			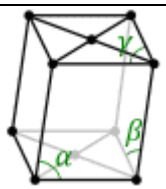
Orthorhombic $a \neq b \neq c$ $\alpha = \beta = \gamma = 90°$	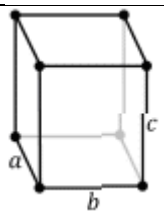	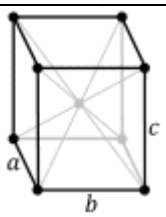	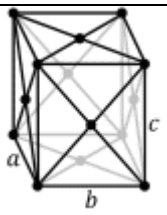	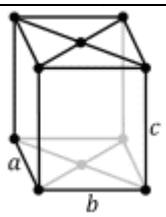
Hexagonal $a = b \neq c$ $\beta = \alpha = 90°$ $\gamma = 120°$	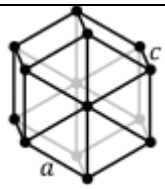			
Trigonal (Rhombohedral) $a = b = c$ $\alpha = \beta = \gamma \neq 90°$	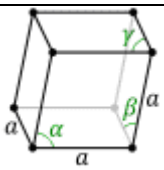			
Tetragonal $a = b \neq c$ $\alpha = \beta = \gamma = 90°$	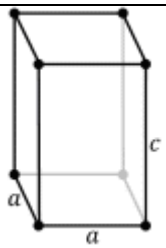	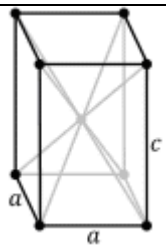		
Cubic $a = b = c$ $\alpha = \beta = \gamma = 90°$			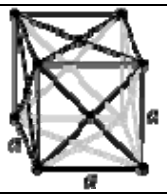	

Depending on the configuration of the molecular chains and their arrangement with respect to one another, any given crystalline structure can be assigned to one of seven crystal systems, which are triclinic, monoclinic, hexagonal, orthorhombic, trigonal, tetragonal, or cubic. The given crystal structure can be shown to have one of the 14 Bravais space lattices.[6] The characteristics of the seven crystal systems and 14 Bravais spaces are given in Table 2.1.

The complete powder diffraction profiles include the following information: (1) the peak positions, (2) the peak intensities, (3) the peak widths and shapes, (4) the background intensity distribution.[7,8] Based on these information, the X-ray diffraction technique can characterize and confirm crystalline materials and their structures, especially determining the unit cell dimensions (*a*, *b*, *c*, α, β, γ) by analysis of the peak positions in the powder diffraction pattern.

Any source of radiation with a wavelength λ is suitable for diffraction or scattering by solids. The scattering of the beam causes a discrete diffraction pattern if the material it penetrates is at least partially crystalline. Different crystal phases existing in the sample display different peaks (2θ) on the diffractogram (Figure 2.2). According to the well-known Bragg equation, or Bragg law:[6]

$$n\lambda = 2d \sin\theta \qquad (2.1)$$

λ is the X-ray wavelength (usually 1.5418Å), d the interplanar spacing and θ one-half the angle of deviation of the diffracted rays from the incident X-rays. Each peak on the diffractogram can be assigned by Miller indices, which are obtained from the unit intercepts by taking their reciprocals and clearing of fractions. For example, if the intercepts of a crystal plane on the coordinate axes (X, Y, Z) are 1a, 2b, 2c respectively (Figure 2.3), and *a*, *b*, *c* are the unit cell parameters, then the reciprocals of intercepts are 1/1, ½ and ½. After clearance of the fraction 2, the Miller indices (hkl) for this crystal plane is (211). Therefore, the process of determination of unit cell parameters is the assignment of Miller indices to every intense diffraction peak obtained. The most widely

used softwares for indexing power diffraction data are CRYSFIRE, DICVOL, ITO and TREOR.[8] Here, more than 30 selected peaks at low diffraction angles (less than 45º) are used to obtain the unit cell parameters of PEO-urea/thiourea complexes with the software DICVOL.

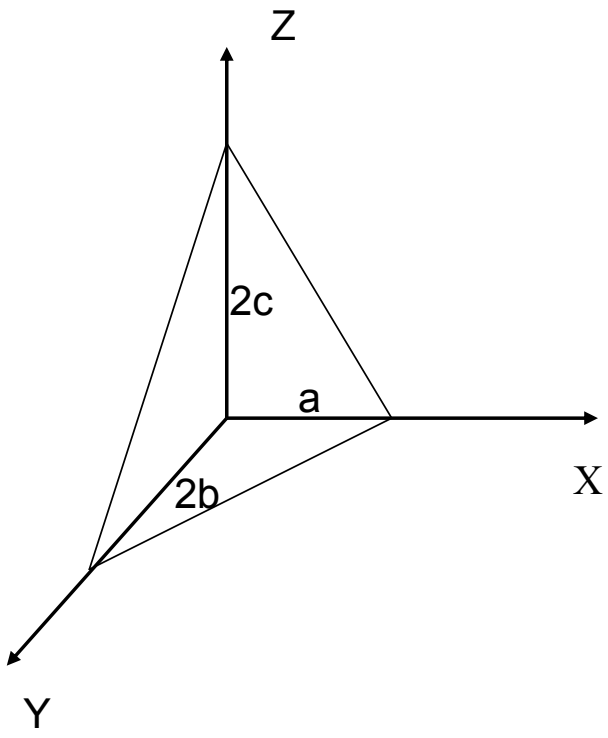

Figure 2.3 Diagram of a plane having the Miller indices of (211).

The diffraction patterns can also be used to analyze the size of crystals, their orientation and the amount of crystallinity. The width of each peak on the diffractogram depends on the crystal size. The crystal size can be calculated by using the Debye-Scherrer equation:

$$\delta(2\theta) = 0.9\lambda / (L\cos\theta) \qquad (2.2)$$

where δ is the width of the peak at half-height, λ is the wavelength of X-rays, L is the crystal size, and 2θ is the angle at which the peak is located. The fraction of crystalline

material present in the sample can also be estimated from the relative area under the crystalline peaks as compared to the area under the amorphous halo. As shown in Figure 2.2, the molten PEO-urea complex is completely amorphous with a wide halo at around 22º. The melt-quenched sample is highly crystallized with only a small amorphous halo under the crystalline peaks.

One issue that may limit the successful structure determination is the sample purity in powder diffraction analysis. If the powder sample contains a second crystalline phase, it will be impossible to find a single unit cell to include all the peak positions in the powder diffraction pattern. Therefore, it is important to prepare samples as pure as possible of the PEO-urea and PEO-thiourea complexes. Several methods were taken to achieve this aim. One is using a low molecular weight PEG to substitute for high molecular weight PEO when preparing the complex precipitate so that the initial components will be easier to eliminate after the formation of the precipitate. Another is waiting a long enough time for the precipitation formation, generally more than one day, and washing the final product several times to get rid of all the uncomplexed components. Another issue that may influence the unit cell parameter assignments is the orientation of the crystallites. Considering the highly aligned electrospun fibers obtained, strong anisotropy can be expected. As a result, some crystal diffractions spots might not appear in the sampling area and the intrinsic relative intensities of the diffraction peaks might deviate from those of the non-oriented specimen. In order to overcome this difficulty, appropriate procedures were carried out to get rid of the preferred orientation, such as cutting the electrospun fibers into pieces and grinding all the samples to a fine powder before testing.

After the unit cell has been determined from the powder diffraction pattern, the unit cell volume is used to calculate its composition and the density of the crystalline structure. The experimental density could be measured with a Sartorius CP224S balance equipped with a YDK01 accessory. The electrospun fibers were pressed into pellets and their density was determined with the equation 2.3

$$\rho = w_a\rho_s/(w_a-w_s) \quad (2.3)$$

where w_a and w_s are the weights of samples measured in air and in a solvent (acetone and benzene were used here) respectively, and ρ_s is the density of the pure solvent. If the unit cell assignment is right, the measured density should be comparable with the calculated one. Another method to justify the unit cell assignment is to check the preferred orientation direction of different crystal planes. Generally, the non-random distribution of crystallite orientation in samples is not welcome in the determination of unit cell parameters. However, once the unit cell has been decided, the preferred orientation of different crystal planes might help to confirm the rightness of this assignment. The angle of the normal direction to the diffraction planes with respect to the fiber direction is fixed and the experimental data should be consistent with the angles calculated from the unit cell parameters, especially for highly oriented electrospun fibers,

After the crystalline structures of the complexes are determined from powder diffraction results, WAXD is also used to research the phase transition properties of those complexes. For example, as shown in Figure 2.4, after melting-cooling, the PEO-urea α complex will convert to urea and PEO-urea β complex. On the other hand, after melting-cooling of PEO-urea β complex, it will convert to α form and crystalline PEO, which can be seen from Figure 2.4. The diffraction peaks of the melt-cooled β complex are the overlap of the peaks from pure PEO and α complex. Combined with the DSC results, a complete phase diagram of PEO/urea and PEO/thiourea systems might be drawn. The specimen used for the phase-transition research were sealed in aluminum pans used for DSC measurements, the temperature was controlled by an STC 200 controller and an LN2-SYS liquid nitrogen cooling system (Instec). A scattering background of an empty DSC pan was subtracted for display.

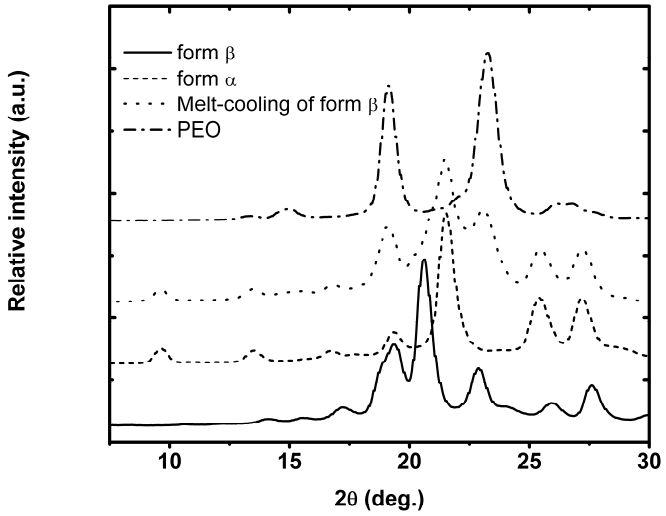

Figure 2.4. WAXD results for PEO, PEO-urea α and β complexes and the melting-cooling of β complexes.

2.2.1.2 Orientation measurement

Orientation in polymers is a phenomenon of great technical and theoretical importance. Polymer orientation refers to molecular-level alignment of the polymer chains, segments of the polymer chains, or of the crystalline regions in the polymer with respect to a macroscopic reference direction.[9] In general, it is either induced by mechanical deformation, such as by drawing, stretching, or rolling, or by other forces, such as electrical and magnetic fields. The mechanism of molecular orientation and macroscopic alignment of electrospun fibers with the rotating cylinder and separate electrodes has been explained in Chapter 1, and it combines both mechanical deformation and electrical field. The electric force is used to stretch the polymer fluids and achieve the polymer chain orientation. While the electrospun fiber diameter dwindles to micro or even nanometers, the molecular orientation is achieved in a single fiber. However, due to the existence of bending instability, the electrospun fibers have to be well aligned on the rotating disk or between the two separate electrodes to maintain

the molecular orientation at the macroscopic level. The results for the electrospun fibers will be provided in Chapters 3, 4 and 6.

The azimuthal intensity of crystalline diffraction peaks observed in WAXD patterns of semicrystalline polymers can be used to characterize the anisotropy quantitatively. Indeed, the scattered intensity at a given azimuthal angle is related to the number of crystals inclined at the same angle with respect to the orientation direction.[10]

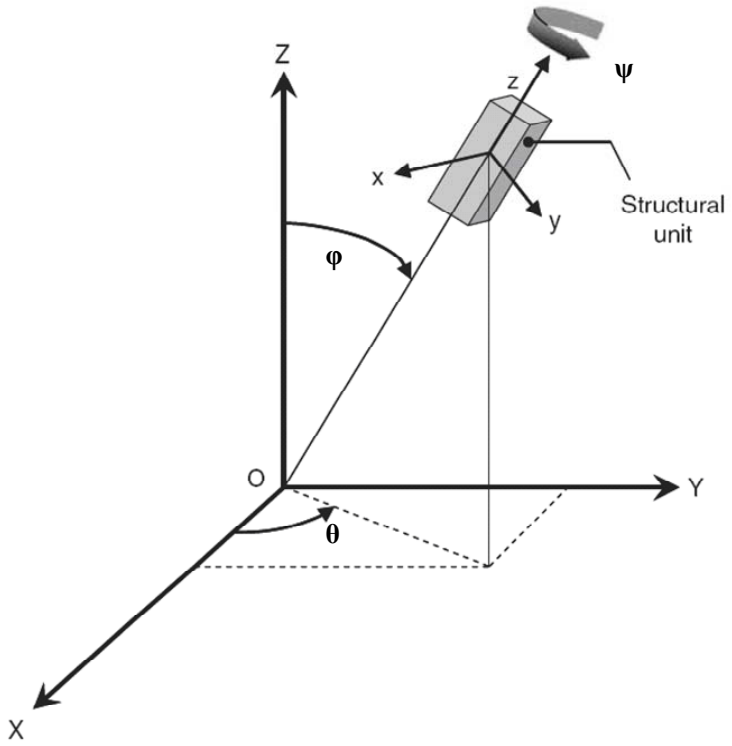

Figure 2.5. Definition of the coordinate system OXYZ with the unit cell system Oxyz and Euler angles θ, φ, and ψ.[11]

In this section, we are concerned only with the use of X-ray diffraction to characterize the orientation level in the crystalline regions of electrospun fibers. In addition to X-ray diffraction, other methods, such as optical birefringence, FT-IR and Raman spectroscopy could be used to measure the overall orientation that prevails in polymer samples, including both amorphous and crystalline regions. The concept of an

orientation function to specify quantitatively the degree of axial orientation in crystalline fibers was developed by Hermans et al.[12,13] In its simplest form, the orientation of the c-axis (Oz) in a given unit cell can be described by the azimuthal angle, which is the angle between c-axis and the Z-axis (OZ). (Figure 2.5). For oriented electrospun fibers, it is assumed that there is only an uniaxial orientation along the fiber axis (Z-axis), and no preferred orientation perpendicular to the fiber axis (XY plane). Both θ and ψ take random values and the P_{lmn}, the associated Legendre polynomials, are non-zero only for m = n = 0.[11] The expression of the first few non-normalized Legendre polynomials averages for a distribution function with uniaxial symmetry about the OZ axis are

$$\langle P_{000}(\cos\varphi)\rangle = 1 \tag{2.4}$$

$$\langle P_{200}(\cos\varphi)\rangle = \frac{3\langle\cos^2\varphi\rangle - 1}{2} \tag{2.5}$$

$$\langle P_{400}(\cos\varphi)\rangle = \frac{1}{8}\langle 3 - 30\cos^2\varphi + 35\cos^4\varphi\rangle \tag{2.6}$$

Where the $<cos^2\varphi>$ and $<cos^4\varphi>$ values, averaged over all the crystallites, represent respectively the mean-square cosine and mean-4th order cosine of the angle between a given crystal plane normal (Oz) and the fiber axis (OZ).[6] To quantify the molecular orientation of the electrospun fibers, the second order orientation parameter, $<P_2(cos\varphi)>$, is often used although the complete determination of the orientation distribution function (ODF) requires the knowledge of all the $<P_{lmn}\,cos(\varphi)>$ coefficients. $<cos^2\varphi>$ was obtained by integrating the intensity of specific 2θ diffraction peaks, $I(\varphi)$, along the azimuthal angle, φ, as:

$$\langle\cos^2\varphi\rangle = \frac{\int_0^{\pi} I(\varphi)\cos^2\varphi\sin\varphi d\varphi}{\int_0^{\pi} I(\varphi)\sin\varphi d\varphi} \tag{2.7}$$

Since the (00l) reflection plane is not available in most X-ray diffraction patterns, the orientation function of the c-axis, $\langle P_2(\cos\varphi)\rangle_c$, was calculated from other reflection planes, assuming uniaxial symmetry, as:

$$\langle P_2(\cos\varphi)\rangle_c = \frac{2}{3\cos^2\sigma - 1}\langle P_2(\cos\varphi)\rangle \qquad (2.8)$$

where σ is the angle between the normal to the (hkl) plane and the c axis. Since the assignment of the (hkl) is not unique for most diffraction peaks, the azimuthal angle of the peak maximum was taken as σ. If the c-axis is along the fiber direction (σ = 0º), the perfect oriented $\langle P_2(\cos\varphi)\rangle_c$ value would be 1; if the c-axis is perpendicular to the fiber direction (σ = 90º), the perfect oriented $\langle P_2(\cos\varphi)\rangle_c$ value would be -1/2; and for random orientation (σ = 53º), the P_2 value would be 0.

In order to obtain an accurate $\langle P_2(\cos\varphi)\rangle_c$ value, it is important to measure the exact intensity of a specific crystalline plane. To achieve this aim, it is rather important to subtract the background completely from the total intensity. As discussed above, oriented electrospun fibers show narrow and sharp arcs for all the diffraction planes. In the first background subtraction method, we reduce to zero the intensity of the signal opposite to the maximum azimuthal angle. In this case, the influence of non-alignment of electrospun fibers is decreased to a minimum and the non-orientation measured come mainly from the contribution of non-oriented polymer chains within the single fibers. In a second method, we subtract the background intensity measured at the same 2θ but at an azimuthal angle 90º away from the maximum of a specific diffraction plane. The isotropic part is due to the contribution from both non-aligned electrospun fibers and non-oriented polymer chains within a single fiber. Therefore, the $\langle P_2(\cos\varphi)\rangle_c$ value obtained is slightly smaller than the one obtained by the former method. In Chapter 3, the data reported come from the first method, and in Chapters 4 and 6, the data come from the second one.

2.2.2 Fourier transform infrared (FT-IR)

Infrared (IR) spectroscopy is one of the most often used spectroscopic methods for the study of polymer materials. Generally, the FT-IR method is rapid, sensitive, and allows relatively easy sampling. IR spectra result from the interactions of the vibrational motions of a molecule with an electromagnetic radiation. There must be a dipole moment variation for absorption to occur and it is only when the frequency of the infrared radiation is corresponding to this dipole moment that the infrared radiation can be absorbed. A vibrational spectrum is usually recorded in wavenumber (cm^{-1}), which is the number of waves per centimeter. The wavenumber of a specific stretching mode of a diatomic molecule A-B can be calculated by equation 2.9. [14]

$$v(cm^{-1}) = \left[k_f \frac{(M_A + M_B)}{M_A M_B} \right]^{1/2} \tag{2.9}$$

where k_f is the force constant, or stiffness of the bond, and M_A and M_B are the masses of the two atoms. The force constant is proportional to the bond order (N_b) and the electronegativities of atoms A and B (X_A and X_B) and is reciprocal to the bond length, which can be expressed in the form [14]

$$k_f \propto N_b \left[\frac{X_A X_B}{d^2} \right]^{3/4} \tag{2.10}$$

For example, when we compare the vibrational frequency of the C=O group in urea and C=S group in thiourea, because the mass of S is larger than that of O and the length of C=S is longer than that of C=O, and because both groups have the same bond order, the vibrational frequency of the C=O group is approximately 1700 cm^{-1} while the C=S group absorbs only at a much lower 725 cm^{-1}.

2.2.2.1 Orientation measurement

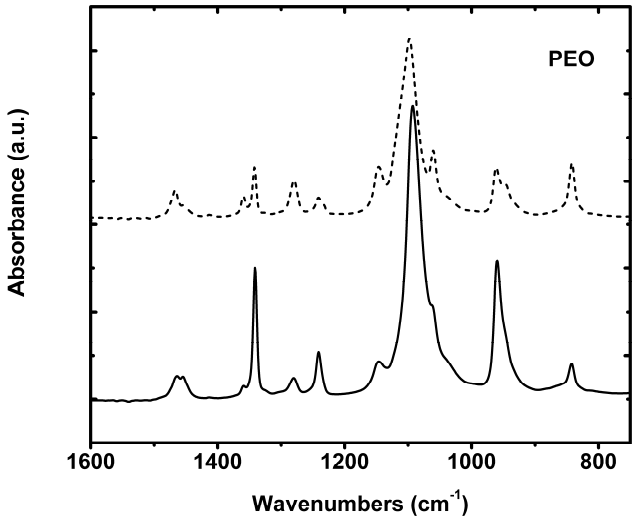

Figure 2.6. Polarized infrared spectra of PEO fibers prepared by electrospinning. Solid and broken lines represent the spectra measured with the radiation polarized parallel and perpendicular to the fiber direction, respectively.

Infrared radiation can be only absorbed when the electric vector of the incident radiation is parallel to the particular transition moment of the vibration. This requirement leads to the application of infrared spectroscopy for the study of molecular orientation in polymers. Here the electrospun fiber direction is taken as reference, and the incident infrared radiation is polarized sequentially parallel or perpendicular to the fiber direction. We then compare the infrared dichroism, which is the differential absorption measured at parallel and perpendicular directions. If the dichroic ratio, D ($A_{//}/A_{\perp}$), is larger than one, this vibrational moment is parallel to the fiber direction. On the other hand, if the dichroic ratio D is less than one, the vibrational moment is perpendicular to the fiber direction. As shown in Figure 2.6, the CH_2 wagging, CH_2 twisting and C-O-C stretching vibration bands of PEO show parallel dichroism at 1342, 1241 and 1098 cm^{-1}, respectively. In contrast, the bands at 1360, 1279 and 1061 show perpendicular dichroism and are therefore more intense in the $A_{\perp}$ spectra. These results indicate that the PEO main chain oriented parallel to the electrospun fibers direction. Considering the

high extensional force caused by the electrospinning process, this is a reasonable result. The IR absorption frequency, the assignment and the dichroic direction of each vibration are listed in Table 2.2.

Table 2.2. Absorption frequencies and assignment of the main bands of electrospun PEO and PEO-urea form α complex. The type of dominant dichroism for the crystalline samples is also indicated.[15,16]

Absorption frequency (cm^{-1})		Assignment	Dominant dichroism
PEO	α complex		
1467	1467	CH_2 symmetric bending	⊥
1455	1454	CH_2 antisymmetric bending	∥
1360	1359	CH_2 wagging and C-C stretching	⊥
1342	1342	CH_2 antisymmetric wagging	∥
1280	1276	CH_2 twisting	⊥
1241	1247	CH_2 antisymmetric twisting	∥
1147	1138	C-C stretching and C-O-C antisymmetric stretching	⊥
	1115	C-O-C symmetric stretching	⊥
1098	1079	C-O-C antisymmetric stretching	∥
1061	1055	C-O-C antisymmetric stretching	⊥
961	945	CH_2 rocking and C-O-C stretching	∥
948	953	CH_2 rocking and C-O-C stretching	⊥

Two methods were used for the FT-IR orientation measurements. Attenuated total reflection (ATR) and transmission. A Seagull variable angle reflectance accessory (Harrick Scientific Products) equipped with a ZnSe hemispherical crystal and a ZnSe wire-grid polarizer was used to measure the polarized spectra of the fibers in the ATR mode. The fibers were aligned perpendicular to the incidence plane and the polarizer

was rotated to record spectra parallel and perpendicular to the fiber axis. For the transmission measurements, a narrow bundle of electrospun fibers was pressed with KBr powder to reduce the scattering of the fibers. The fiber direction was then observed using optical microscopy. During the measurement, the polarizer was rotated either parallel or perpendicular to the fiber axis.

2.2.2.2 Conformation analysis

Conformation refers to the relative steric arrangement of atoms or groups that can be altered by rotation of the atoms or groups around a single bond. For the bond sequence O-C-C-O in PEO chains, different conformations, such as TTT, TGT, TGG(TG^-G^-), TGG^- etc., (the dihedral angle is 180º for trans and 60º (-60 º) for G and G^-, respectively) have been observed in either crystalline PEO or its complexes. As discussed in Chapter 1, the most commonly observed PEO structure is 7_2 helical conformation with trans-gauche-trans (TGT) sequences,[17] and another less observed form is the all-trans (TTT) planar zigzag conformation which can be obtained by stretching two folds[18] or by freeze-drying in a dilute solution.[19] The polarized FT-IR spectra of electrospun PEO nanofibers are shown in Figure 2.6. The vibrational bands of PEO could be divided into two groups, parallel bands ($\parallel$) and perpendicular bands ($\perp$) based on the dichroic measurements.[20] But there are conflicting opinions about the assignment of CH_2 wagging, twisting and rocking vibrations to helical or to all-trans conformations because of the difficulties in preparing PEO in a single phase. Marcos et al.[21] assigned the 1342, 1241 and 959 cm^{-1} vibrational bands in PEO/PMMA blends to be due to all-trans conformation and those at 1359, 1279, 1060 and 947 cm^{-1} to be due to helical structure, but Strake et al.[22] pointed out that the assumption about the presence of relatively high concentration of all-trans conformation in PEO/PMMA blends is not well-founded. As shown in Table 2.2, the relatively intense CH_2 wagging, twisting and rocking vibrations at 1341, 1241 and 959 cm^{-1} are all parallel bands and the relatively weak CH_2 wagging, twisting and rocking vibrations bands at 1359, 1279 and 947 cm^{-1} are all perpendicular bands. Therefore, the question comes down to whether these bands are connected with dichroic properties or represent different conformational structures.

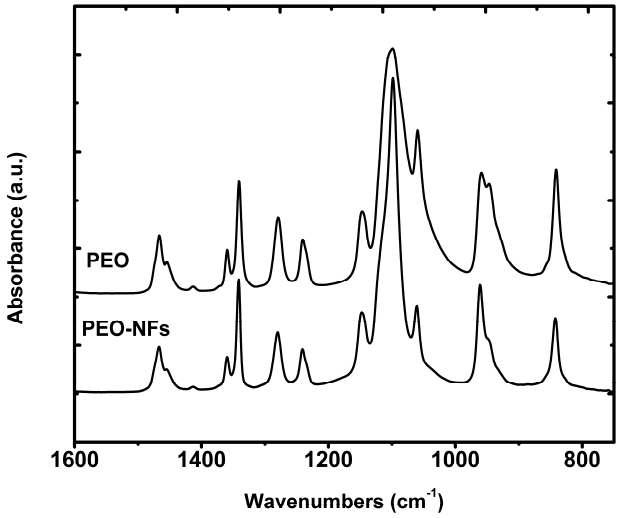

Figure 2.7. FT-IR spectra of bulk PEO and electrospun PEO nanofibers (NFs).

More recently, Liedberg,[23-26] Vanderah[27-29] and Grunze[30] et al. obtained the molecular conformation of highly oriented oligo(ethylene glycol)-terminated $(EO)_x$ self-assembled monolayers on gold or silver surfaces. They suggested that $(EO)_5$ is the shortest $(EO)_x$ segment capable of forming a helical conformation with the specific vibrational bands at 1345, 1244, 1114 and 964 cm^{-1}. When x is less than 5, all those peaks were absent, which suggest that the $(EO)_x$ ($x \leq 4$) chains assemble predominantly in the all-trans conformation with specific bands at 1144, 1060, 938 cm^{-1}. As to the conformation of electrospun PEO fibers, as shown in Figure 2.7, all the bands assigned to all-trans by Liedberg,[23-26] Vanderah[27-29] and Grunze[30] et al. either keep similar intensity (1147 cm^{-1}) or become less intense (1061 and 948 cm^{-1}) than the corresponding bands of bulk PEO. Therefore we suggest that the electrospinning process only orient the PEO chains in the parallel direction rather than change the conformation from helical to all-trans, as reported by some authors.[31]

As to the PEO-urea α complex, Chenite and Brisse[3] suggested an approximately 4_1 helical conformation close to TGT. Ye et al.[4] proposed a TGG^- conformation for the melt-quenched PEO-urea complex, that is form β with excess urea. But the advance per

chemical unit measured is only 0.231 and 0.258 nm for PEO-urea form α and β, respectively, much less than the conventional TGT (0.278 nm) and $TGGTG^-G^-$ (0.294 nm) conformations obtained for the PEO and the PEO-$HgCl_2$ complex. The dichrioism and the possible conformation of PEO in the PEO-urea complexes will be analyzed in Chapters 4 and 5.

2.2.2.3 PEO and urea/thiourea chain orientation direction in complexes

Both pure urea and thiourea adopt a planar molecular structure, but with a different crystal structure. The urea crystal has a tetragonal lattice with unit cell parameters of $a = b = 5.661$ Å and $c = 4.712$ Å.[32] Thiourea has an orthorhombic lattice with unit cell parameters of $a = 7.655$, $b = 8.537$ Å and $c = 5.520$ Å at room temperature. The urea molecules are thought to take a chain structure linked by two head-to-tail H-bonds along the c axis. The neighboring chains are mutually orthogonal and go to opposite directions with the adjacent chains (antiparallel).[33-37] The thiourea molecules adopt a ribbon structure linked by centrosymmetric H-bonds.[38] As a result, the two hydrogen bonds on a sulfur atom come from two different neighboring thiourea molecules in the same ribbon, unlike the urea chain structure in which both hydrogen bonds on the oxygen come from the same neighboring urea molecule.[33,34] The assembly of urea and thiourea molecules in the PEO complexes is still unknown, although it is well known that the bands coming from urea or thiourea show large differences after complex formation. To determine the structure of the PEO-urea and PEO-thiourea complexes, it is helpful to know the relative assembly of PEO with urea or thiourea in the complexes. The orientation and assembly of urea and thiouea molecules were researched via polarized FT-IR in Chapters 4 and 6.

2.2.3 Microscopy

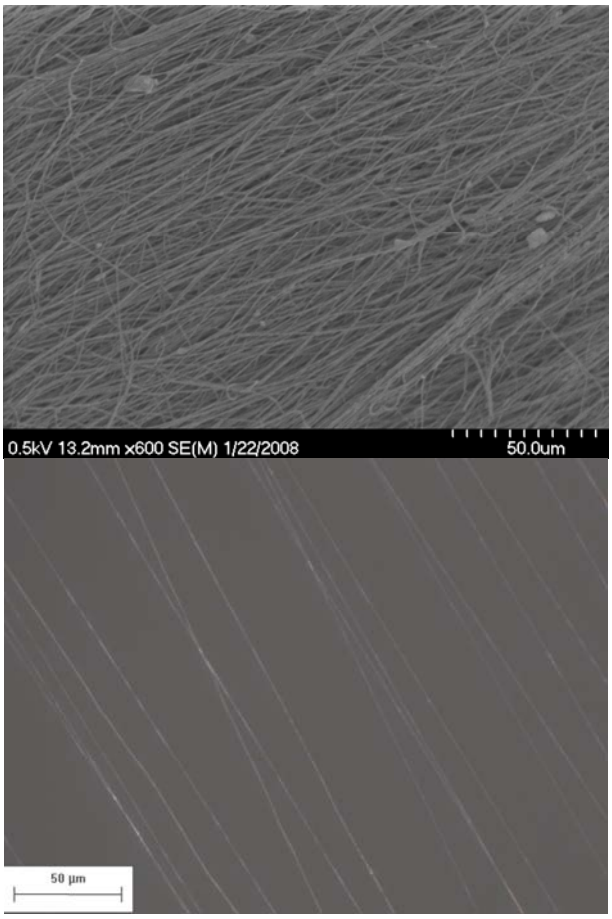

Figure 2.8. SEM image of PEO-urea IC α form (top) and cross-polarized optical micrograph of PEO fibers (bottom).

Another application of optical microscopy is the observation of birefringence with the help of two crossed polarizers. Birefringence is one of the simplest methods for the characterization of molecular orientation. For an isotropic sample, the refractive index is the same in all directions, thus a single averaged macroscopic refractive index is observed. For an anisotropic sample, such as electrospun fibers, the polarizability of the specimen is usually not equivalent in all directions, which leads to two or three independent refractive indices along its main axes. The three birefringence indices, Δn_{ij} (i, j = X, Y, Z), can be obtained by measuring the refractive index, n, along the

machine (Z), transverse (X) and normal (Y) directions of the specimen. For a sample with uniaxial orientation, such as the electrospun fibers, only a single birefringence is required to evaluate the orientation, Δn_{ZX} or Δn_{ZY}, because n_X is equal to n_Y. Or more generally,

$$\Delta n_{ZY} = \Delta n_{ZX} = n_Z - \frac{(n_X + n_Y)}{2} \tag{2.11}$$

When the PEO-urea complexes are spin-coated on glass or silicon substrates or experienced melt-cooling, the polymer chains crystalize to form spherulite structures. Spherulite formation is a very common form of self-assembly observed during polymer crystallization. The formation of PEO-urea complex spherulites starts on a nucleation site in both the melt-cooling process and from high concentration solutions. Then it will extend radially outwards to take the spherical shape until a neighboring spherulite is reached (Figure 2.9). On most occasions, the chains fold direction within the lamellae is perpendicular to the crystal growth direction (radial direction). When a spherulite is observed by optical microscopy between crossed polarizers, it exhibits birefringence and shows a cross-like extinction, called "Maltese Cross". A pattern also sometimes observed is concentric ringed spherulite that show periodic extinction along the radial direction, which is commonly believed to be due to lamellar twisting along the radial direction during crystal growth so that alternating dark and bright bands appear. Generally speaking, the birefringence property of spherulites is mainly dependent on the orientation of the lamellae which constitute the spherulites. If the highest refractive index of the spherulites is in the radial direction (Z) of the spherulites, then n_Z □ n_X and n_Y (X and Y are normal directions to Z), Δn_{ZX} or Δn_{ZY} is positive and such spherulite is called positive spherulite. On the other hand, if the highest refractive index of the spherulite is in the tangential direction, which is perpendicular to the radial direction, then n_Z □ n_X or n_Y and Δn_{ZX} or Δn_{ZY} is negative, such kind of spherulite is called negative spherulite. The positive or negative spherulites can be observed under crossed polarizer and analyzer with a sensitive color plate (λ waveplate). For a positive

spherulites, the first and third quadrants are blue, and the second and fourth quadrants are yellow, while a reversed arrangement of the quadrants is observed for a negative spherulite. As shown in Figure 2.9, both PEO-urea α and β complexes form spherulites, PEO-urea α complex forms positive spherulites while that of the PEO-urea β complex is negative. When the β complex melts and converts to the α complex, the sign of the spherulites is also altereed. It might be attributed to the channel and layer structures, as will be discussed in Chapter 4.

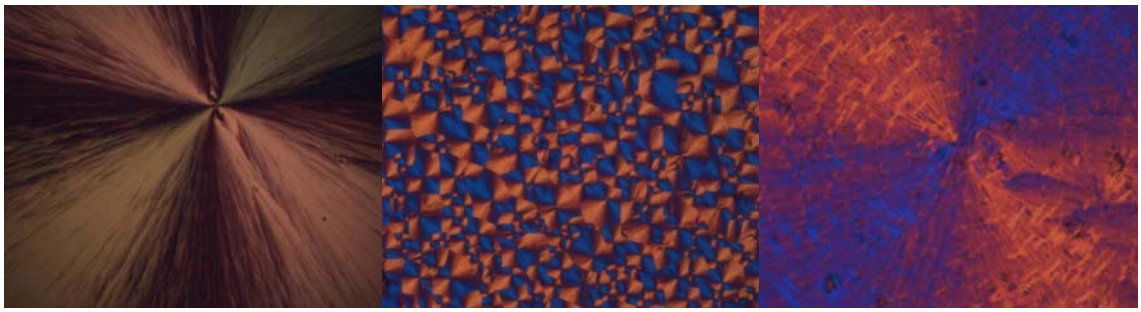

Figure 2.9. Spin-coated PEO-urea α complex (left), PEO-urea β complex (middle), and β complex after melting and cooling to 25 ºC (right).

2.2.4 Thermal analysis

Thermal analysis can designate any technique that involves the measurement of a physical quantity while the temperature is changed or maintained. Here, thermogravimetric analysis (TGA) and differential scanning calorimetry (DSC) are used to characterize the composition and the decomposition temperature of the complexes, and to study the first order transition properties of the complexes, such as their melting and crystallization processes, to yield information concerning structure of the complexes and to draw the phase diagram. Generally, thermal analysis techniques are among the easiest and most available of techniques and are often the first techniques used to analytically describe a specimen.

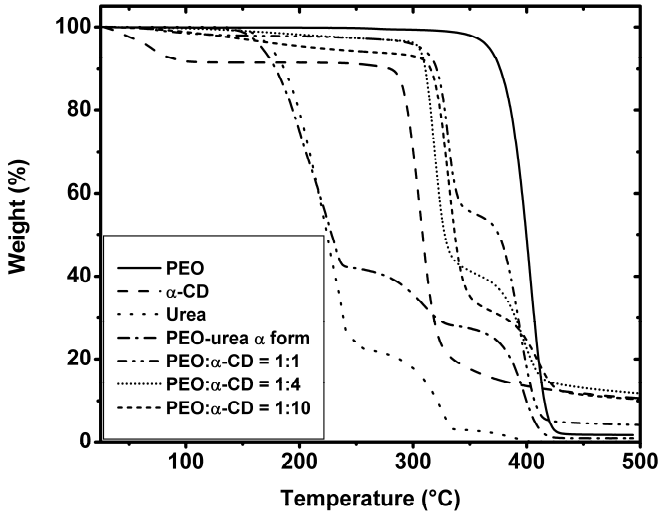

Figure 2.10. Thermogravimetric analysis plots of pure PEO, α-CD, urea, PEO-urea complex form α and PEO-α-CD complexes with various mass ratios.

TGA provides a quantitative measurement of the mass change associated with the thermal degradation of a material. When used in combination with FT-IR, TGA/FT-IR is capable of the analysis of evolved gases produced from TGA. Here TGA is used to characterize the composition of PEO-urea, thiourea or CD complexes prepared by the co-crystallization method (Figure 2.10). PEO-urea α form presents a stoichiometric PEO:urea molar ratio, in agreement with the literature value reported in single crystal.[3] But PEO-α-CD complex is not stoichiometric, and as more α-CD is added in, PEO chains are covered more. This could be attributed to the different formation processes of PEO-urea and PEO-α CD complexes. The threading process of CD to the polymer chains is slow and there is a large resistance to pass through the whole polymer chain, especially for high molecular weight polymers.

The DSC instrument is composed of two identical cells in which the sample and the reference (an empty pan) are placed. Both cells are heated with a constant heat flow with two heaters. If the sample undergoes a thermal transition, such as a glass transition, melting or crystallization, thermal energy is added to either the sample or reference pans

in order to maintain both sample and reference at the same temperature. The output of DSC is a plot of heat flow (W/g) versus temperature at a specific temperature ramp rate. For polymer samples, significant broadening of the thermal transition, such as melting, is normal and this is associated with the structural and kinetic features of the polymer melting, or the previous crystallization process. To obtain precise results, the instrument is usually calibrated with a pure metal that displays a sharp melting transition, such as indium (T_m = 155.8 ºC). The complexes prepared here are highly crystalline specimens, and the melting temperature is broad as for conventional polymers. The enthalpy of melting is determined by integrating the endothermic peak, and the enthalpy of crystallization is the integration of the corresponding exothermic peak, given by $\Delta H = \int C_p dT$. Since the heat flow increases with temperature ramping rates, higher heating rates lead to more sensitive thermograms but, also to lower resolution of the transition, and might have consequences for transitions displaying kinetic features. We also observed that, for the same sample, different crystals can be obtained if the cooling rate is changed, the details will be shown in Chapter 5. If not specified, the data reported here are with a 10 ºC /min ramp. Based on the DSC results, the phase diagrams of PEO-urea and PEO-thiourea systems are set up and the compositions of the stable crystalline complexes are decided.

According to the DSC results on different compositions of PEO/urea or PEO/thiourea systems, a complete phase diagram might be drawn. Wagner et al.[39] previously obtained the temperature-composition phase diagram of PEO/urea system. As shown in Figure 2.11, the phase diagram clearly indicates the formation of PEO-urea α complex, which displays a congruent melting, which means the composition of the liquid after melting is the same as the composition of the solid. The stoichiometric composition could be derived from the temperature-composition phase diagram. Unfortunately, although the authors observed a melting of the PEO/urea system at ca. 90 ºC with high ratio of PEO in the heating cycle of DSC (not shown), they did not realize that it came from a new crystal phase (β form), but assigned it to the melting of pure PEO. Here we obtained a series of electrospun specimens with various PEO/urea and

PEO/thiourea compositions and hoped to obtain a complete phase diagram to explain the phase composition and phase transition properties of the two systems.

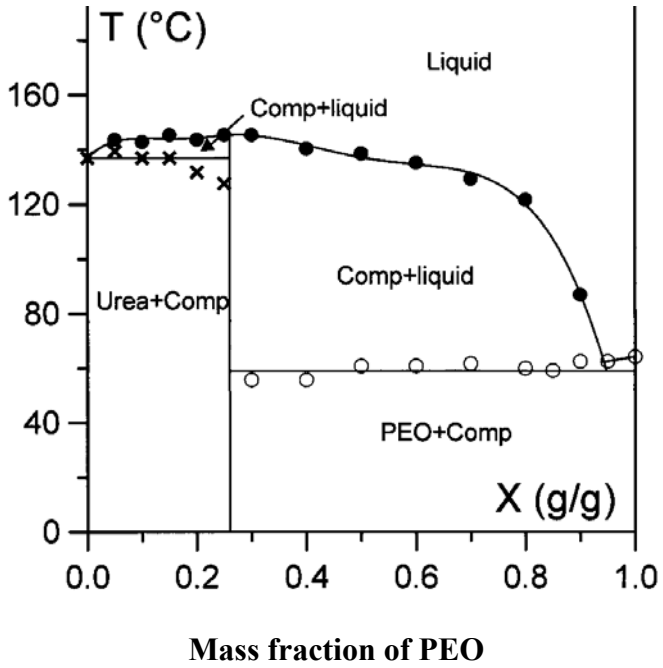

Figure 2.11. Phase diagram of PEO/urea system as a function of PEO composition, Comp represents the PEO-urea complex.[39]

2.3 References

1. Tadokoro, H.; Yoshihara, T.; Chatani, Y.; Murahashi, S. *J. Polym. Sci. B* **1964**, 2, 363.
2. Vasanthan, N.; Shin, I. D.; Tonelli, A. E. *Macromolecules* **1996**, 29, 263.
3. Chenite, A.; Brisse, F. *Macromolecules* **1991**, 24, 2221.
4. Ye, H. M.; Peng, M.; Xu, J.; Guo, B. H.; Chen, Q.; Yun, T. L.; Ma, H. *Polymer* **2007**, 48, 7364.
5. Teo, W. E.; Ramakrishna, S. *Nanotechnology* **2005**, 16, 1878.
6. Alexander, L. E., *X-Ray Diffraction Methods in Polymer Science*. John Wiley & Sons, Inc.: New York, 1969.
7. http://en.wikipedia.org/wiki/Crystal_structure
8. Harris, K. D. M.; Cheung, E. Y. *Chem. Soc. Rev.* **2004**, 33, 526.
9. Ward, I. M., *Structure and Properties of Oriented Polymers*. 2nd ed.; Chapman & Hall: London, 1997.
10. Vancso, G. J. *Polymer Bulletin* **1990**, 24, 266.
11. Lefevre, T.; Pellerin, C.; Pezolet, M., *Comprehensive Analytical Chemistry*. Elsevier: Oxford, 2008; Vol. 53, p 295.
12. Hermans, P. H.; Platzek, P. *Kolloid Z.* **1939**, 88, 68.
13. Hermans, J. J.; Hermans, P. H.; Vermaas, D.; Weidinger, A. *Rec. Trav. Chim. Pays-Bas* **1946**, 65, 427.
14. Koenig, J. L., *Spectroscopy of Polymers*. Elsevier Science Inc.: New York, 1999.
15. Matsuura, H.; Miyazawa, T. *J. Polym. Sci. part A-2* **1969**, 7 1735.
16. Dissanayake, M. A. K. L.; Frech, R. *Macromolecules* **1995**, 28, 5312.
17. Tadokoro, H.; Yoshihara, T.; Tahara, S.; Murahashi, S. *Makromol. Chem.* **1964**, 73, 109.
18. Takahashi, Y.; Sumita, I.; Tadokoro, H. *J. Polym. Sci. Polym. Phy. Ed.* **1973**, 11, 2113.
19. Gu, F.; Bu, H.; Zhang, Z. *Polymer* **2000**, 41, 7605.
20. Miyazawa, T.; Fukushima, K.; Ideguchi, Y. *J. Chem. Phys.* **1962**, 37, 2764.
21. Marcos, J. I.; Orlandi, E.; Zerbi, G. *Polymer* **1990**, 31, 1899.

22. Straka, J.; Schmidt, P.; Dybal, J.; Schneider, B.; Spevacek, J. *Polymer* **1995**, 36, 1147.
23. Valiokas, R.; Svedhem, S.; Svensson, S. C. T.; Liedberg, B. *Langmuir* **1999**, 15, 3390.
24. Malysheva, L.; Onipko, A.; Valiokas, R.; Liedberg, B. *J. Phys. Chem. A* **2005**, 109, 7788.
25. Malysheva, L.; Onipko, A.; Valiokas, R.; Liedberg, B. *J. Phys. Chem. B* **2005**, 109, 13221.
26. Ostblom, M.; Valiokas, R.; Konradsson, P.; Svensson, S. C. T.; Liedberg, B.; Garrett, M.; Allara, D. L. *J. Phys. Chem. B* **2006**, 110, 1830.
27. Vanderah, D. J.; Pham, C. P.; Springer, S. K.; Silin, V.; Meuse, C. W. *Langmuir* **2000**, 16, 6527.
28. Vanderah, D. J.; Meuse, C. W.; Silin, V.; Plant, A. L. *Langmuir* **1998**, 14, 6916.
29. Vanderah, D. J.; Arsenault, J.; La, H.; Gates, R. S.; Silin, V.; Meuse, C. W. *Langmuir* **2003**, 19, 3752.
30. Harder, P.; Grunze, M.; Dahint, R.; Whitesides, G. M.; Laibinis, P. E. *J. Phys. Chem. B* **1998**, 102, 426.
31. Kim, G.-M.; Wutzler, A.; Radusch, H.-J.; Michler, G. H.; Simon, P.; Sperling, R. A.; Parak, W. J. *Chem. Mater.* **2005**, 17, 4949.
32. Vaughan, P.; Donohue, J. *Acta Crystallogr.* **1952**, 5, 530.
33. Masunov, A.; Dannenberg, J. J. *J. Phys. Chem. A* **1999**, 103, 178.
34. Masunov, A.; Dannenberg, J. J. *J. Phys. Chem. B* **2000**, 104, 806.
35. Gora, R. W.; Bartkowiak, W.; Roszak, S.; Leszczynski, J. *J. Chem. Phys,* **2002**, 117, 1031.
36. Rinderknecht, S.; J.Brisson. *Macromolecules* **1999**, 32, 8509.
37. Lamelas, F. J.; Dreger, Z. A.; Gupta, Y. M. *J. Phys. Chem. B* **2005**, 109, 8206.
38. Truter, M. R. *Acta Crystallogr.* **1967**, 22, 556.
39. Wagner, J.-F.; Dosière, M.; Guenet, J.-M. *Macromol. Symp.* **2005**, 222, 121.

Chapter 3 : Highly Oriented Electrospun Fibers of Self-Assembled Inclusion Complexes of Poly(ethylene oxide) and Urea

3.1 Résumé

L'électrofilage a été utilisé pour la première fois pour préparer des nanofils hautement orientés de complexes auto-assemblés entre de petites molécules formant des canaux (urée) et des chaînes de polymère (poly(oxyde d'éthylène), PEO). La structure du complexe d'inclusion est préservée dans les nanofils électrofilés. La diffraction des rayons X aux grands angles révèle une fonction d'orientation de 0.89 pour les fibres. A notre connaissance, ceci est la valeur d'orientation moléculaire la plus élevée rapportée à ce jour pour des fibres électrofilées.

3.2 Abstract

Electrospinning was used for the first time to prepare highly oriented fibers of self-assembled inclusion complexes (IC) between channel-forming small molecules (urea) and guest polymer chains (poly(ethylene oxide), PEO). The structure of the bulk IC was preserved in the electrospun fibers. Wide-angle X-ray diffraction revealed an orientation function of 0.89 for the fibers. This constitutes, to our knowledge, the largest molecular orientation ever reported for a polymer in electrospun fibers.

3.3 Introduction

Electrospinning is a technique that allows production of polymeric fibers with diameters ranging from nanometers to a few microns, and thus with an inherent high surface-to-volume ratio.[1-3] These fibers are finding potential applications in drug delivery, tissue engineering, membranes, nanocomposites, etc. While electrospinning was initially used to prepare disordered mats, it is now possible to produce aligned fibers using various collectors[1,2,4] However, it is important to not only control the macroscopic alignment of fibers but also their molecular orientation because it strongly influences most mechanical, optical, and electrical properties of polymers.[5] Conventional spinning methods allow the production of fibers with a very large molecular orientation, leading to ultra-high modulus, but these are typically several microns or tens of microns in diameter.[5] In contrast, the molecular orientation is generally modest in electrospun nano- or micro-fibers.[2,6-8]

An independent method for preparing highly structured materials is the self-assembled formation of inclusion complexes (IC) of polymeric guests inside a small molecule host matrix. For instance, poly(ethylene oxide) (PEO) has been complexed with urea,[9-11] mercuric chloride,[12] cyclodextrins,[13] etc. In their urea inclusion complexes, polymers are packed in one-dimensional channels constructed from an essentially infinite three-dimensional network of hydrogen-bonded urea molecules.[14] The polymer chains are thus highly extended at the molecular scale, but they are not aligned at the macroscopic level.

In this work, we have used electrospinning to prepare highly oriented and well aligned fibers of the self-assembled inclusion complex between urea and high molecular weight (400 000 g/mol) PEO. The IC was prepared by a co-crystallization method and the resulting 20% w/v suspension was electrospun, under a 17 kV potential difference, onto a target composed of two metallic counter electrodes separated by a 5 cm gap. The details of the sample preparation, electrospinning conditions and sample characterization

are provided in the Supporting Information. To our knowledge, it is the first time that such IC fibers were prepared and characterized.

3.4 Results and discussion

Figure 3.1 shows a crossed-polarized optical micrograph of a sample obtained by electrospinning the PEO-urea IC suspension. Cylindrical fibers having a 1 to 2 μm diameter are observed, clearly demonstrating that the PEO-urea inclusion complex can form fibers in spite of its rather poor film forming properties. The fibers do not show any beading and are mostly continuous over the 5 cm gap between the counter electrodes. A few breakage points can nevertheless be observed, most likely because of a high level of crystallinity (vide infra) that makes the material brittle. The fibers transmit light when observed under crossed polarizers, indicating that they possess a significant level of molecular orientation.

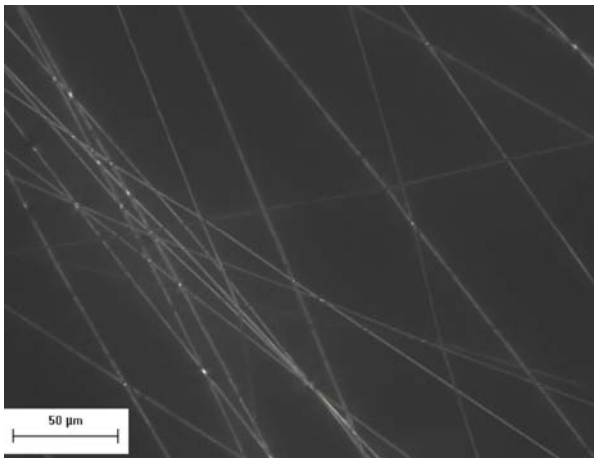

Figure 3.1. Crossed-polarized optical micrograph of electrospun fibers of the PEO-urea inclusion complex.

For comparison, control PEO fibers electrospun under similar conditions had a diameter in the 400-700 nm range. This significant difference can be explained by the large concentration difference necessary to reach a similar viscosity, 5% for pure PEO

vs. 20% for the inclusion complex. It is well accepted that higher concentrations lead to fibers with larger diameters.[15] Interestingly, thermogravimetric analysis (see Supporting Information) revealed a 3:1 urea:PEO mass ratio, thus suggesting a similar PEO concentration in both solutions. This corresponds to a ~9:4 urea:PEO molar ratio, in agreement with the reported value for this complex.[9]

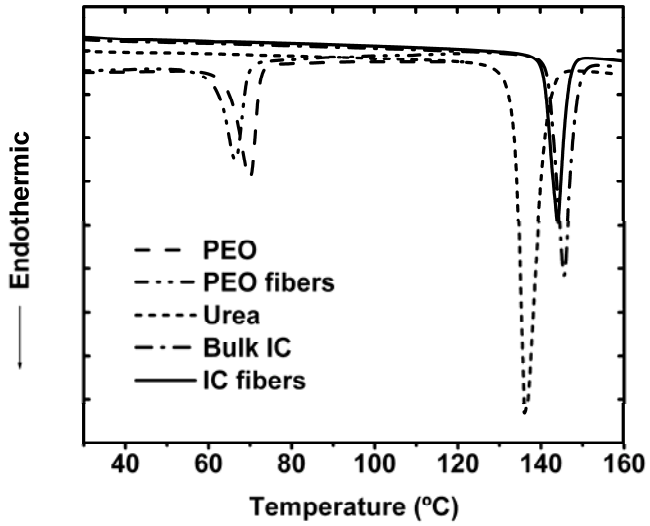

Figure 3.2. DSC thermograms of the bulk PEO, urea and inclusion complex (IC), as well as those of the pure PEO and PEO-urea IC electrospun fibers.

Figure 3.1 shows that fibers can be electrospun but it does not establish that they are composed of the inclusion complex. Figure 3.2 compares the DSC thermograms of the bulk PEO, urea and IC, as well as those of the pure PEO and IC electrospun fibers. A single endothermic peak, attributed to the melting of the crystalline phase, can be observed for all samples. The melting temperature of the bulk inclusion complex is found at 146 °C, clearly above those of pure PEO (69 °C) and pure urea (136 °C) and in agreement with the literature value.[11] The melting peak is observed at ~144 °C for the fibers electrospun from the IC suspension, very close to that of the bulk sample. It is thus a good indication that the fibers are truly composed of the inclusion complex. The

melting temperature difference between the fibers and bulk IC is similar to that (1-3 degrees) observed between the fibers and bulk of pure PEO.

These conclusions are supported by infrared spectroscopy measurements (see Supporting Information). Indeed, the infrared spectra of the bulk IC and the electrospun IC fibers are very similar, but are markedly different from those of pure PEO and urea. Tonelli et al. studied the infrared spectra of bulk PEO-urea IC and suggested that the urea bands are modified by the new hydrogen bonding network and that PEO chains adopt a more extended conformation than the usual trans-gauche-trans (TGT) conformation found in pure crystalline PEO around the O-C-C-O linkages.[11]

It can be observed in Figure 3.2 that the thermograms of the bulk IC and of the fibers do not present any significant transition at the melting temperatures of either pure PEO or urea. This indicates that the sample preparation procedure removed most if not all free urea and PEO from the inclusion complex. In addition, thermogravimetric analysis (see Supporting Information) of the fibers shows that the electrospinning process does not alter the composition of the inclusion complex. The crystallinity level could not be determined quantitatively because the melting enthalpy of the 100% crystalline IC is not known. However, the absence of a glass transition temperature and of a crystallization exotherm suggests that the degree of crystallinity is large for both IC samples.

The two-dimensional WAXD patterns and 2θ diagrams obtained for the bulk and electrospun IC are shown in Figure 3.3a. Very similar 2θ diagrams can be observed, indicating that the crystalline structure remains essentially the same after electrospinning. Both samples show intense and narrow diffraction peaks and no significant amorphous halo, further suggesting a high crystallinity level. It is noteworthy that the most intense diffraction peaks of pure PEO (23.5°) and urea (22.5°) are not observed in the X-ray diagrams, confirming that no residual pure (crystalline) products are present.

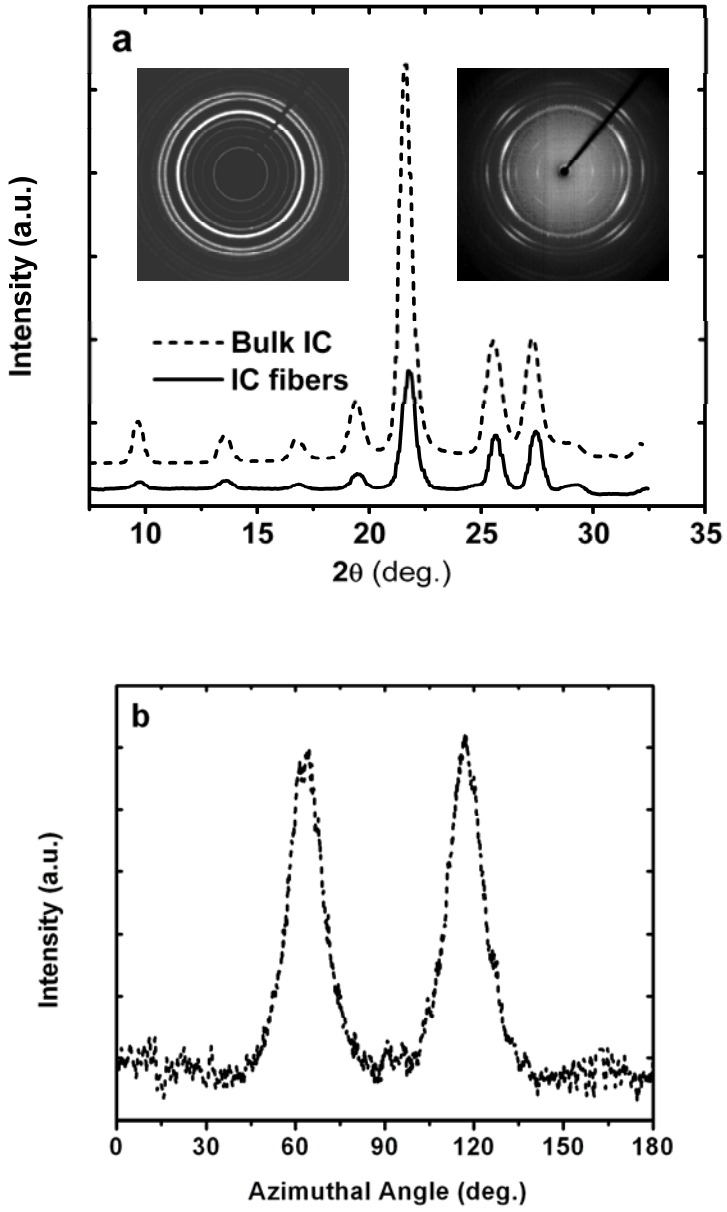

Figure 3.3. a) Wide-angle X-ray diffraction 2θ diagrams for the bulk and electrospun fibers of the PEO-urea inclusion complex (IC) and two-dimensional diffraction patterns of bulk IC (left inset) and electrospun fibers (right inset). b) Azimuthal profile of the WAXD pattern for electrospun PEO-urea IC at 2θ=21.6º.

In addition to providing structural information, X-ray diffraction can be used to probe the molecular orientation in polymers. While a uniform azimuthal intensity distribution is observed for the bulk IC (left inset of Figure 3.3a), the electrospun fibers present a highly inhomogeneous diffraction intensity distribution (right inset). The azimuthal scan for the 2θ = 21.6° diffraction plane of the electrospun fibers is shown in Figure 3.3b. A narrow peak with a full width at half height (FWHH) of ~13º can be observed because of the strongly anisotropic distribution of the crystals in the fibers. Similar values are obtained for the other intense 2θ diffraction peaks, as shown in Table 3.1.

The second order moment of the orientation distribution function of the c-axis, $<P_2(\cos\varphi)>_c$, was calculated to quantify the molecular orientation in the fibers. Since the (00l) reflection plane is not available, the orientation function was calculated from other reflection planes, assuming uniaxial symmetry, as:

$$< P_2(\cos\varphi) >_c = \frac{2}{3\cos^2\sigma - 1} \cdot \frac{3 < \cos^2\varphi > -1}{2} \tag{3.1}$$

where σ is the angle between the normal to the (hkl) plane and the c axis. Since the assignment of the (hkl) is not unique for most diffraction peaks, the azimuthal angle of the peak maximum was taken as σ. The average $<\cos^2\varphi>$ was calculated by integrating the intensity of specific 2θ diffraction peaks along the azimuthal angle, φ, as:

$$< \cos^2\varphi >= \frac{\int_0^{\pi} I(\varphi)\cos^2\varphi \sin\varphi d\varphi}{\int_0^{\pi} I(\varphi)\sin\varphi d\varphi} \tag{3.2}$$

Table 3.1 shows that an average $<P_2(\cos\varphi)>_c$ value of 0.89 is obtained for the electrospun fibers of the inclusion complex. This unusually large molecular orientation

is very close to the maximum theoretical value of 1 that would be obtained for a sample perfectly oriented along the reference direction.[5] In contrast, a $<P_2(\cos\varphi)>_c$ value of ~0 would be obtained for an isotropic sample, as for the bulk IC.

Table 3.1. WAXD characterization of the degree of orientation for PEO-urea inclusion complex electrospun fibers.

2θ peak	21.6º	25.5º	27.2º
FWHH*	13º	13º	13º
$<P_2(\cos\varphi)>_c$	0.90	0.91	0.85
Plane attribution§	102; 201; 012; 021	210; 120	211; 121

*FWHH: Full width at half height of the diffraction peaks in the azimuthal scan.
§Plane attribution: Calculated based on the unit cell data reported in ref. 13.

To the best of our knowledge, it is the first time that such high orientation level is reported not only for self-assembled inclusion complexes but also for polymers in electrospun fibers. The largest quantitative values we have found in the literature were obtained by Reneker, Cheng et al. for nanocomposite fibers of poly(acrylonitrile) (PAN) and multiwalled carbon nanotubes (MWCNT).[16] $<P_2(\cos\varphi)>$ values of 0.62 and 0.90 were obtained for the PAN and MWCNT, respectively. It should be noted that a rotating collector was used in these experiments and imposed an approx. 8.4 m/s linear velocity on the fibers. It was shown for pure PAN fibers that increasing the take-up speed from 0 to 9.84 m/s increases the orientation function from 0 to 0.23,[7] partly because of better macroscopic alignment but also because of drawing. In contrast, the PEO-urea IC fibers prepared in this work were collected between two static metallic rods, ensuring that no force acted on the fibers apart from the electrospinning process itself. Low molecular orientation values were observed for electrospun fibers in most other studies. For

instance, Dersch et al. reported no orientation in poly(lactic acid) fibers,[2] while a modest orientation function of 0.092 was found in electrospun silk fibroin.[8]

It is worth noting that the orientation functions of Table 3.1 were calculated assuming that all fibers are perfectly aligned during the WAXD measurements, although Figure 3.1 shows that this is not the case. The values obtained here are thus low estimates of the molecular orientation. In future work, we will attempt determining the orientation of single fibers, thus avoiding the uncertainties due to imperfect fiber alignment.

3.5 Acknowledgments

The financial support of the Natural Sciences and Engineering Research Council of Canada (NSERC), the Fonds Québécois de Recherche sur la Nature et les Technologies (FQRNT) and the Canada Foundation for Innovation (CFI) is acknowledged. We also thank S. Essiembre for his technical assistance.

3.6 Supporting information

3.6.1 Sample preparation

PEO with a weight-average molecular weight of 400 000 g/mol (Scientific Polymer Products), urea and methanol (Fisher Scientific) were used without further purification. PEO-urea inclusion complexes were prepared via a co-crystallization method. Four grams of PEO were dissolved at 65 °C in 100 ml of a methanol solution saturated with 20 grams of urea. After complete dissolution, the solution was cooled to room temperature and a white gel-like precipitate formed gradually during one day. The precipitate was filtered and washed several times with methanol to eliminate any uncomplexed urea and PEO. Following these steps, the gel-like sample had a total (urea and PEO) concentration of 20% w/v. A part of the sample was dried under vacuum to

prepare bulk PEO-urea inclusion complex. The second part was directly introduced in a syringe equipped with a 0.41mm diameter needle in order to prepare PEO-urea IC fibers by electrospinning. A 15 kV positive voltage was applied on the needle tip using a CZE 100R high-voltage power supply (Spellman High Voltage Electronics), while a 2 kV negative potential (Power Designs) was imposed on two metallic counter electrodes separated by a 5 cm gap. The distance between the flat-end needle and the counter electrodes was 15 cm. The flow rate of the solution was fixed to 0.01 ml/min using a PHD 2000 syringe pump (Harvard Apparatus). PEO control samples were prepared using a 5% w/v solution in water, which was shown to possess the same viscosity as that of the 20% PEO-urea IC suspension using an AR2000 Rheometer (TA Instruments), the shear rates varied from 0 to 1000 s^{-1} and the shear viscosity was measured under room temperature. Bulk sample was prepared by solvent-casting, while pure PEO nanofibers were electrospun using identical experimental conditions as those used for the PEO-urea IC fibers.

3.6.2 Characterization

An Axioskop 40 optical microscope (Carl Zeiss) equipped with a 40X polarizing objective and a QImaging digital camera was used to observe the electrospun fibers. The birefringence of the samples was qualitatively verified under crossed polarization geometry. Differential scanning calorimetry (DSC) measurements were conducted at a heating rate of 10 °C/min using a TA Instruments 2910 calorimeter calibrated with indium. The decomposition processes of PEO, urea, and of the bulk and fibers of the PEO-urea IC were followed using a TGA 2950 thermogravimetric analyzer (TA Instruments). The experiments were performed under a nitrogen atmosphere at a heating rate of 20 ºC/min. Infrared spectra were recorded on a Vertex 70 FT-IR spectrometer (Bruker Optics) equipped with a liquid nitrogen-cooled HgCdTe detector. Spectra with a resolution of 4 cm^{-1} were collected in the attenuated total reflection (ATR) mode using a MIRacle single reflection accessory (Pike Technologies) equipped with a silicon crystal.

Wide angle X-ray diffraction measurements were carried out using a Bruker AXS diffractometer (Siemens Kristalloflex 780 generator), operated at 40 kV and 40 mA, using the Cu Kα (0.1542 nm) radiation collimated by a graphite monochromator and a 0.5 mm pinhole. The diffraction patterns were captured by a HI-STAR area detector. Characterization of the electrospun fibers was performed with the incident X-ray beam perpendicular to the (vertically aligned) fiber direction. The acquisition time was 15 min for the bulk IC and 60 min for the electrospun fibers. A scattering background was subtracted from the signal of the samples.

3.6.3 Thermogravimetric analysis

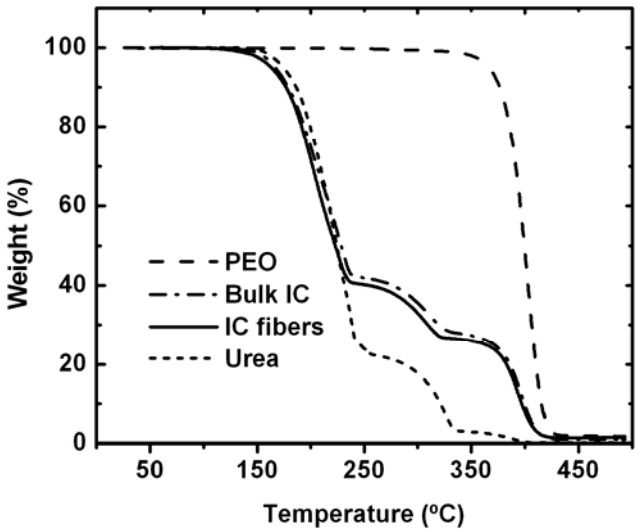

Figure S-3.1. Thermogravimetric analysis plots of pure PEO and urea, and of the bulk and fibers of the PEO-urea inclusion complex (IC).

The urea:PEO molar fraction in the inclusion complexes can be determined using thermogravimetric analysis. Figure S-3.1 shows that the degradation of pure PEO occurs in a single stage, as compared to three steps for pure urea. The degradation curves of the two types of PEO-urea IC samples present the decomposition processes of both urea and PEO. From the ratio of the first two (urea) and the third (almost exclusively PEO)

weight losses, a 3:1 urea:PEO mass ratio can be calculated. This corresponds to a 9:4 urea:PEO molar ratio, in agreement with the literature value (Chenite, A.; Brisse, F. *Macromolecules* **1991,** 24, 2221)

3.6.4 Infrared spectroscopy

Figure S-3.2 shows the infrared spectra of pure urea and PEO, and of the bulk and fibers of the PEO-urea inclusion complex. It is clear that the spectrum of the inclusion complex is not a linear sum of those of pure urea and PEO, confirming that the system is not barely a physical mixture. The main differences are observed for the bands due to urea (C=O stretching, N-H bending and N-C-N stretchings) and to the C-O-C stretching bands of PEO. The very close similarity between infrared spectra of the bulk and electrospun fibers of the PEO-urea IC indicates that the crystalline structure of the inclusion complex and the conformation of the PEO chains are not significantly influenced by the electrospinning process.

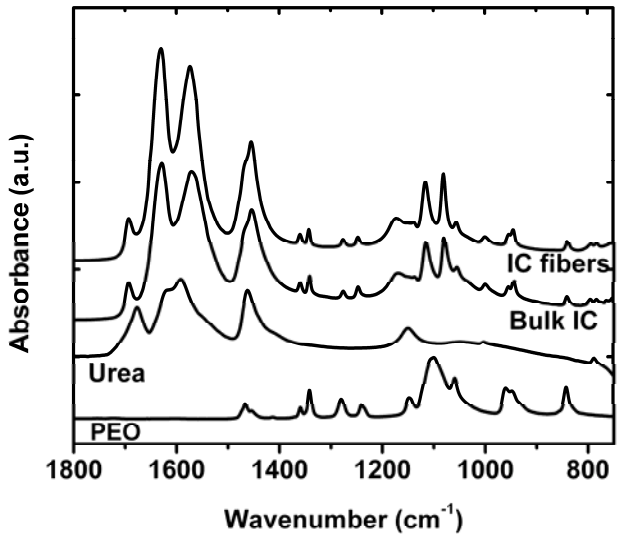

Figure S-3.2. Infrared spectra of pure PEO and urea, and of the bulk and fibers of the PEO-urea inclusion complex (IC).

3.7 References

(1) Theron, A.; Zussman, E.; Yarin, A. L. *Nanotechnology* **2001,** 12, 384; Kameoka, J.; Craighead, H. G. *Appl. Phys. Lett.* **2003,** 83, 371; Li, D.; Wang, Y.; Xia, Y. *Adv. Mater.* **2004,** 16, 361; Ko, F.; Gogotsi, Y.; Ali, A.; Naguib, N.; Ye, H.; Yang, G.; Li, C.; Willis, P. *Adv. Mater.* **2003,** 15, 1161; Katta, P.; Alessandro, M.; Ramsier, R. D.; Chase, G. G. *Nano Lett.* **2004,** 4, 2215.

(2) Dersch, R.; Liu, T.; Schaper, A. K.; Greiner, A.; Wendorff, J. H. *J. Polym. Sci. Part A: Polym. Chem.* **2003,** 41, 545.

(3) Burger, C.; Hsiao, B. S.; Chu, B. *Annu. Rev. Mater. Res* **2006,** 36, 333.

(4) Teo, W. E.; Kotaki, M.; Mo, X. M.; Ramakrishna, S. *Nanotechnology* **2005,** 16, 918.

(5) Ward, I. M., *Structure and Properties of Oriented Polymers*. 2nd ed.; Chapman & Hall: London, 1997.

(6) Zong, X. H.; Ran, S. F.; Fang, D. F.; Hsiao, B. S.; Chu, B. *Polymer* **2003,** 44, 4959.

(7) Fennessey, S. F.; Farris, R. J. *Polymer* **2004,** 45, 4217.

(8) Wang, M.; Yu, J. H.; Kaplan, D. L.; Rutledge, G. C. *Macromolecules* **2006** 39, 1102.

(9) Chenite, A.; Brisse, F. *Macromolecules* **1991,** 24, 2221.

(10) Suehiro, K.; Nagano, Y. *Makromol. Chem.* **1983,** 184, 669; Tadokoro, H.; Yoshihara, T.; Chatani, Y.; Murahashi, S. *J. Polym. Sci. B* **1964,** 2, 363; Tonelli, A. E. *Macromolecules* **1990,** 23, 3134.

(11) Vasanthan, N.; Shin, I. D.; Tonelli, A. E. *Macromolecules* **1996,** 29, 263.

(12) Iwamoto, R.; Saito, Y.; Ishihara, H.; Tadokoro, H. *J. Polym. Sci. part A-2* **1968,** 6, 1509; Yokoyama, M.; Ishihara, H.; Iwamoto, R.; Tadokoro, H. *Macromolecules* **1969,** 2, 184.

(13) Girardeau, T. E.; Zhao, T.; Leisen, J.; Beckham, H. W.; Bucknall, D. G. *Macromolecules* **2005,** 38, 2261; Harada, A.; Li, J.; Kamachi, M. *Nature* **1992,** 356, 325.

(14) Lee, S. O.; Kariuki, B.; Richardson, A. L.; Harris, K. D. M. *J. Am. Chem. Soc.* **2001,** 123, 12684.

(15) Deitzel, J. M.; Kleinmeyer, J.; Harris, D.; Tan, N. C. B. *Polymer* **2001,** 42, 261.

(16) Ge, J. J.; Hou, H.; Li, Q.; Graham, M. J.; Greiner, A.; Reneker, D. H.; Harris, F. W.; Cheng, S. Z. D. *J. Am. Chem. Soc.* **2004,** 126, 15754.

Chapter 4 : Characterization of the Stable and Metastable Poly(ethylene oxide)-Urea Complexes in Electrospun Fibers

4.1 Résumé

L'électrofilage de solutions a été utilisé pour la première fois pour préparer des nanofibres des complexes stable (α) et métastable (β) se formant entre le poly(oxyde d'éthylène) (PEO) et l'urée. Les deux types de fibres sont hautement cristallines et présentent un grand degré d'orientation moléculaire. Le complexe β, qui était très mal connu, a été caractérisé en détail avec la diffraction de rayons X aux grands angles, la spectroscopie infrarouge et la calorimétrie différentielle à balayage. Les résultats ont révélé que la stoechiométrie du complexe PEO:urée est 3:2 et qu'il est orthorhombique avec a = 1.907 nm, b = 0.862 nm, et c = 0.773 nm. Les chaînes de PEO sont orientées selon l'axe de la fibre et leur conformation est affectée de façon significative par les ponts hydrogène avec l'urée comparativement au polymère pur et au complexe stable. Une structure en couches est suggérée pour le complexe métastable, dans laquelle les molécules d'urée seraient arrangées en rubans intercalés entre deux couches de PEO.

4.2 Abstract

Solution electrospinning was used for the first time to prepare nanofibers of the stable (α) and metastable (β) complexes between poly(ethylene oxide) (PEO) and urea. Both types of fibers were highly crystalline and presented a large level of molecular orientation. Detailed characterization of the ill-studied β complex was performed using wide-angle X-ray diffraction, infrared spectroscopy and differential scanning calorimetry. Results reveal that it possesses a 3:2 PEO:urea stoichiometry and suggest that it belongs to the orthorhombic system with a = 1.907 nm, b = 0.862 nm, and c = 0.773 nm. The PEO chains are oriented along the fiber axis and present a conformation significantly affected by strong hydrogen bonding with urea as compared to the pure polymer and the stable complex. A layered structure model is suggested for the metastable complex, in which the urea molecules would be arranged into a ribbon-like structure intercalated between two PEO layers.

4.3 Introduction

Electrospinning is a simple and flexible technique that allows preparing nanofibers of most polymeric materials by the application of a large electric field on a concentrated polymer solution. These fibers are drawing much interest for applications in the life and materials sciences. Interestingly, electrospinning often produces fibers in which the polymers are in unusual or metastable crystalline forms because of the rapid solvent evaporation and the strong electric field and elongational forces involved in the process. For instance, nylon-6 fibers with the γ structure[1,2] and poly(1-butene) fibers with form II crystals[3] could be obtained instead of their usual stable structures. However, polymer chains usually present a low level of molecular orientation in electrospun fibers while, in contrast, extended structures such as carbon nanotubes develop a high level of anisotropy.[4]

It is possible to compel a polymer chain to adopt an extended structure by forming inclusion complexes (IC) with small molecules like urea.[5-7] A stable IC between

poly(ethylene oxide) (PEO) and urea (that we will call form α) was first reported by Tadokoro et al.[8] As in most urea ICs, the guest chains are packed inside narrow channels constructed from an essentially infinite network of hydrogen-bonded urea molecules.[9,10] Brisse and Chenite[11] showed that its stoichiometry is $(EO)_4$-$(urea)_9$, with 6 urea molecules forming the channel structures that include the remaining 3 urea molecules and 4 EO segments. We have recently demonstrated that it is possible to prepare fibers of the α PEO-urea complex by electrospinning a gel-like suspension of the previously co-crystallized IC.[12] The trigonal crystal structure was preserved and the fibers presented a very large molecular orientation, as hypothesized based on the extended structure of PEO inside the channels.

A second type of PEO-urea complex, called form β hereon, has also been prepared by quenching the molten α complex to room temperature.[13-18] It can convert back to the stable α form by heating to 90°C, and was recently reported to be metastable below its transition temperature.[18] The X-ray diffraction patterns of the metastable complex show the presence of residual pure urea crystals, indicating that it is enriched in PEO as compared to the well-studied α complex, but that the sample consists of a mixture. Nevertheless, because of the challenge of preparing a large quantity of the β complex in a pure state (without residual urea), its structure and even its stoichiometry have not been established firmly yet.

Considering the potential of electrospinning to produce unusual polymer structures, we attempted to use it for preparing fibers of the pure stable and metastable forms of the PEO-urea complex in order to characterize their fiber and solid-state structures. We show for the first time that it is possible to prepare highly oriented and crystalline nanofibers of both the stable and metastable PEO-urea complexes by electrospinning solutions (rather than suspensions) with appropriate molar ratios. The structure of the metastable complex was studied using wide angle X-ray diffraction (WAXD), Fourier transform infrared spectroscopy (FT-IR), and differential scanning calorimetry (DSC). The results indicate that the β complex possesses an orthorhombic

crystalline structure with a $(EO)_3$-$(urea)_2$ stoichiometry and allow suggesting a new layered structural model.

4.4 Experimental section

Sample preparation. PEO with a weight-average molecular weight of 400 000 g/mol (Scientific Polymer Products), urea and methanol (Fisher Scientific) were used without further purification. PEO-urea inclusion complexes were prepared by dissolving 0.46 g of PEO in 10 ml of methanol, then adding an appropriate amount of urea to obtain PEO:urea mixtures with mass ratios of 1:0, 1:0.25, 1:0.75, 1:0.91, 1:1.36 and 1:3.06. Full dissolution of PEO and urea was possible by increasing the temperature to 65 ºC. The solutions were introduced in a syringe equipped with a 0.41mm diameter flat-end needle in order to prepare PEO-urea IC fibers by electrospinning. A 15 kV positive voltage was applied on the needle tip using a CZE 100R high-voltage power supply (Spellman High Voltage Electronics), while a 2 kV negative potential (Power Designs) was imposed on two metallic counter-electrodes separated by a 5 cm gap. The distance between the needle and the counter-electrodes was 15 cm, and the solution flow rate was fixed to 0.02 ml/min using a PHD 2000 syringe pump (Harvard Apparatus). Solvent cast films with various mass ratios were prepared as control samples by evaporating the methanol overnight in a vacuum oven.

Characterization. An Axioskop 40 optical microscope (Carl Zeiss) equipped with a 40X polarizing objective and a QImaging digital camera was used to observe the electrospun fibers. The birefringence of the samples was qualitatively verified under crossed polarization geometry. Average fiber diameters were determined using a Hitachi S-4700 scanning electron microscope. Differential scanning calorimetry (DSC) measurements were conducted at a heating rate of 10 °C/min using a TA Instrument 2910 calorimeter calibrated with indium. Infrared spectra were recorded on a Vertex 70 FT-IR spectrometer (Bruker Optics) equipped with a liquid nitrogen-cooled HgCdTe detector. Spectra with a resolution of 4 cm^{-1} were collected in the attenuated total reflection

(ATR) mode using a MIRacle single reflection accessory (Pike Technologies) equipped with a silicon crystal. A Seagull variable angle reflectance accessory (Harrick Scientific Products) equipped with a ZnSe hemispherical crystal and a ZnSe wire-grid polarizer was used to measure the polarized spectra of the fibers. The fibers were aligned perpendicular to the incidence plane and the polarizer was rotated to record spectra parallel and perpendicular to the fiber axis.

Unless otherwise noted, wide angle X-ray diffraction measurements were carried out using a Bruker AXS diffractometer (Siemens Kristalloflex 780 generator) operated at 40 kV and 40 mA, using the Cu Kα (0.1542 nm) radiation collimated by a graphite monochromator and a 0.5 mm pinhole. The fibers were assembled into a bundle and inserted in the path of the incident X-ray beam with the fiber axis along the meridian. The diffraction patterns were captured by a HI-STAR two-dimensional detector. The acquisition time was 30 min for all samples. A scattering background, recorded for the same time but without the sample, was subtracted for display purposes in Figs 4.2 and 4.5a, but the orientation functions were calculated using the original data. To determine the crystal structure of PEO-urea β complex, a higher resolution diffraction pattern was recorded with a Bruker AXS D8 Advance powder diffractometer using an increment of 0.0084º from 15º to 40º. For this experiment only, the fibers were ground into a fine powder and mixed with grease to obtain a smooth sample surface. To avoid any possible subtraction artifact, the data (Fig. 4.7) is presented without any scattering or grease subtraction. The density of the electrospun fibers was measured using a Sartorius CP224S balance equipped with a YDK01 accessory. The fibers were pressed into pellets and their density was determined using both acetone and benzene.

4.5 Results and discussion

4.5.1 Solution electrospinning of the PEO-urea complexes

In a previous work, fibers of the stable α PEO-urea IC were prepared by electrospinning suspensions of the previously co-crystallized complex. This method was quite limitative since the molar composition of the suspension could not be easily controlled. It was later realized that solutions of PEO-urea mixtures could be electrospun directly, as long as spinning is performed sufficiently fast after solution preparation in order to prevent precipitation of the stable inclusion complex. This allowed electrospinning fibers with various PEO:urea ratios to explore the possibility of preparing samples of the pure β form complex. Fig. 4.1 shows two representative examples of crossed-polarized optical micrographs recorded for fibers obtained by electrospinning solutions with 1:0.91 and 1:3.06 PEO:urea mass ratios. The latter corresponds to the 4:9 stoichiometry of the stable α form of the complex. All fibers are smooth and bead-free, and present average diameters of 550±200 nm. They show a strong preferential macroscopic alignment in the direction perpendicular to the rod-like counter-electrodes. All fibers also transmit light when observed under crossed polarizers and are thus birefringent, indicating that they possess a significant level of molecular orientation.

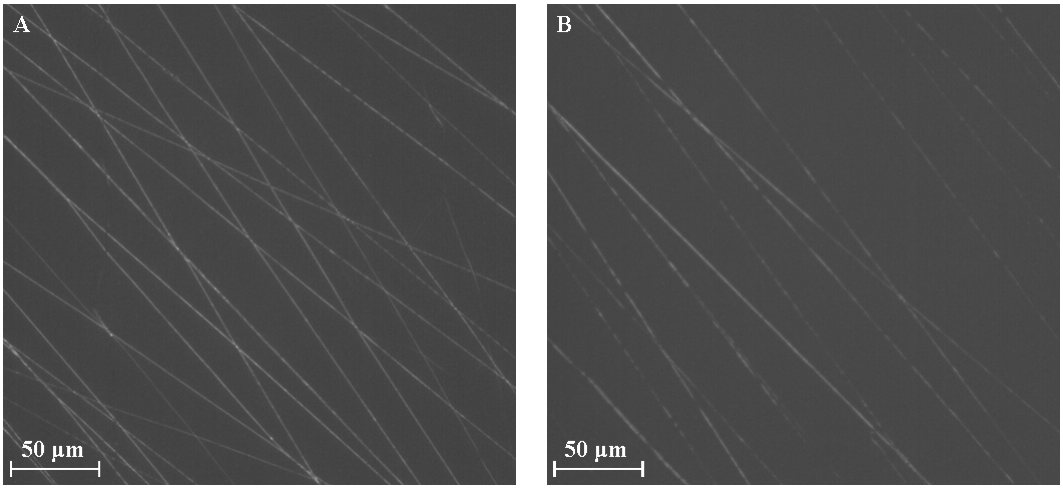

Figure 4.1. Representative crossed-polarized optical micrographs of fibers prepared by electrospinning solutions with A) 4:9 and B) 3:2 PEO:urea molar ratios.

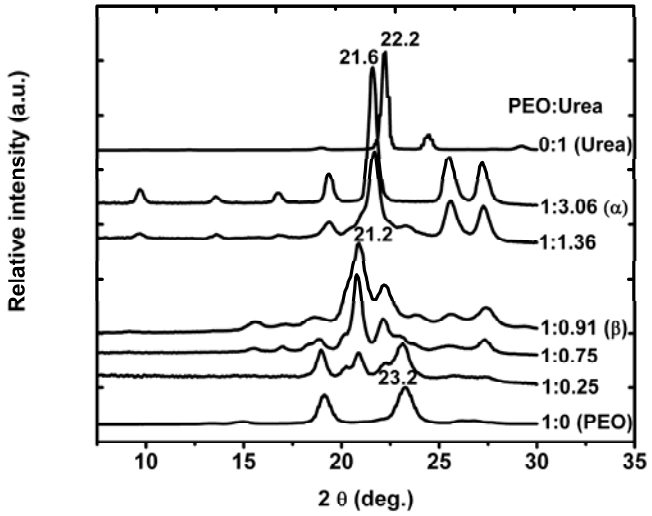

Figure 4.2. Wide-angle X-ray diffraction patterns of electrospun fibers with different PEO:urea mass ratios.

Fibers with different PEO:urea compositions were analyzed by WAXD (Fig. 4.2) and FT-IR spectroscopy (Fig. 4.3). The X-ray diffraction pattern for the 1:3.06 fibers is identical to those reported for the form α IC, either prepared in the bulk by the co-crystallization method[11,17] or as fibers by electrospinning a suspension.[12] This indicates that the crystal structure of this stable IC is independent of the preparation method and thus that solution electrospinning can be an appropriate procedure to prepare nanofibers of inclusion complexes. The WAXD pattern contains only a very weak amorphous halo, suggesting that co-crystallization is both thermodynamically favorable and kinetically rapid. It can also be noted that no peaks due to pure PEO or urea crystals can be observed in this pattern, indicating that complex formation is nearly quantitative when electrospinning solutions with the appropriate stoichiometry.

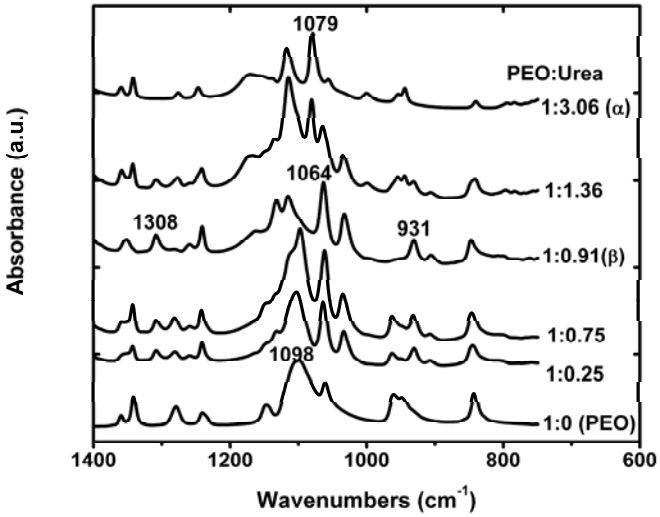

Figure 4.3. Infrared spectra of electrospun fibers with different PEO:urea mass ratios.

When the mass fraction of urea is decreased to 1:1.36, the diffraction pattern is still dominated by the peaks of the α complex, notably by the most intense one at 21.6°, but the sample also contains a significant amount of pure PEO crystals, as revealed by the diffraction at 23.2°. A similar mixture was obtained when slowly evaporating the solvent. Nevertheless, the presence of a shoulder can be noted on the low angle side of the 21.6° peak. This new diffraction peak becomes dominant, with a maximum at 21.2°, when the PEO:urea composition is 1:0.91. The diffraction pattern for this system is completely different from those of pure PEO and of the form α complex, and can be assigned to the form β complex. This specific composition corresponds to a PEO:urea molar ratio of 3:2, a reasonable stoichiometry for such complex. Fig. 4.2 shows that a further decrease in urea content leads to diffraction patterns containing characteristic peaks at both 23.2º and 21.2º, and thus to mixtures of the form β complex with pure PEO.

Table 4.1. Assignment and dichroism of the main infrared absorption bands for pure PEO and the form α and β PEO-urea complexes.[19-21]

Pure PEO	β complex	α complex	Assignment
1359 (⊥)	1351 (∥)	1359 (⊥)	CH_2 wagging
1341 (∥)	1308 (∥)	1341 (∥)	
1279 (⊥)	1259 (∥)	1275 (⊥)	CH_2 twisting
1241 (∥)	1240 (⊥)	1246 (∥)	
1147 (⊥)	1132 (⊥)	1138 (⊥)	C-O-C stretching and C-C stretching
1098 (⊥)	1116 (∥)	1116 (⊥)	
1093 (∥)	1064 (∥)	1079 (∥)	
1059(⊥)	1032 (⊥)	1055 (⊥)	
959 (∥)	931 (∥)	954 (⊥)	CH_2 rocking and C-O-C stretching
947 (⊥)	905 (⊥)	944 (∥)	

FT-IR spectra recorded for the various electrospun fibers confirm the 3:2 PEO:urea stoichiometry for the β complex as established by WAXD. Fig. 4.3 shows significant differences between the spectra of pure PEO and those of the two complexes (also see Table 4.1 for band assignments[19-21]). The spectrum of pure PEO is characterized by two intense and highly overlapped C-O-C stretching bands close to 1098 cm^{-1}, and by the splitting of the CH_2 wagging vibration at 1341 and 1359 cm^{-1}. As expected, the spectrum of the 1:3.06 PEO-urea fiber is identical to that previously reported for the stable α complex.[8,17] It also features the splitting of the CH_2 wagging band, as for pure PEO, but one of the C-O-C stretching bands is red-shifted to 1079 cm^{-1}. In contrast with these two samples, the spectrum of the form β fiber does not show any splitting of the CH_2 wagging but rather a single band at 1351 cm^{-1}. It also features a new band at 1308 cm^{-1}, a further red shift of the C-O-C stretching band to 1064 cm^{-1}, and a red shift of the CH_2 rocking band to 931 cm^{-1}. Based on the presence of these different characteristic bands, it can be confirmed from Fig. 4.3 that both pure PEO and form β

complex are present when the PEO:urea mass ratio is less than 1:0.91, while ternary mixtures of form α, form β and pure PEO are obtained when electrospinning mixtures with compositions between 1:0.91 and 1:3.06. These results support a 3:2 PEO:urea stoichiometry for the β complex, rather than the 1:1 stoichiometry reported for the IC of urea with poly(ethylene glycol) oligomers[22] and suggested for the metastable PEO-urea complex.[18]

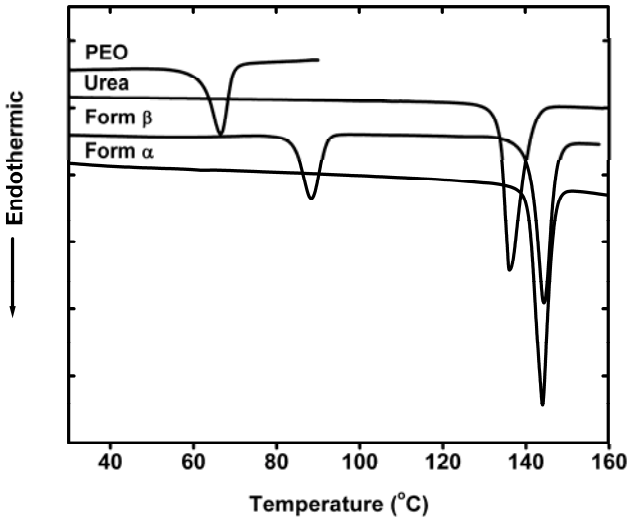

Figure 4.4. DSC thermograms recorded for pure PEO and urea, and for the electrospun fibers of the form β and form α PEO-urea complexes.

Differential scanning calorimetry (DSC) was used to characterize the thermal properties of the complex fibers. The thermograms of Fig. 4.4 show that the α complex fibers present a single melting temperature of 143 °C, well above those of pure PEO (65 °C) and urea (135 °C). This is in excellent agreement with the value obtained for fibers electrospun from a suspension (144 °C),[12] further confirming that the solution process produces unaltered α crystals with no trace of residual pure starting products. The thermogram of the β complex shows two endothermic events at 89 and 143 °C. The latter corresponds to the melting temperature of the α crystal, although the WAXD and

FT-IR data of Figs. 4.2 and 4.3 did not reveal the presence of any α complex in the original sample. The endotherm at 89 °C must then correspond to a melt-recrystallization transition from the β to the α complex. Since the PEO:urea stoichiometry is 3:2 for the former and 4:9 for the latter, the process must release most of the PEO to create a liquid PEO phase, since the melting temperature of pure PEO (65 °C) is well below the β to α transition.

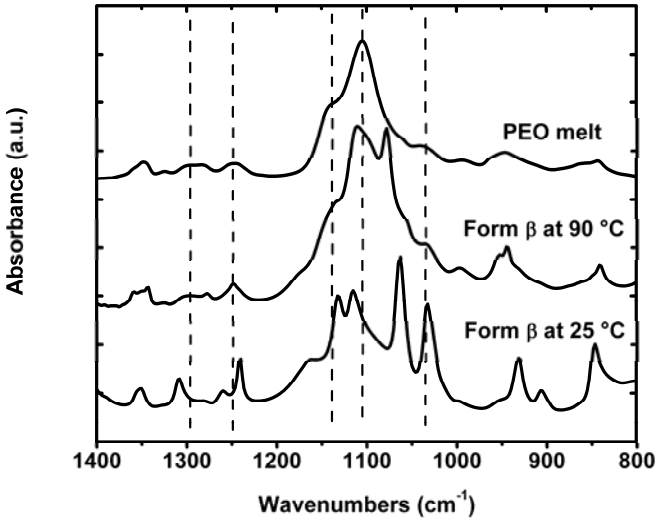

Figure 4.5. Infrared spectra of the form β PEO-urea complex recorded at 25 and 90 ºC, and of pure PEO in the melt state.

This suggestion can be verified by examining the infrared spectra of Fig. 4.5, in which several changes can be observed when heating the β complex from 25 to 90 °C. In particular, the 1064 cm^{-1} C-O stretching band of the β complex shifts to 1080 cm^{-1}, a position characteristic of the α complex. A partial splitting of the CH_2 wagging band around 1350 cm^{-1} is also apparent due to the formation of the stable complex. In addition, various bands indicated by dashed lines confirm the formation of a PEO melt at 90 °C. In particular, the CH_2 twisting and C-O stretching bands become much wider in the high

temperature spectrum than at 25 °C, and appear at the same position as those in the spectrum of pure molten PEO.

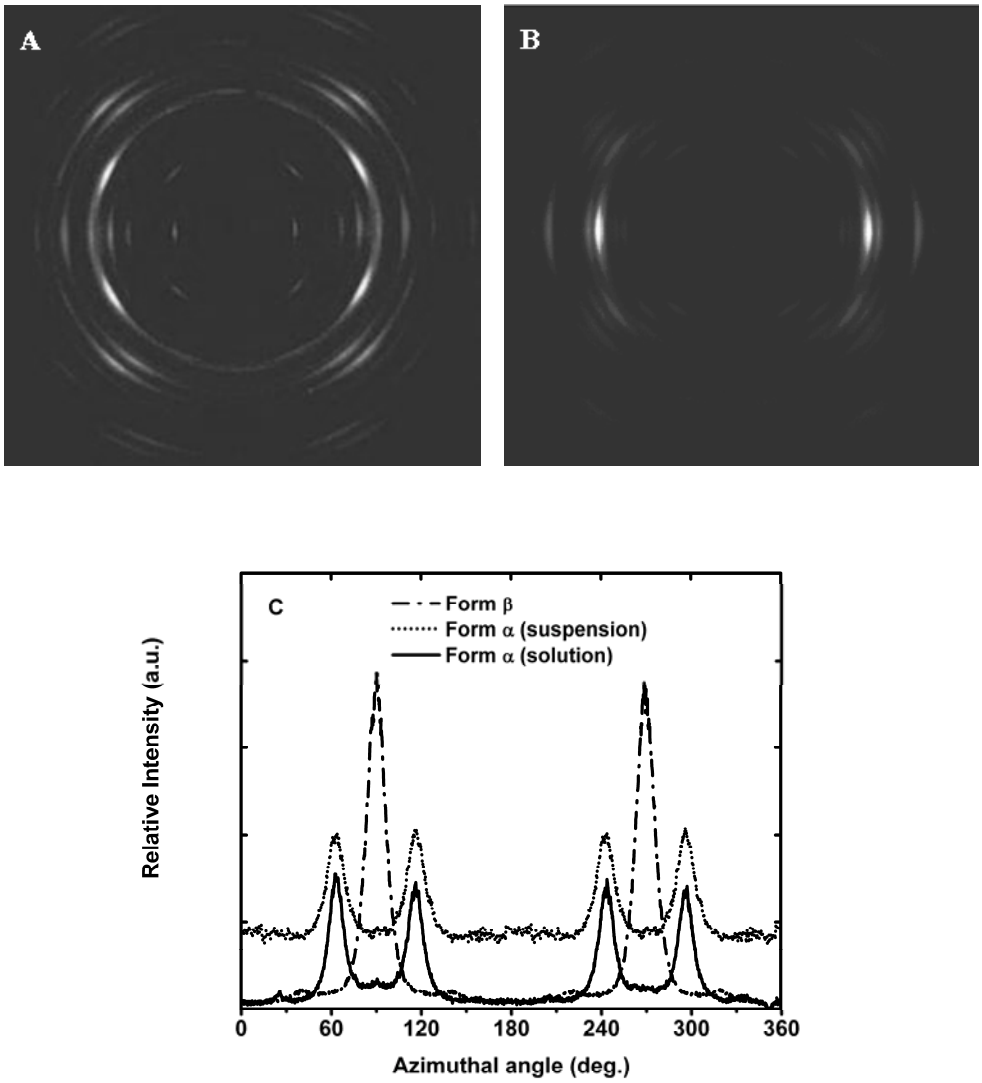

Figure 4.6. Two-dimensional WAXD patterns of the A) form α and B) form β PEO-urea complexes, and C) azimuthal profiles recorded for the form β (2θ = 21.2º) and form α (2θ = 21.6º) fibers prepared by electrospinning of suspensions and solutions.

Although multiple methods have been developed to prepare highly aligned electrospun nanofibers,[23] only a limited number of papers have reported the

development of large molecular orientation.[4,12,24,25] As mentioned above, fibers of the form α IC electrospun from a suspension develop a very large orientation level, which could be explained by the reorientation of the pre-existing crystals as rigid units during the spinning process.[12] This is similar to the "pseudo-affine" model for the orientation development in deformed semi-crystalline bulk polymers.[26] Two-dimensional WAXD patterns were recorded to determine the orientation level for the fibers electrospun from solutions. Figs. 4.6A and 4.6B show that both α and β complexes present relatively sharp X-ray reflections with highly inhomogeneous azimuthal intensity distributions for all crystalline planes. Fig. 4.6C shows the azimuthal scans obtained by integrating the intensity of specific 2θ peaks along the azimuthal angle, φ. Results for the most intense diffraction planes at 2θ = 21.2° and 21.6° are shown for the form β and α fibers, respectively, but similar results were obtained using various diffraction planes. In all cases, narrow peaks with full widths at half height (FWHH) of ca. 13º are observed in the azimuthal intensity plots, indicating strongly anisotropic distribution of the crystals in the fibers.

Assuming uniaxial symmetry along the fiber direction, it is possible to quantify the orientation level by calculating the orientation function, $<P_2(\cos\varphi)>_c$, as:

$$< P_2(\cos\varphi) >_c = \frac{2}{3\cos^2\sigma - 1}\frac{3 < \cos^2\varphi > -1}{2} \qquad (4.1)$$

where σ is the angle between the normal to the plane and the c axis, and the brackets indicate a mean value over the distribution of orientation. The $<\cos^2\varphi>$ value was determined using:

$$< \cos^2\varphi >= \frac{\int_0^{\pi} I(\varphi)\cos^2\varphi\sin\varphi d\varphi}{\int_0^{\pi} I(\varphi)\sin\varphi d\varphi} \qquad (4.2)$$

The background intensity was determined by interpolating the diffraction intensity (without air scattering subtraction) at 2θ positions above and below the diffraction peak of interest, at the azimuthal position furthest away from the diffraction peak. Average $\langle P_2(\cos\varphi)\rangle_c$ values of 0.75 and 0.79 were obtained for the α and β complex fibers, respectively. It should be emphasized that such $\langle P_2(\cos\varphi)\rangle_c$ values are quite large, considering that a maximum orientation function of 1 would be obtained for a perfectly oriented sample. This suggests that the development of a large molecular orientation does not require the presence of pre-existing crystals in the spinning dope.[12] It is plausible that the elongational forces at work during the whipping process lead to the formation of oriented crystallization nuclei, and that the following crystal growth is highly directionalized. This whipping mode is due to charge-charge repulsion and causes a chaotic bending of the electrospun jet and a drastic decrease in fiber diameter. Considering the stoichiometry of the β crystal, 3 PEO repeat units for 2 urea molecules, the urea may not form a channel structure as in the α co-crystal, as will be discussed later. Nevertheless, relatively strong hydrogen bonding interactions between PEO and urea could contribute to the orientation development in the complex by rigidifying the macroconformation of PEO.

4.5.2 Structure of the form β PEO-urea complex

Our attempts to prepare pure β complex samples by solvent casting or co-crystallization of solutions have led to various mixtures of PEO and the two types of complexes, even when the appropriate 3:2 PEO:urea stoichiometry was used. Its successful preparation by electrospinning could then be attributed to the fast solvent evaporation that occurs on a millisecond time scale.[27] This suggests that formation of the β complex requires kinetically preventing the formation of the stable α complex, in agreement with the report that the β complex is metastable.[18] While single crystals of the form β complex could not be grown, the fact that the electrospun fibers are highly crystalline and oriented can help determining its lattice parameters.

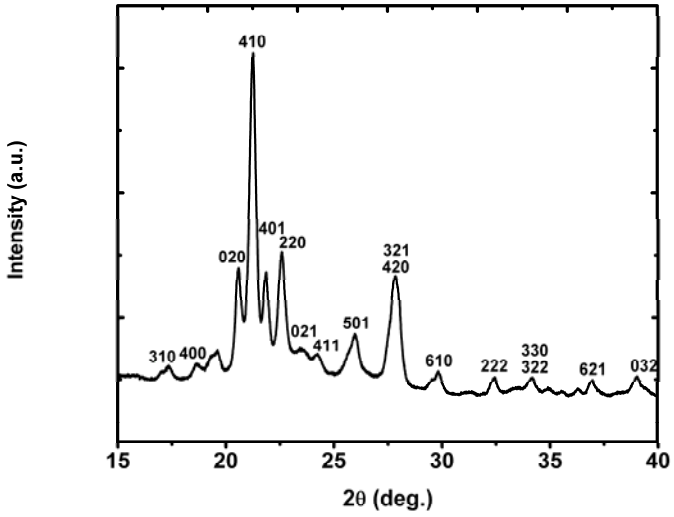

Figure 4.7. Higher resolution WAXD pattern of the form β PEO-urea complex.

A WAXD pattern of the β complex was recorded with a better 2θ resolution and is shown in Fig. 4.7. After careful analysis, it is proposed that the β complex crystal could possess an orthorhombic structure with a = 1.907 nm, b = 0.862 nm and c = 0.773 nm. Table 4.2 provides the suggested assignment for the most intense diffraction peaks. Because the electrospun fibers are highly oriented, it is possible to further support these new assignments by comparing σ, the calculated angle between the normal direction to a given hkl plane and the c axis, with the experimentally measured maximum azimuthal angle, φ_{max}, between the plane normal and the fiber axis. It can be seen in Table 4.2 that the calculated angles are in good agreement with the experimentally observed values, further supporting the orthorhombic unit cell parameters. In contrast, significant angle mismatches are found when considering the tetragonal unit cell of the poly(ethylene glycol)-urea complex, [22] suggesting that their structures are different.

Table 4.2. Crystal plane attribution for the form β PEO-urea complex based on an orthorhombic unit cell with a = 1.907 nm, b = 0.862 nm and c = 0.773 nm. σ is the calculated angle between the normal of an hkl plane and the c axis, while φ_{max} is the measured maximum of the azimuthal angle.

2θ peak	17.3	18.6	20.6	21.2	21.9	22.6	24.2	25.9
Plane attribution	310	400	020	410	401	220	411	501
σ cal (°)	90	90	90	90	58.3	90	62	63.7
φ_{max} exp (°)	90	90	90	90	55	90	57	55

Even if the crystalline structure cannot be determined at this point, it is interesting to sketch a model for the organization of the PEO and urea molecules in the β complex based on the currently available information. Considering that the lattice dimensions yield a unit cell volume of 1.271 nm^3 and that the PEO:urea stoichiometry is 3:2, it is likely that there are 12 PEO repeat units and 8 urea molecules $[(EO)_{12}(urea)_8]$ in each unit cell. This leads to a calculated density of 1.317 g/cm^3, very close to that of pure urea (1.314 g/cm^3) and slightly lower than that of the form α IC (1.331 g/cm^3) at room temperature.[11] The experimentally measured densities were 1.313, 1.286, and 1.317 g/cm^3 for pure urea, the β complex, and the α IC, respectively, in good agreement with the calculated values. The density of pure urea was almost identical to the expected value, while those of the form α and β complexes were 1-3% below the calculated ones. This can be explained by the fact that the samples are not 100% crystalline and that imperfect crystal structures can be obtained by electrospinning.

Infrared spectroscopy can provide additional information about the organization of PEO and urea in the complex. It is well known that the conformation of pure crystalline PEO is a 7_2 helix with trans-gauche-trans (TGT) O-C-C-O sequences.[28] Brisse and Chenite[11] have described the conformation of PEO in the stable α complex as an approximate 4_1 helix with a distorted TGT structure. The distances per repeat unit are 0.278 nm in pure PEO and a slightly squashed 0.231 nm in the α complex. Fig. 4.3 and Table 4.1 show that the infrared bands related to the CH_2 wagging, twisting and rocking

vibrations are very similar for these two samples, suggesting that the C-C bonds remain mostly in a gauche conformation. More significant shifts occur in the C-O-C stretching region, where pure PEO shows a broad band consisting of components at 1098 and 1093 cm^{-1} that are shifted to 1116 cm^{-1} and 1079 cm^{-1} in the α complex. The latter band positions are quite similar to those observed in the spectrum of dioxane, for which a gauche conformation around the C-O bonds is imposed by a cyclic structure.[29] On the other hand, pure PEO also shows absorption at 1080 cm^{-1} when dissolved in water, with which it forms hydrogen bonds, but not in its pure melt even if a range of conformations are present. These observations suggest that hydrogen bonding is at the origin of the C-O conformation distortion in the α complex.

As noted above, the infrared spectrum of the β complex is quite different from those of pure PEO and of the α complex. The low-frequency C-O-C stretching band is further red-shifted to 1064 cm^{-1}, suggesting stronger hydrogen bonding and distortion of the conformation around the C-O bonds. In agreement with this, Fig. 4.8 reveals that the N-H stretching bands also appear at lower frequencies in the spectrum of the β complex than in that of the α complex. The CH_2 wagging vibration is also quite different as it appears as a single band at 1351 cm^{-1} rather than as a doublet, and a new band appears at 1308 cm^{-1}, suggesting a significant conformational change around the C-C bonds. It has been reported that the spectrum of mechanically deformed PEO contains a new band with parallel dichroism at 1301 cm^{-1}, similar to that observed at 1308 cm^{-1} in Fig. 4.9, and was ascribed to the formation of an all-trans (TTT) planar-zigzag structure.[30,31] It is thus possible that the torsion angle of the C-C bond strongly departs from gauche in the β complex.

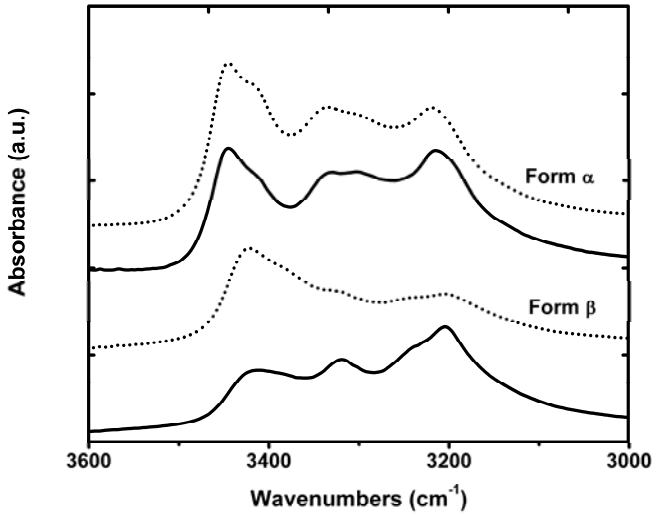

Figure 4.8. Polarized infrared spectra of the form α and form β PEO-urea complex fibers in the N-H stretching region. Solid and broken lines represent spectra measured with the radiation polarized parallel and perpendicular to the fiber direction, respectively.

The polarized infrared spectra of Fig. 4.9 reveal a parallel dichroism for the transition dipole moments of the CH_2 wagging and C-O-C stretching vibrations, indicating that the PEO chains are oriented along the fiber direction. Considering that c = 0.773 nm in the orthorhombic unit cell, it can be concluded that there are 3 EO repeat units along the c direction with a repeat distance of 0.258 nm. Indeed, fitting 4 EO units would only leave 0.193 nm per repeat unit, while 2 EO units would lead to a repeat distance (0.386 nm) longer than that of the fully extended all-trans conformation (0.365 nm). Since there are 12 EO units per cell, 4 PEO chains should pass through the ab plane, as observed in the case of pure PEO.[28] It can be noted that a repeat length of 0.258 nm is intermediate between the values found in pure PEO (0.278 nm)[28] and in the form α complex (0.231 nm)[11]. This is in agreement with the infrared spectroscopy results that suggested distorted C-O bonds, which would make the chains more compact than the

pure PEO helix, but also C-C bonds with some trans character, that would make it slightly more extended than in the α complex.

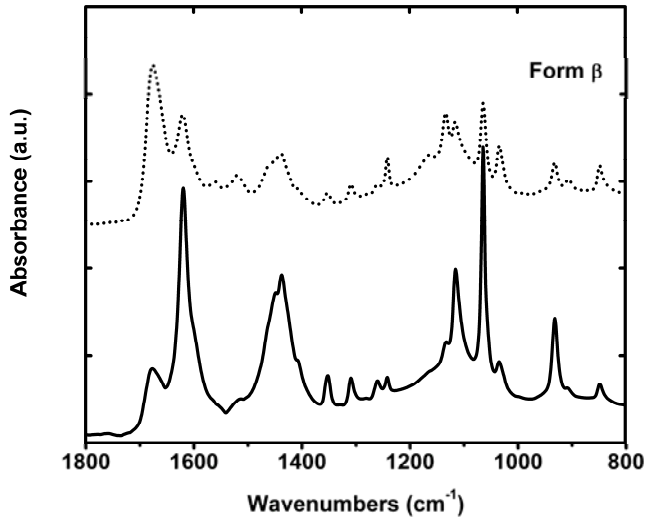

Figure 4.9. Polarized infrared spectra of the form β PEO-urea complex fibers prepared by electrospinning. Solid and broken lines represent the spectra measured with the radiation polarized parallel and perpendicular to the fiber direction, respectively.

Taking into account the crystal dimensions, the hydrogen bonding interactions between the N-H groups of urea and the ether groups of PEO, and the orientation of the PEO chains along the fiber axis, two model structures can be drawn as in Scheme 4.1. Both correspond to a sandwich-like structure in which the PEO chains are in the corners of the ab plane and are separated (in the larger a direction) by a layer composed of either chains or ribbons of urea molecules. Indeed, it has been suggested that urea can form stable hydrogen-bonded networks of both types,[32,33] with chains being observed in pure urea.[34,35] Information about the urea organization, and discrimination between the two models, can be obtained from the polarized infrared spectra of Figs. 4.8 and 4.9. The N-

H stretching bands show a relatively strong dichroism in Fig. 4.8, with the antisymmetric stretching vibration (3407 cm^{-1}) perpendicular to the fiber axis and the symmetric stretching vibration (3309 cm^{-1}) parallel to it. Such dichroism strongly supports the ribbon structure of model II as compared to the chains of model I. Indeed, these two bands have transition dipole moments that are oriented mostly parallel and perpendicular, respectively, to the carbonyl group. Supporting evidence is provided in Fig. 4.9 by the strong parallel dichroism of the C-N antisymmetric stretching vibration at 1470 cm^{-1}, as well as by the perpendicular dichroism of the NH_2 rocking vibration at 1150 cm^{-1}.

It is interesting to note that, in contrast with the previous case, the N-H stretching bands of the α complex fibers show very little infrared dichroism in Fig. 4.8, in spite their large WAXD orientation function. This can be understood by considering that in the crystal structure of the α complex, the channel-forming urea molecules and those included inside the channels orient in different directions, leading to a low average orientation.[11] The strong urea orientation observed in Figs. 4.8 and 4.9 for the β complex fibers is thus consistent with a much simpler structure. Normally, one could have used the amide bands in the 1700 – 1500 cm^{-1} region to determine the orientation of urea in the complex. However, in spite of abundant work, there still remains uncertainty about the assignment of these bands even for pure urea. Some authors[36,37] assigned the higher wavenumber band to C=O stretching and the lower ones to NH_2 deformations, as for simple amide groups, while others[38,39] made the opposite assignment. It is possible to attribute these bands in the spectrum of the form β PEO-urea complex based on their dichroism in Fig. 4.9. Since the C=O groups are perpendicular to the fiber axis in model II, the C=O stretching-dominated amide I band must be the one showing perpendicular dichroism at 1677 cm^{-1}, while NH_2 deformation would contribute mostly to the parallel band at 1619 cm^{-1}.

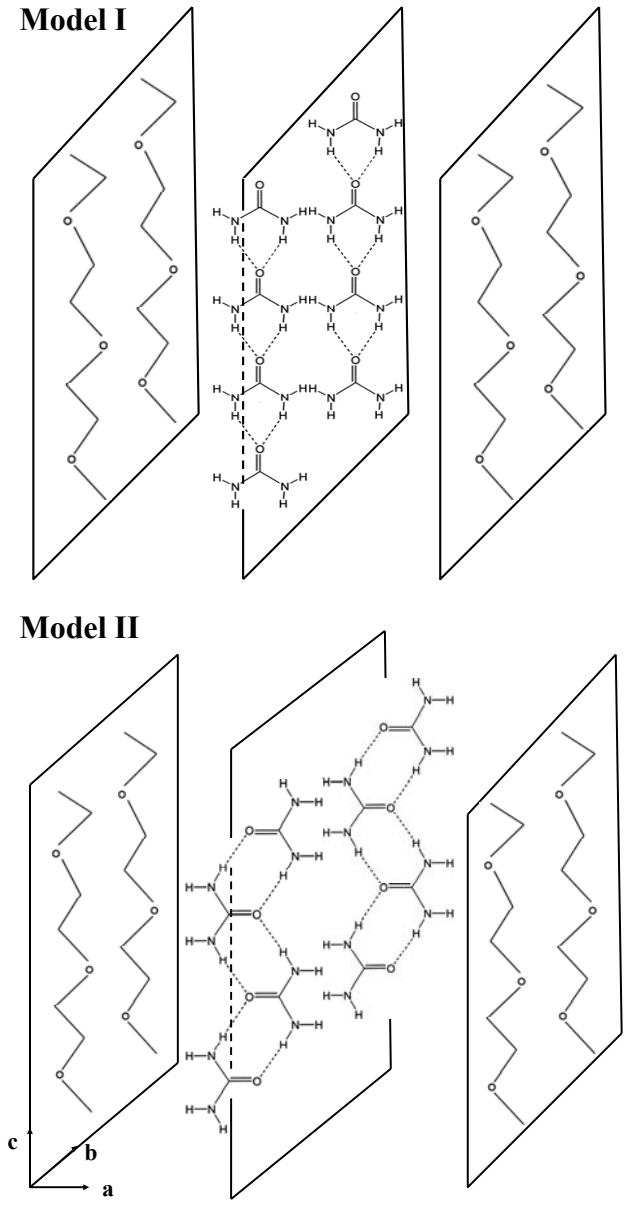

Scheme 4.1. Two possible structural models for the orthorhombic PEO-urea β complex.

It can be noted that the suggested model II appears plausible when considering the a and b dimensions determined by X-ray diffraction for the β complex. Indeed, the unit cell of pure PEO, which also contains 4 chains in the ab plane, has a and b

dimensions of 0.805 and 1.304 nm.[28] The first is quite close to the b length proposed here for the β complex, which would similarly contain only PEO chains. A difference of 0.603 nm is found between the proposed a axis for the complex and the b dimension of pure PEO. Such difference is, at least qualitatively, consistent with the intercalation of a ribbon of interdigitated urea molecules.

The putative model II is also consistent with the DSC results of Fig. 4.4, in which the melting temperature was found to increase in the order of PEO < β complex < urea < α complex. The higher transition temperature for the β complex as compared to pure PEO can be explained by the strength of the intermolecular interactions in the crystal. While the polymer chains are only held by van der Waals forces in pure PEO crystals, additional stronger PEO-urea and urea-urea hydrogen bonds exist in the β complex. The fact that the transition temperature of the α complex is 54 ºC higher than that of the β complex can be rationalized by considering the strength of the intermolecular interactions. All molecules in the first form a continuous three-dimensional network of hydrogen bonds because the PEO chains are included in continuous channels and do not interact directly with one another.[11] This is not he case in the β complex because of its layered structure. Obviously, all molecules in pure urea crystals also form a continuous network of hydrogen bonds. The observation of a 9 °C higher melting point for the α complex could be explained by a smaller entropy of fusion in the complex. Indeed, polymer chains gain much less entropy upon melting than small molecules do. A higher melting temperature is then reasonable even if the enthalpy of fusion is potentially smaller for the complex.

4.6 Conclusions

It was shown for the first time that solution-based electrospinning can be used to prepare nanofibers of the pure stable (form α) and "metastable" (form β) PEO-urea complexes. Both types of fibers present a high degree of crystallinity and a large level of molecular orientation, with WAXD orientation functions of ~0.77. The form α fibers

possess the expected $(EO)_4(urea)_9$ stoichiometry and a structure identical to that of fibers prepared from a suspension of the inclusion complex. The stoichiometry of the form β complex was shown to be $(EO)_3(urea)_2$ by WAXD and infrared spectroscopy, and its crystals is proposed to belong to the orthorhombic system (a = 1.907 nm, b = 0.862 nm and c = 0.773 nm) with a unit cell that contains 12 PEO repeat units and 8 urea molecules. Infrared spectroscopy indicates that the PEO chains are oriented along the c direction (fiber axis) and possess a conformation that significantly departs from those of pure PEO or the α complex, likely because of strong hydrogen bonding with urea. A model structure is suggested, in which 4 PEO chains would pass through the ab plane (with 3 repeat units along the c axis) to form two PEO layers along the a axis, while the 8 urea molecules would form an intercalated ribbon-like layer. Such a model explains the relative melting temperature observed for the pure compounds and the two types of complex. The possibility of preparing bulk amounts of the β PEO-urea complex will facilitate the in-depth characterization of the phase behavior of the PEO-urea system.

4.7 Acknowledgements

The financial support of the Natural Sciences and Engineering Research Council of Canada (NSERC), the Fonds Québécois de Recherche sur la Nature et les Technologies (FQRNT) and the Canada Foundation for Innovation (CFI) is acknowledged. HA also thanks NSERC for an undergraduate student research award. The authors thank Dr. Thierry Maris and Huguette Dinel for their help with the higher resolution XRD experiments and the density measurements, respectively.

4.8 References

(1) Liu, Y.; Cui, L.; Guan, F.; Gao, Y.; Hedin, N. E.; Zhu, L.; Fong, H. *Macromolecules* **2007**, 40, 6283.

(2) Stephens, J. S.; Chase, D. B.; Rabolt, J. F. *Macromolecules* **2004**, 37, 877.

(3) Lee, K.-H.; Snively, C. M.; Givens, S.; Chase, D. B.; Rabolt, J. F. *Macromolecules* **2007**, 40, 2590.

(4) Ge, J. J.; Hou, H.; Li, Q.; Graham, M. J.; Greiner, A.; Reneker, D. H.; Harris, F. W.; Cheng, S. Z. D. *J. Am. Chem. Soc.* **2004**, 126, 15754.

(5) Tonelli, A. E. *Macromolecules* **1990**, 23, 3134.

(6) Tonelli, A. E. *Macromolecules* **1991**, 24, 1275.

(7) Tonelli, A. E. *Macromolecules* **1992**, 25, 3581.

(8) Tadokoro, H.; Yoshihara, T.; Chatani, Y.; Murahashi, S. *J. Polym. Sci. B* **1964**, 2, 363.

(9) Hollingsworth, M. D.; Harris, K. D. M., *Comprehensive Supramolecular Chemistry*. Elsevier Science Ltd.: Oxford, 1996; Vol. 6, p 177.

(10) Harris, K. D. M. *Chem. Soc. Rev.* **1997**, 26, 279.

(11) Chenite, A.; Brisse, F. *Macromolecules* **1991**, 24, 2221.

(12) Liu, Y.; Pellerin, C. *Macromolecules* **2006**, 39, 8886.

(13) Bogdanov, B.; Michailov, M.; Uzov, C.; Gavrailova, G. *Makromol. Chem.* **1994**, 195, 2227.

(14) Bogdanov, B.; Mikhailov, M.; Uzov, K.; Gavrailova, G. *Angew. Makromol. Chem.* **1992**, 195, 165.

(15) Bogdanov, B.; Mikhailov, M.; Uzov, K.; Gavrailova, G. *J. Polym. Sci. Part B: Polym. Phys.* **1994**, 32, 387.

(16) Bogdanov, B.; Uzov, C.; Gavrailova, G. *Acta Polym.* **1994**, 45, 381.

(17) Vasanthan, N.; Shin, I. D.; Tonelli, A. E. *Macromolecules* **1996**, 29, 263.

(18) Ye, H. M.; Peng, M.; Xu, J.; Guo, B. H.; Chen, Q.; Yun, T. L.; Ma, H. *Polymer* **2007**, 48, 7364.

(19) Miyazawa, T.; Fukushima, K.; Ideguchi, Y. *J. Chem. Phys.* **1962**, 37, 2764.

(20) Matsuura, H.; Miyazawa, T. *J. Polym. Sci. part A-2* **1969**, 7 1735.

(21) Dissanayake, M. A. K. L.; Frech, R. *Macromolecules* **1995**, 28, 5312.

(22) Suehiro, K.; Nagano, Y. *Makromol. Chem.* **1983**, 184, 669.

(23) Li, D.; Wang, Y.; Xia, Y. *Adv. Mater.* **2004**, 16, 361.

(24) Kakade, M. V.; Givens, S.; Gardner, K.; Lee, K. H.; Chase, D. B.; Rabolt, J. F. *J. Am. Chem. Soc.* **2007**, 129, 2777.

(25) Kim, G.-M.; Wutzler, A.; Radusch, H.-J.; Michler, G. H.; Simon, P.; Sperling, R. A.; Parak, W. J. *Chem. Mater.* **2005**, 17, 4949.

(26) Ward, I. M., *Structure and Properties of Oriented Polymers*. 2nd ed.; Chapman & Hall: London, 1997.

(27) Greiner, A.; Wendorff, J. H. *Angew. Chem. Int. Ed.* **2007**, 46, 5670.

(28) Tadokoro, H.; Yoshihara, T.; Tahara, S.; Murahashi, S. *Makromol. Chem.* **1964**, 73, 109.

(29) Liu, K. J.; Parsons, J. L. *Macromolecules* **1969**, 2, 529.

(30) Takahashi, Y.; Sumita, I.; Tadokoro, H. *J. Polym. Sci. Polym. Phys. Ed.* **1973**, 11, 2113.

(31) Tashiro, K.; Tadokoro, H. *Rep. Prog. Polym. Phys. Jpn.* **1978**, XXI, 417.

(32) Masunov, A.; Dannenberg, J. J. *J. Phys. Chem. A* **1999**, 103, 178.

(33) Masunov, A.; Dannenberg, J. J. *J. Phys. Chem. B* **2000**, 104, 806.

(34) Keller, W. E. *J. Chem. Phys.* **1948**, 16, 1003.

(35) Waldron, R. D.; Badger, R. M. *J. Chem. Phys.* **1950**, 18, 566.

(36) Ha, T. K.; Puebla, C. *Chem. Phys.* **1994**, 181, 47.

(37) Vijay, A.; Sathyanarayana, D. N. *J. Mol. Struct.* **1993**, 295, 245.

(38) Keuleers, R.; Desseyn, H. O.; Rousseau, B.; Alsenoy, C. V. *J. Phys. Chem. A* **1999**, 103, 4621.

(39) Grdadolnika, J.; Marechal, Y. *J. Mol. Struct.* **2002**, 615, 177.

Chapter 5 : Stability and Phase Behavior of the Poly(ethylene oxide)-Urea Complexes Prepared by Electrospinning

5.1 Résumé

Le système binaire poly(oxyde d'éthylène)-urée forme un complexe stable (α) qui peut être trempé à partir du fondu pour donner un mélange d'urée et d'un second complexe (β) ayant une stoechiométrie différente. Nos résultats confirment que ce mélange est métastable, mais que la transition solide-solide $\beta - \alpha$ est beaucoup plus lente que ce qui avait été suggéré auparavant. En contraste avec le mélange trempé à partir du fondu, il a été observé pour la première fois que le complexe β pur, préparé par électrofilage, est thermodynamiquement stable jusqu'à sa température de fusion. Cette fusion est incongruente et mène à la formation de complexe cristallin α et de PEO liquide. Un diagramme de phases a été tracé sur toute la gamme de compositions et a permis d'interpréter la formation de plusieurs mélanges hors d'équilibre qui sont observés expérimentalement. Ce travail démontre aussi une nouvelle possibilité intéressante de l'électrofilage: la préparation de composés thermodynamiquement stables qui seraient inaccessibles autrement à cause de la formation de produits gelés cinétiquement.

5.2 Abstract

The poly(ethylene oxide) – urea binary system forms a stable (α) complex that can be melt-quenched into a mixture of urea and a second (β) complex with a different stoichiometry. Our results confirm that this mixture is metastable, but that the β – α solid-solid transition is much slower than previously reported. In contrast with the melt-quenched mixture, we observe for the first time that the pure β complex, prepared by electrospinning, is thermodynamically stable up to its melting temperature. This melting is incongruent and leads to the formation of the crystalline α complex and liquid PEO. A phase diagram is drawn over the complete composition range and allows interpreting the formation of the various out-of-equilibrium mixtures observed experimentally. This work also demonstrates an interesting new possibility of electrospinning: the preparation of thermodynamically stable compounds that are otherwise inaccessible because of the formation of kinetically frozen products.

5.3 Introduction

The molecular complexes of poly(ethylene oxide) (PEO) and urea have received renewed attention in recent years. For instance, it was shown that they can form highly oriented fibers through electrospinning that could lead to new applications. [1,2] Nevertheless, a complete phase diagram has not yet been obtained for this binary system and the stability of the different complex forms is not fully established. [3-6] Up to now, three crystalline modifications have been reported for PEO-urea system. The stable α complex, with a $(EO)_4$-$(urea)_9$ stoichiometry, was first reported by Tadokoro et al. [3] Brisse and Chenite prepared single crystals and showed that it belongs to the trigonal system with $a = b = 1.054$ nm, $c = 0.912$ nm, and $\gamma = 120°$ at 173 K. [4] A different crystalline structure was reported for the complex of urea with low molecular weight PEO (M_w = 400 Da), with a 1:1 PEO:urea molar ratio and a tetragonal unit cell ($a = b =$ 0.73 nm, $c = 1.951$ nm). [7] Finally, Bogdanov et al. prepared a third crystalline PEO-urea complex (called "melt-quenched" β hereon) by quenching the α complex from above its

melting temperature. [8-11] It has been hypothesized [5] that it could adopt the hexagonal structure ($a = b = 0.819$ nm, $c = 1.103$ nm) observed for the urea complexes with other polymers [12-14] and small molecules, [15] or that it adopts the tetragonal structure of the low molecular weight PEO-urea complex. [16]

The observation of two stoichiometric complexes has also been reported by Damman et al. for PEO with other host molecules, such as resorcinol [17] and p-nitrophenol. [18-20] In both cases, the β form was found to be metastable and to rapidly transform into the stable α form. [21] In contrast, two thermodynamically stable complexes were observed for the PEO system with 2-methyl resorcinol (MRES). [22,23] The low-melting point complex (7:2 PEO:MRES molar ratio) possesses a layered structure, while the 3:1 complex forms a tight hydrogen-bonded network and shows a higher melting temperature. It is well known that the melt-quenched PEO-urea β samples can rapidly convert back to the α form when heated above 90 °C. [8-11] Importantly, Ye et al. have recently showed that a solid-solid β – α transition can take place slowly at much lower temperatures, even at room temperature, suggesting that the complex is in fact metastable. [16]

A limiting factor in the study of the PEO-urea system has always been the preparation of pure samples of the β complex. In spite of efforts to isolate it, wide-angle X-ray diffraction (WAXD) patterns of the melt-quenched sample usually reveal the presence of some residual urea or α complex. This experimental difficulty has left open the question of whether the β complex is stable or metastable by itself, therefore preventing the drawing of a complete phase diagram and a proper understanding of the complex phase behavior.

In a recent paper, we have shown that it is possible to prepare almost pure samples of both α and β complexes in bulk amounts using electrospinning. [2] In this technique, a large electric field is applied to an entangled polymer solution to produce nanofibers. [24-26] It has been shown that electrospinning can impart molecular orientation parallel to the fiber axis [1,27,28] and that it sometimes produces metastable structures. [29,30]

In our previous work, the α and β complex fibers presented a high level of crystallinity and orientation without the need for a thermal annealing or mechanical deformation. [2] WAXD and Fourier transform infrared (FT-IR) spectroscopy characterization of these electrospun fibers revealed that the stoichiometry of the pure β complex is $(EO)_3$-$(urea)_2$, and suggested a layered orthorhombic crystal structure with a = 1.907 nm, b = 0.862 nm and c = 0.773 nm [2]. This layered structure is reminiscent of that of the stable low-melting point complex of PEO with MRES. [22] The availability of these samples now allows revisiting the stability and phase diagram of the PEO-urea complexes. It will be shown using variable-temperature WAXD and FT-IR that the pure β complex is stable, in contrast with the melt-quenched sample. A phase diagram drawn using samples prepared by electrospinning will allow interpreting the rich phase behavior of the PEO-urea system.

5.4 Experimental section

5.4.1 Sample preparation

PEO with a weight-average molecular weight of 400 000 g/mol (Scientific Polymer Products) and, urea (Fisher Scientific) were used without further purification. The α complex was prepared using a previously described co-crystallization method. [1] The melt-quenched β sample was prepared by heating the α complex to 160 °C (17 °C above its melting point) and cooling it to room temperature at a rate of at least 10 °C/min. The pure β complex and the various samples used to determine the phase diagram were prepared by electrospinning solutions of PEO and urea in water. 0.5 g of PEO was dissolved in 10 ml of distilled water and an appropriate amount of urea was added to obtain mixtures with various PEO:urea molar ratios. A PEO:urea molar ratio of 3:2 was used to prepare samples of almost pure β complex. The solutions were introduced in a syringe equipped with a 0.41 mm diameter flat-end needle. A 15 kV positive voltage was applied on the needle tip using a CZE 1000R high-voltage power supply (Spellman High Voltage Electronics) while a 2 kV negative potential (Power Designs) was imposed on a rotating cylinder collector to collect the electrospun fibers.

The as-prepared electrospun fibers were folded and ground to obtain randomly oriented samples for the following DSC, FT-IR and WAXD characterization.

5.4.2 Sample characterization

DSC measurements were conducted using TA Instruments 2910 or Q1000 calorimeters calibrated with ultra-pure indium. The heating rate was 10 °C/min and the cooling rate was either 10 or 3 °C/min. Infrared spectra with a resolution of 4 cm^{-1} were recorded on a Vertex 70 FT-IR spectrometer (Bruker Optics) equipped with a liquid nitrogen-cooled HgCdTe detector. Spectra were collected in the attenuated total reflection (ATR) mode using a MIRacle accessory (Pike Technologies) or a temperature-controlled GoldenGate accessory (Specac). Wide-angle X-ray diffraction measurements were carried out using a Bruker AXS diffractometer (Siemens Kristalloflex 780 generator), operated at 40 kV and 40 mA, using the Cu Kα (0.1542 nm) radiation collimated by a graphite monochromator and a 0.5 mm pinhole. The diffraction patterns were captured by a HI-STAR area detector. The samples were sealed in aluminum pans and their temperature was controlled by an STC 200 controller and an LN2-SYS liquid nitrogen cooling system (Instec). A scattering background was subtracted for display.

5.5 Results and discussion

5.5.1 Phase transitions of the α and melt-quenched complexes

Although the crystalline structure of the α complex has been established for many years, its phase behavior is still not fully understood. Fig. 5.1 shows the DSC thermograms of this complex during a heat-cool-heat cycle. During the first heating scan, the crystalline α complex melts at 143 °C, higher than the melting points of pure PEO (67 °C) and urea (135 °C). Two exothermic peaks appear during the cooling cycle at 10 °C/min, under conditions that produce the melt-quenched β complex. The first peak at 90 °C is very narrow and indicates a fast crystallization that is more typical of

small molecules than polymers. The second exotherm at 65 °C, which has not been reported in the literature, is much broader, characteristic of the slower crystallization rate of polymers. The exothermic peak at 95 °C observed during the second heating ramp can be attributed to the β - α phase transition. The newly formed α complex melts at 140 °C and the melting enthalpy is 30% smaller than in the first heating scan, indicating a decreased level of crystallinity and less perfect crystals than in the original sample.

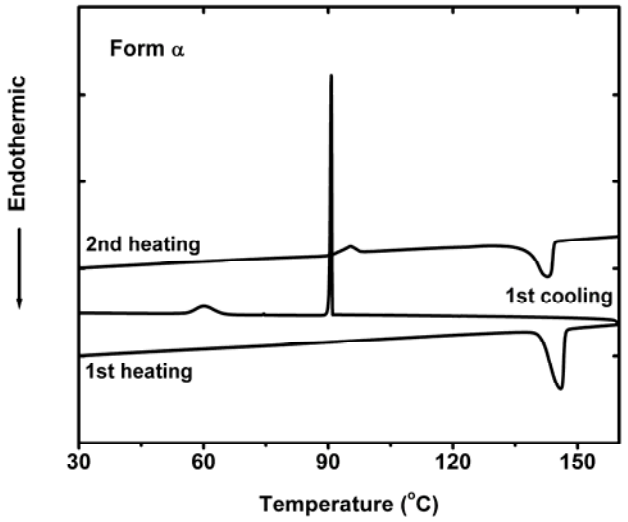

Figure 5.1. DSC thermograms recorded for the PEO-urea α complex.

A firm attribution of these various thermal events is established by performing WAXD and FT-IR measurements during similar heat-cool-heat sequences. [31,32] Fig. 5.2 shows that the WAXD pattern of the original sample (top curve) only presents the characteristic peaks of the α complex, most notably the intense peak at 21.6° due to the 201 plane. Heating the sample to 160 °C melts the complex and only an amorphous halo is observed. Several crystalline reflections appear when temperature is decreased below 90 °C, with the most intense peak appearing at a 2θ angle of 22.2°. All these peaks can be indexed using the tetragonal unit cell of pure urea, [33,34] confirming that the narrow exotherm at 90 °C in the cooling run of Fig. 5.1 is due to pure urea crystallization. This crystallization temperature is somewhat lower than for pure urea (101 °C) because the presence of PEO in the liquid phase increases the entropic cost of crystallization. The

characteristic 410 reflection of the β complex appears at a 2θ angle of 21.2° when temperature reaches 65 °C and it becomes more prominent as temperature is further decreased. Meanwhile, the intensity of the pure urea peaks is maintained, proving that the melt-quenched sample is composed of a mixture of urea and the β complex. This is consistent with the stoichiometry of the two complexes, with PEO:urea molar ratios of 4:9 and 3:2 for the α and β complexes, respectively. Finally, the β complex and urea peaks disappear simultaneously and are replaced by those of the α complex when reheating the sample to 95 °C, confirming the β - α transition exotherm during the second heating cycle of Fig. 5.1. This phase transition occurs instantaneously on the time scale of WAXD at this temperature but the kinetics of the process at lower temperatures will be discussed below.

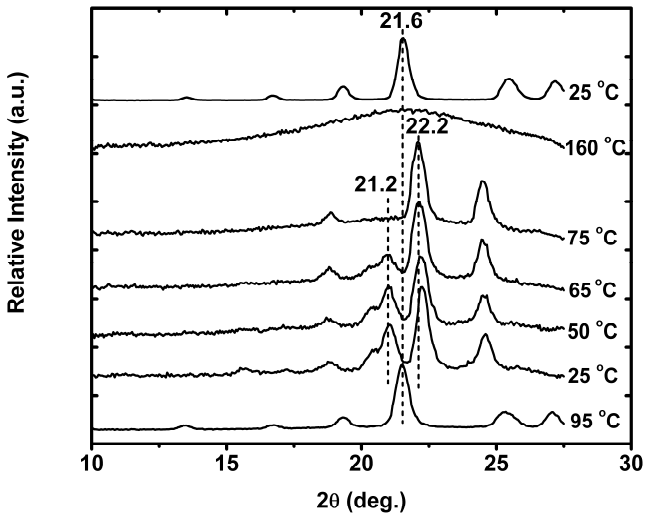

Figure 5.2. WAXD patterns of the PEO-urea α complex recorded at 25 °C (top curve), after heating to the liquid state (160 °C), cooling to 75, 65, 50 and 25 °C, and finally after a second heating to 95 °C (bottom trace).

It is noteworthy that it is urea, and not the α complex, that partially crystallizes at 90 °C even if the latter has a higher melting point. This can be explained by a slower

nucleation rate for the α complex due to the incorporation of PEO chains in the crystals. Polymers generally require a large degree of undercooling to crystallize at significant rates because of a slow nucleation process at temperatures close to their melting point. Urea crystals are therefore produced for kinetic and not for thermodynamic reasons. As a matter of fact, cooling the α complex melt at a slower rate of 3 °C/min only produces the thermodynamic product, the α complex crystals, and not a kinetically frozen mixture of urea and β complex.

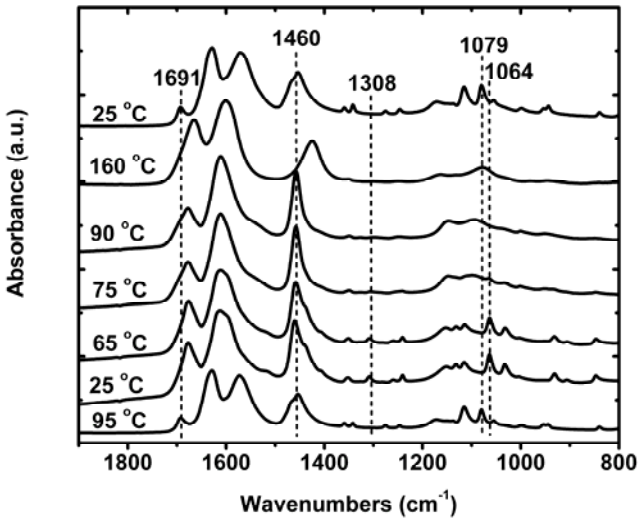

Figure 5.3. FT-IR spectra of the PEO-urea α complex recorded at 25 °C (top curve), after heating to the liquid state (160 °C), cooling to 90, 75, 65 and 25 °C, and finally after a second heating to 95 °C (bottom trace).

The temperature-controlled FT-IR spectra shown in Fig. 5.3 confirm the WAXD results and provide additional molecular insight on this system. The spectrum of the initial α complex sample (top curve) is characterized by the presence of a urea amide band at 1691 cm^{-1} and by a PEO C-O-C stretching mode at 1079 cm^{-1}, as compared to 1098 cm^{-1} for pure PEO. The 1691 cm^{-1} band completely disappears and the C-O-C band becomes much broader upon melting the sample at 160 °C. When temperature is decreased to below 90 °C, the partial crystallization of urea is clearly observed through

the blue shift of the C=O stretching and NH_2 deformation vibrations, and by the shift and narrowing of the C-N stretching band around 1460 cm^{-1}. Meanwhile, most PEO bands do not change with the exception of the C-O-C stretch that shifts to ~1090 cm^{-1}. This position indicates that the PEO chains are still hydrogen-bonded with urea in a melt with the β complex composition. These favorable enthalpic interactions decrease the Gibbs free energy of urea in the melt and explain the fact that urea only partially crystallizes during the DSC cooling scan. When temperature reaches 65 °C, the PEO bands become narrower and adopt the positions characteristic of the crystalline β complex, including a single CH_2 wagging band at 1351 cm^{-1}, a new band at 1308 cm^{-1}, and the C-O-C stretching band at 1064 cm^{-1}. [2,16] Shoulders on the urea bands around 1600 and 1518 cm^{-1} also indicate the coexistence of the solid β complex with pure crystalline urea. [35] The infrared spectra finally confirm β - α transition when temperature is increased above 95 °C.

5.5.2 Phase transitions of the pure β complex

The phase behavior of the pure β complex has never been studied in detail before. The first heating DSC thermogram of Fig. 5.4 shows two transitions at 89 and 143 °C. These temperatures are quite similar to those observed in the second heating cycle of Fig. 5.1 for the melt-quenched mixture. A noteworthy difference is that the first thermal event is endothermic in Fig. 5.4 and not exothermic as in Fig. 5.1. We have previously shown using FT-IR spectroscopy that this peak is due to the conversion of the β complex into a mixture of the α complex and liquid PEO. [2] Assuming that the melting enthalpy of the α complex is 228 J/g (assuming in first approximation that the pure α complex is 100% crystalline), the 131 J/g melting enthalpy observed at 143 °C corresponds to a ~91% β – α conversion yield. Two exothermic peaks appear in the cooling run, as was observed in Fig. 5.1 for the α complex, but at temperatures ~15 °C lower. The exotherm at 75 °C is narrow, although not as much as for the urea crystallization in Fig. 5.1, while the peak at 40 °C is broad. Two endothermic peaks appear in the second heating ramp at 65 and 140 °C, close to the melting temperatures of pure PEO and of the α complex, respectively.

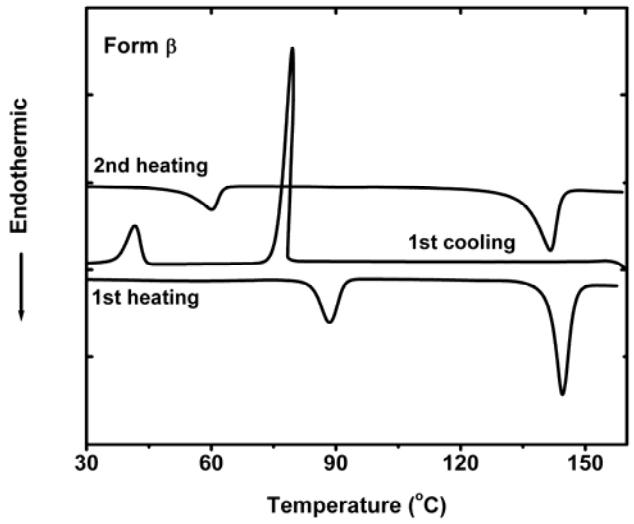

Figure 5.4. DSC thermograms recorded for the pure PEO-urea β complex.

The temperature-controlled WAXD experiments of Fig. 5.5 were performed to confirm the nature of the phases in presence. The original specimen at 25 °C only shows the characteristic reflections of the β complex, thereby confirming that electrospinning is a powerful method to prepare pure samples of this complex. When temperature is increased to 90 °C, all peaks disappear abruptly and are replaced by those of the α complex. A significant amorphous halo simultaneously develops, consistent with the presence of residual liquid PEO after the β – α conversion. After complete melting at 160 °C, the α complex diffraction peaks reappear directly when cooling to 75 °C at a rate of 10 °C/min. Crystallization of the α complex is slower than that of pure urea because of the involvement of the polymeric PEO chains, justifying the observation of a broader peak in Fig. 5.4 as compared to the urea crystallization in Fig. 5.1. Further cooling the sample below the broad exothermic transition at 40 °C provokes the crystallization of pure PEO, as confirmed by the characteristic 120 and 032 peaks of PEO at 19.0° and 23.2°, respectively. Degrees of crystallinity of ca. 70% and 61% are calculated for the α complex and for PEO assuming melting enthalpies of 228 and 182.7 J/g, respectively. [36] This is consistent with the weak amorphous halo observed in the WAXD pattern of Fig. 5.5 at the end of the cooling ramp. Finally, the second heating

cycle sees the successive melting of the PEO and α complex crystals, as expected from Fig. 5.4. It is interesting to note that melt-cooling the α complex yields a mixture containing the β complex, while melt-cooling the β complex produces a mixture that contains the α complex. In order to explain this behavior, it is important to establish whether the pure β complex is stable or metastable.

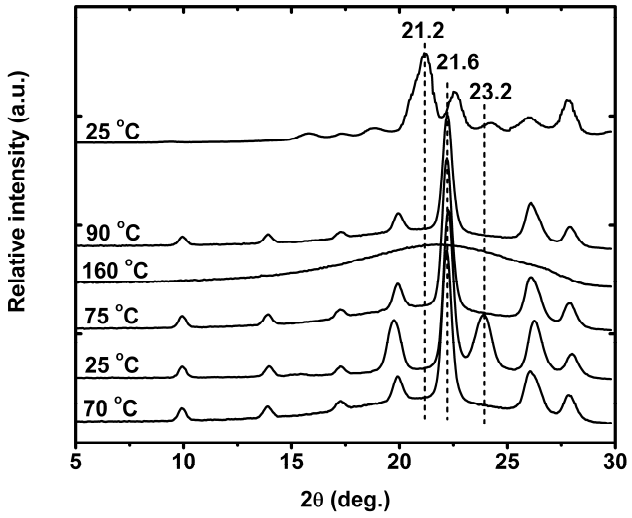

Figure 5.5. WAXD patterns of the pure PEO-urea β complex recorded at 25 °C (top curve), after heating slightly above the phase transition temperature (90 °C) and in the melt state (160 °C), after cooling to 75 and 25 °C (middle curves), and finally after a second heating scan to 70 °C (bottom trace).

5.5.3 β – α transition and stability of the pure β complex

It is now established that the melt-quenched β mixture can convert rapidly to the α form at 95 °C, [8-11] as seen in Fig. 5.1, or more slowly at lower temperatures through a solid-solid transition. [16] Ye et al. have recently used infrared spectroscopy to follow the β – α transition kinetics during the annealing of melt-quenched samples and determined an activation energy of 222 kJ/mol for the process. [16] FT-IR spectroscopy and WAXD were employed here to obtain additional insight on this phenomenon. At first hand, Fig

5.6A confirms that the phase transition occurs quite rapidly at 60 °C, 35 °C below the DSC transition temperature. Indeed, all infrared bands of the β complex, including those at 1351 and 1308 cm^{-1} and the C-O-C stretch at 1064 cm^{-1}, disappear almost completely

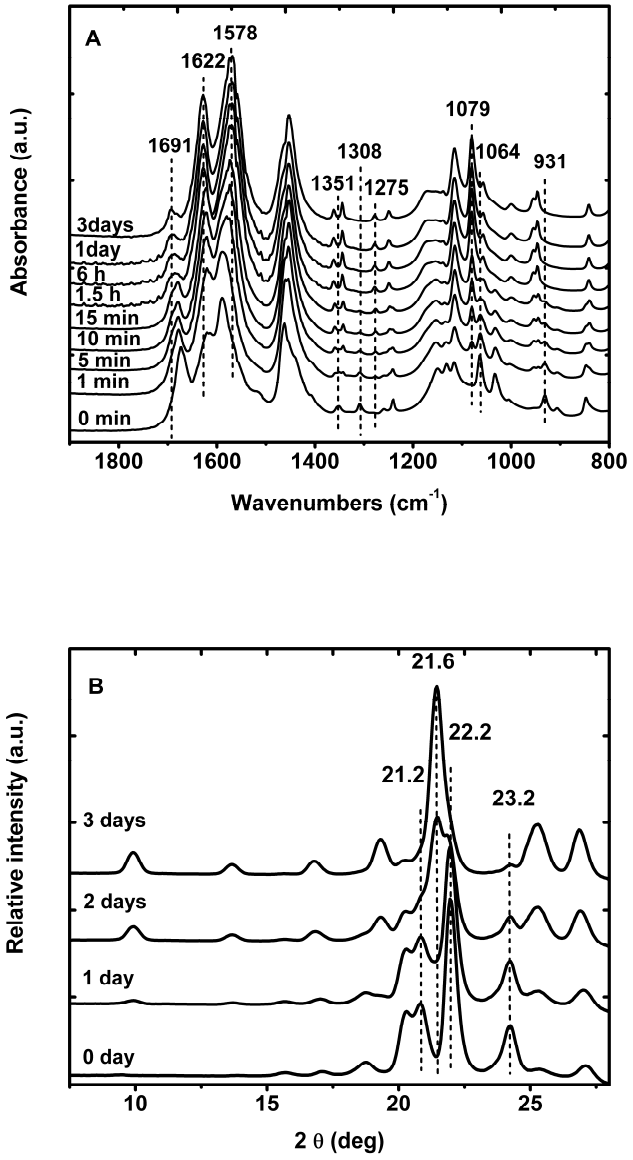

Figure 5.6. A) FT-IR spectra and B) WAXD profiles of the melt-quenched β mixture recorded as a function of time during an annealing at 60 °C.

in less than 15 min and are replaced by bands of the α complex. The use of attenuated total reflectance (ATR) in this study allows following bands that were saturated in the transmission spectra of reference 16. As expected, the intense C=O and NH_2 modes at 1619 and 1589 cm^{-1} also shift to their final position in about 15 min. In sharp contrast, the 1675 cm^{-1} band continues blue shifting and only stabilizes at 1691 cm^{-1} after almost three days of annealing. Second derivative spectra show that this shift is actually due to the decrease of a β complex band at 1675 cm^{-1} coupled with the concomitant increase of an α complex band at 1691 cm^{-1}. Nevertheless, this result indicates that while the local scale conformational changes occur rapidly in a few minutes, the overall phase transition process is actually two orders of magnitude slower than previously thought.

This conclusion is confirmed by the WAXD measurements of Fig. 5.6B, in which the β complex and urea peaks at 21.2° and 22.2°, respectively, still largely dominate after one day of annealing at 60 °C. The α complex peak at 21.6° increases gradually and dominates the diffraction pattern after three days of annealing, with traces of β complex and urea left. The apparent position of 1691 cm^{-1} infrared band can therefore be used as an indicator of the large scale crystalline modifications as observed through X-ray diffraction. Similar behavior was observed at other temperatures, including at room temperature. In that case, the PEO infrared bands evolved from β to α over several hours, but the WAXD peaks only showed obvious α complex presence after weeks, taking several months to complete the solid-solid phase transition.

At first sight, it would appear that the pure β complex is also metastable since it features a similar β – α transition at 90-95 °C in the thermogram of Fig. 5.4. However, the infrared spectra of Fig. 5.7A show that the pure β complex remains unaffected by 24 hours of annealing at 60 °C. This is to be contrasted with Fig. 5.6A, in which the occurrence of the solid-solid phase transition was clear after less than one minute for the melt-quenched sample. WAXD measurements (not shown) did not reveal any change either after more than a day of annealing, as was expected since the infrared spectra are much more sensitive to the local conformational changes occurring in initial stage of

phase transition. Since the β – α DSC transition is lower for the pure β complex than for the melt-quenched sample (89 vs. 95 °C), one would rather have predicted a faster phase

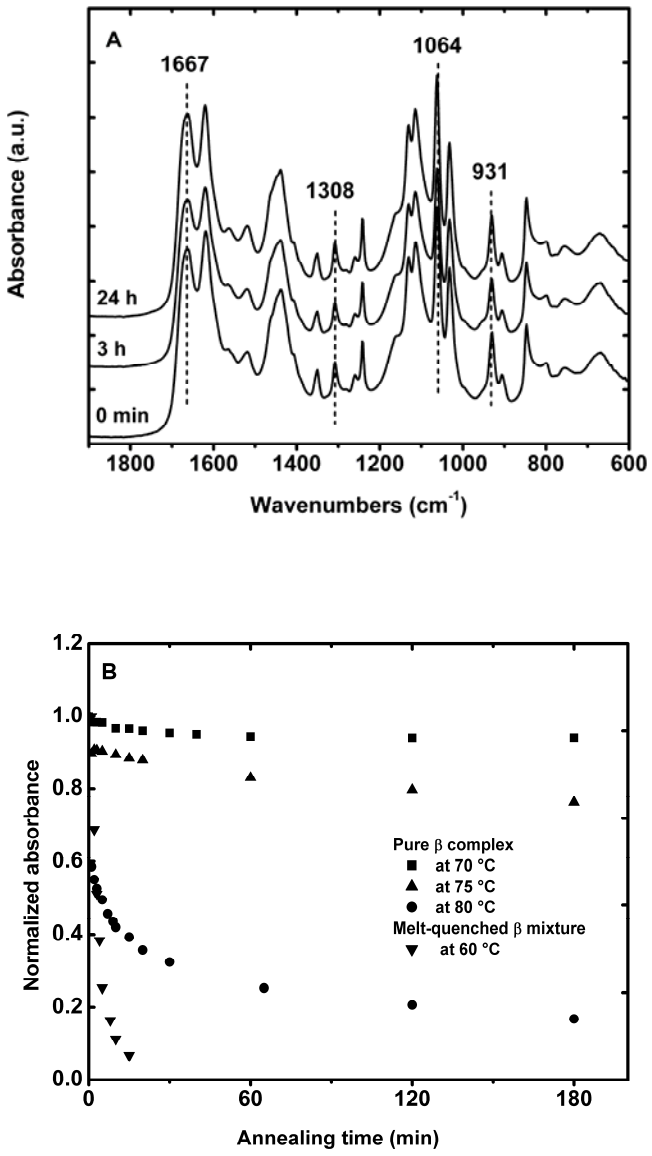

Figure 5.7. A) FT-IR spectra of the pure β complex recorded as a function of time during an annealing at 60 °C; B) Time evolution of the normalized absorbance of the 1308 cm^{-1} β complex band during annealings at 70, 75 and 80 °C for the pure β complex and at 60 °C for the melt-quenched β mixture.

transition, assuming an equivalent activation energy. Fig. 5.7B shows the time evolution of the absorbance of the 1308 cm^{-1} band, which is well isolated and is characteristic of the β complex. It can be seen that, after 3 hours of annealing, the β – α transition is limited to 5% at 70 °C and 20% at 75 °C. A 24 hours annealing at 75 °C, the apparent onset temperature of the DSC transition peak, only amounted to the equivalent of approximately 1 min at 60 °C for the metastable melt-quenched sample. Pure β complex shows an almost complete formation of the α complex only when the annealing is performed at or above 80 °C, which corresponds to the maximum of the DSC endotherm at a scanning rate of 1 °C/min.

These results strongly suggest that the phase transition of the pure β complex is a thermodynamic process and not a kinetic transition, and that the metastability observed for the melt-quenched sample is due to the presence of residual urea. The partial transition occurring at 75 °C in Fig. 5.7B can be attributed to the incongruent melting of smaller or defective crystals, while larger crystals require a higher temperature to melt. The endothermic phase transition observed by DSC in Fig. 5.4 is therefore due to the overlap of the endothermic melting of the β crystals with the exothermic crystallization of the α complex. The pronounced temperature dependence of the transition kinetics observed in Fig. 5.7B further supports the thermodynamic stability of the pure β complex. If the β – α transition were a kinetic process, one would have expected it to possess a lower activation energy than the 222 kJ/mol determined for the melt-quenched sample. [16] Indeed, the latter requires disruption of urea crystals much below their melting temperature in order to form the channel structure of the α complex, while converting the pure β complex to the α complex only requires ejection of highly mobile PEO chains since they are well above their melting point of 67 °C.

5.5.4 Phase diagram of the PEO-urea system

Considering the newfound stability of the pure β complex, it is now possible to draw a complete phase diagram of the PEO-urea binary system. Fig. 5.8 is obtained by

measuring the DSC thermograms of samples prepared by electrospinning solutions with various PEO:urea molar ratios. The nature of the different phases was confirmed by infrared spectroscopy and WAXD. The phase diagram contains two stable stoichiometric complexes at urea molar fractions (X_U) of 0.692 (α complex) and 0.4 (β complex). The α complex melts congruently at a higher temperature (143 °C) than the two starting components because of the strong hydrogen-bonded network between PEO and urea as well as the decreased melting entropy compared with pure urea due to the presence of the polymeric guest. In contrast, the β complex melts incongruently [37] at 89 °C and converts to liquid PEO and α complex. It is interesting to note that the layered complex of PEO with MRES, which was found to be thermodynamically stable, can also melt incongruently to generate the higher melting point complex. [22] The lower melting temperature of the β complex is due to its sandwich structure, in which urea and PEO layers are joined by hydrogen bonds but only van der Waals forces exist within the PEO layers. [2] A liquid phase characterized by significant hydrogen bonding between the urea and PEO is formed above the melting point of the α complex.

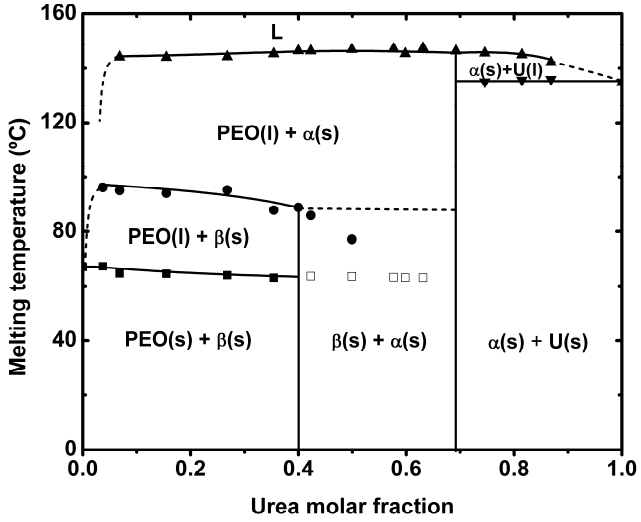

Figure 5.8. Phase diagram of PEO-urea binary system. The open symbols represent the melting events due to kinetic products and the dashed lines the expected behavior under thermodynamic conditions.

The phase separation observed upon melt-cooling the α (Fig. 5.1) and β (Fig. 5.4) complexes can be interpreted in view of the new phase diagram. In both cases, crystallization of the stoichiometric complex is slower and/or requires a larger undercooling than that of the next stable urea-rich compound. In the case of the α complex, crystallization of pure urea is kinetically favored and occurs around 90 °C, a temperature at which a "pseudo-tie line" on the phase diagram leads to a second phase with the β complex composition. As predicted from the phase diagram, cooling the melt α complex at a slow rate leads to the direct formation of the thermodynamic product: the solid α complex. In the case of the β complex, the system must first be cooled through a large temperature range, between 143 and 89 °C, where the two equilibrium phases are solid α complex and liquid PEO. It is therefore not surprising that those phases are obtained experimentally (Figs. 5.4 and 5.5) in spite of the stability of the complex. The crystallization peak for the α complex is observed at 75 °C in Fig. 5.4, a temperature below the melting point of the β complex but at which the undercooling is still insufficient for rapid β complex nucleation. Support for this interpretation is obtained by quenching the melt β complex in liquid nitrogen. In such case, the temperature quickly reaches a sufficient undercooling and only the stable β complex is produced.

The phase diagram can further be separated in three main composition ranges. When $X_U > 0.692$, the samples consist of a mixture of solid urea and α complex that sequentially melt at 135 and 143 °C. When $X_U < 0.4$, samples consist of a mixture of PEO with the β complex, in agreement with the conclusion of thermodynamic stability. Otherwise, a tie-line would have rather predicted the coexistence of solid PEO and α complex. While a fraction of the PEO chains certainly exist in the amorphous state, its crystallinity level is high and a glass transition temperature is hardly observed except for the pure polymer. Finally, samples with $0.4 > X_U > 0.692$ should in principle be composed of a mixture of the two solid complexes, but a weak PEO melting event is systematically observed, as noted with open squares in Fig. 5.8. This is explained by the relative crystallization kinetics for the different species. It was shown above that the α complex crystallization is much faster than that of the β complex. As a consequence, more α crystals are formed during the rapid electrospinning process than would be

expected under equilibrium conditions. Since the α complex contains more urea than the β complex, this excess crystallization leads to residual pure PEO in the system. When composition is very close to $X_U = 0.692$, the α complex formation is so efficient that almost all urea becomes included in it and the sample consist of a mixture of α complex with a small amount of PEO and only traces of the β complex. We believe that the equilibrium phase diagram should not feature this PEO melting event but rather the β complex melting at a constant temperature marked by the dashed line, but preparing equilibrium samples has proven difficult.

It is interesting to point out that the observation of the stability of the β complex could open up an intriguing new avenue for electrospinning. While the method is normally used to prepare nanofibers of various polymers and complex polymeric systems, it has also been used to prepare unusual or metastable crystal structure.[29,30] This was actually a rationale for using it in the first place to prepare pure β complex samples. The results obtained here demonstrate that electrospinning can also be used to prepare thermodynamically stable compounds that would otherwise be inaccessible under normal sample preparation conditions because of the formation of kinetically frozen products. The method does not require thermal annealing of the as-prepared electrospun fibers. This is especially the case for compounds that melt incongruently and are therefore prone to phase separation upon cooling or solvent evaporation at slower rates than that occurring during an electrospinning experiment.

5.6 Conclusions

This study has revisited the poly(ethylene oxide)-urea system to better understand the thermodynamic stability and phase behavior of its two molecular complexes. It was demonstrated that the β complex is stable when it is pure, in contrast with the metastable mixture of β complex and urea obtained by melt-quenching the α complex. It was found that the kinetic solid-solid β – α phase transition of such melt-quenched sample occurs over a much longer timescale than previously reported, with a fast local scale reorganization occurring in a few minutes at 60 °C but completion of the

inclusion complex formation requiring days. Melt-cooling the pure β complex can also lead to a phase-separated mixture of PEO and α complex due to slower crystallization kinetics. A complete phase diagram was obtained from DSC, WAXD and FT-IR studies and was used to understand the many phases that can coexist under various sample preparation conditions. These results help us to better understand the properties of the important class materials that are polymeric host-guest systems, in particular in view of their application as electrospun nanofibers. More generally, this work also demonstrates that electrospinning is not only a method of choice to prepare metastable structures, but that it can also be used to gain access to stable systems that are otherwise inaccessible due to kinetic freezing. We are currently extending this approach to the preparation of other polymeric host-guest systems.

5.7 Acknowledgements

The financial support of the Natural Sciences and Engineering Research Council of Canada (NSERC) and the Fonds Québécois de Recherche sur la Nature et les Technologies (FQRNT) is acknowledged.

5.8 References

1. Liu, Y.; Pellerin, C. *Macromolecules* **2006**, 39, 8886.
2. Liu, Y.; Antaya, H.; Pellerin, C. *J. Polym. Sci. Part B: Polym. Phys.* **2008**, 46, 1903.
3. Tadokoro, H.; Yoshihara, T.; Chatani, Y.; Murahashi, S. *J. Polym. Sci. B* **1964**, 2, 363.
4. Chenite, A.; Brisse, F. *Macromolecules* **1991**, 24, 2221.
5. Vasanthan, N.; Shin, I. D.; Tonelli, A. E. *Macromolecules* **1996**, 29, 263.
6. Wagner, J.-F.; Dosière, M.; Guenet, J.-M. *Macromol. Symp.* **2005**, 222, 121.
7. Suehiro, K.; Nagano, Y. *Makromol. Chem.* **1983**, 184, 669.

8. Bogdanov, B.; Michailov, M.; Uzov, C.; Gavrailova, G. *Makromol. Chem.* **1994**, 195, 2227.
9. Bogdanov, B.; Mikhailov, M.; Uzov, K.; Gavrailova, G. *Angew. Makromol. Chem.* **1992**, 195, 165.
10. Bogdanov, B.; Mikhailov, M.; Uzov, K.; Gavrailova, G. *J. Polym. Sci. Part B: Polym. Phys.* **1994**, 32, 387.
11. Bogdanov, B.; Uzov, C.; Gavrailova, G. *Acta Polym.* **1994**, 45, 381.
12. Choi, C.; Davis, D. D.; Tonelli, A. E. *Macromolecules* **1993**, 26, 1468.
13. Vasanthan, N.; Shin, I. D.; Tonelli, A. E. *Macromolecules* **1994**, 27, 6515.
14. Howe, C.; Vasanthan, N.; MacClamrock, C.; Sankar, S.; Shin, I. D.; Simonsen, I. K.; Tonelli, A. E. *Macromolecules* **1994**, 27, 7433.
15. Hollingsworth, M. D.; Harris, K. D. M., *Comprehensive Supramolecular Chemistry*. Elsevier Science Ltd.: Oxford, 1996; Vol. 6, p 177.
16. Ye, H. M.; Peng, M.; Xu, J.; Guo, B. H.; Chen, Q.; Yun, T. L.; Ma, H. *Polymer* **2007**, 48, 7364.
17. Delaite, E.; Point, J. J.; Damman, P.; Dosière, M. *Macromolecules* **1992**, 25, 4768.
18. Damman, P.; Point, J. J. *Macromolecules* **1993**, 26, 1722.
19. Damman, P.; Point, J. J. *Macromolecules* **1994**, 27, 3919.
20. Damman, P.; Point, J. J. *Macromolecules* **1995**, 28, 2050.
21. Spevacek, J.; Paternostre, L.; Damman, P.; Draye, A. C.; Dosière, M. *Macromolecules* **1998**, 31, 3612.
22. Paternostre, L.; Damman, P.; Dosière, M. *Macromolecules* **1999**, 32, 153.
23. Iannelli, P.; Damman, P.; Dosière, M.; Moulin, J.-F. *Macromolecules* **1999**, 32, 2293.
24. Greiner, A.; Wendorff, J. H. *Angew. Chem. Int. Ed.* **2007**, 46, 5670.
25. Yarin, A. L.; Koombhongse, S.; Reneker, D. H. *J. Appl. Phys.* **2001**, 89, 3018.
26. Burger, C.; Hsiao, B. S.; Chu, B. *Annu. Rev. Mater. Sci.* **2006**, 36, 333.
27. Kakade, M. V.; Givens, S.; Gardner, K.; Lee, K. H.; Chase, D. B.; Rabolt, J. F. *J. Am. Chem. Soc.* **2007**, 129, 2777.

28. Kongkhlang, T.; Tashiro, K.; Kotaki, M.; Chirachanchai, S. *J. Am. Chem. Soc.* **2008**, 130, 15460.
29. Stephens, J. S.; Chase, D. B.; Rabolt, J. F. *Macromolecules* **2004**, 37, 877.
30. Lee, K.-H.; Snively, C. M.; Givens, S.; Chase, D. B.; Rabolt, J. F. *Macromolecules* **2007**, 40, 2590.
31. Gowd, E. B.; Shibayama, N.; Tashiro, K. *Macromolecules* **2007**, 40, 6291.
32. Gowd, E. B.; Shibayama, N.; Tashiro, K. *Macromolecules* **2008**, 41, 2541.
33. Vaughan, P.; Donohue, J. *Acta Crystallogr.* **1952**, 5, 530.
34. Zavodnik, V.; Stash, A.; Tsirelson, R.; Vries, R.; Feil, D. *Acta Crystallogr. B* **1999**, B55, 45.
35. Zhang, H.; Xuan, X.; Wang, J.; Wang, H. *J. Phys. Chem. B* **2004**, 108, 1563.
36. Brandrup, J.; Immergut, E. H.; Grulke, E. A., *Polymer Handbook, 4th ed.* John Wiley & Sons: Hoboken, 1999.
37. White, M. A.; Harnish, R. S. *Chem. Mater.* **1998**, 10, 833.

Chapter 6: Structure and Phase Behavior of the Poly(ethylene oxide)-Thiourea Complex Prepared by Electrospinning

6.1 Résumé

La formation de complexes moléculaires entre le poly(oxyde d'éthylène) (PEO) et la thiourée a été étudiée par différentes méthodes expérimentales, comme la DSC, le WAXD et la spectroscopie FT-IR. L'électrofilage ainsi que la méthode conventionnelle de co-cristallisation ont été utilisées avec succès pour préparer les spécimens. Un rapport molaire de 3:2 de PEO:thiourée a été déduit à partir du diagramme de phases obtenu par DSC. Lorsque le complexe moléculaire est chauffé, il se transforme spontanément en une phase liquide et en thiourée cristalline (fusion péritectique). L'analyse d'échantillons de fibres électrofilées et du complexe avec le PEG de faible masse moléculaire (M_w = 1000) a permis de déterminer que la maille élémentaire était monoclinique avec a = 9.15 Å, b = 18.88 Å, c = 8.25 Å et β = 92.35º. Elle contient 12 unités de répétition de PEO et 8 molécules de thiourée. Une structure cristalline en couches a été proposée sur la base de l'empilement moléculaire et des paramètres de diffraction des rayons X. Elle serait constituée de couches alternées de PEO et de thiourée stabilisées par des ponts hydrogène intermoléculaires. Cette structure en couches pourrait expliquer la température de fusion beaucoup plus basse (110 ºC) du complexe de PEO-thiourée par rapport au complexe en canaux de PEO-urée (143 ºC). Les spectres FT-IR de ce complexe montrent que les vibrations du PEO sont très affectées par la complexation.

6.2 Abstract

Electrospinning was used for the first time to prepare nanofibers of the host/guest complex between poly(ethylene oxide) (PEO) and thiourea. It is shown by differential scanning calorimetry (DSC) and wide-angle X-ray diffraction (WAXD) that the stoichiometry of the complex is $(EO)_{12}$-$(thiourea)_8$, settling a series of conflicting values in literature reports. The complex crystallizes in a monoclinic unit cell with a = 9.15 Å, b = 18.88 Å, c = 8.25 Å and β = 92.35º. Based on WAXD, infrared spectroscopy and polarized Raman scattering measurements, it is proposed that the complex adopts a layered structure in which alternating PEO and thiourea layers are stabilized by intermolecular hydrogen bonds. This structure is highly reminiscent of that of the β complex between PEO and urea. A phase diagram was determined and shows that the complex melts incongruently at 110 °C to form a peritectic liquid and crystals of pure thiourea. The nanofibers of the PEO-thiourea present a very large molecular orientation with a $<P_2(\cos\varphi)>_c$ value of 0.76, amongst the largest reported for electrospun materials.

6.3 Introduction

The host/guest complexes between polymers and small molecules, such as urea, thiourea and cyclodextrins (CD), have received significant attention over the last decades. Complex formation has been used, for instance, for chiral recognition[1] and for conducting stereospecific polymerizations.[2] In most (thio)urea complexes, the guests are included inside one-dimensional channels constructed from a crystalline network of hydrogen-bonded (thio)urea molecules. The crystal structure is often independent of the specific guest, with urea complexes frequently adopting an hexagonal structure and thiourea complexes forming monoclinic or rhombohedral crystals.[3] Many guest molecules tend to form an inclusion complex with either urea or thiourea, but not both, because of the difference in their channel diameter (5.0-5.5 Å vs. 5.8-7.1 Å, respectively). In a similar way, most polymers form a stable complex with only one of α-, β-, or γ-CD, depending on their size relative to the CD diameter.[4]

Poly(ethylene oxide) (PEO) is an interesting exception to this rule since it has been reported to complex with thiourea[5-8], urea[9-12], α-CD[13] and γ-CD[14]. In spite of several studies, the structure, phase diagram and even the stoichiometry of the PEO-thiourea complex remain open questions. Bailey et al. reported that the complex has a 1:2 PEO:thiourea molar ratio and that its melting temperature is lower than that of pure thiourea.[5,6] In contrast, Tarnrutskii et al. concluded that its molar ratio is 1:0.7 and that it does not adopt the usual structure of thiourea complexes.[7] Most recently, Campo et al. studied the dynamics of PEO chains in PEO-thiourea samples prepared with a 1:4 molar ratio.[8] An excess of thiourea was used to ensure a full encapsulation of the PEO chains. Nevertheless, it was reported that only a small amount of free thiourea was present in the sample, implying a complex stoichiometry close to the initial 1:4 molar ratio. Clearly, more work is needed in order to properly understand this system. These studies can be guided by the observations made for the PEO-urea complexes since this system is now much better understood.

The first stable (α) PEO-urea complex was initially reported in 1964 by Tadokoro et al.[9] and was later shown to belong to the trigonal system ($a = b = 10.54$ Å and $c = 9.12$ Å at 173 K)[10]. It possesses an $(EO)_4$-$(urea)_9$ stoichiometry, with 6 urea molecules forming the channel walls and the remaining 3 urea molecules and 4 EO segments included as guests in the channel.[10] In contrast with the PEO-thiourea complex, the PEO-urea α complex melts at a higher temperature (+8 °C) than pure urea. Melt-quenching the α complex yields a mixture containing a second (β) complex and pure urea crystals.[11,12] This mixture was shown to be metastable and to convert back to the α complex with time, even at room temperature.[12] We have very recently shown that electrospinning, a technique used to prepare nanofibers by applying a high electric field on a concentrated polymer solution, is an efficient method for preparing pure samples of both the α and β PEO-urea complexes.[15,16] Our results revealed that the β complex is in fact thermodynamically stable when pure. It possesses a drastically different $(EO)_{12}$-$(urea)_8$ stoichiometry and adopts a layered-structure rather than forming inclusion channels. Interestingly, its melting temperature (89 ºC) is lower than that of pure urea (135 ºC), as was reported for the PEO-thiourea complex.[6]

In this work, we have used the electrospinning method to prepare pure samples of the PEO-thiourea complex. Characterization of the nanofibers was performed using wide-angle X-ray diffraction (WAXD), infrared spectroscopy, Raman scattering and differential scanning calorimetry (DSC). Results allowed determining the stoichiometry of the complex, suggesting its molecular structure, and tracing a phase diagram for the system. It will be shown that the PEO-thiourea complex shares several structural and thermodynamic characteristics with the PEO-urea β complex.

6.4 Experimental section

Sample preparation. PEO with weight-average molecular weights (M_w) of 400, 1000 and 400 000 g/mol (Scientific Polymer Products), urea, thiourea and methanol (Fisher Scientific) were used without further purification. PEO-thiourea complexes were prepared by cocrystallization and by electrospinning. In the first method, 0.5g of PEO were dissolved in 10 ml of a methanol solution saturated with thiourea. The solution was stirred until a white precipitate appeared. In the electrospinning method, aqueous solutions with various PEO:thiourea molar ratios were prepared by adding an appropriate mass of thiourea to 5% (w/v) PEO solutions. The solutions were introduced in a syringe equipped with a 0.41 mm diameter flat-end needle. A 15 kV positive voltage was applied on the needle tip using a CZE 1000R high-voltage power supply (Spellman High Voltage Electronics), while a 2 kV negative potential (Power Designs) was imposed on a rotating cylinder or two-rods collector to collect the electrospun fibers.

Characterization. An Axioskop 40 optical microscope (Carl Zeiss) was used to observe the electrospun fibers. The density of the fibers was measured by pycnometry using a Sartorius CP224S balance equipped with a YDK01 pycnometer. The fibers were pressed into pellets and their density was determined using two displacement liquids, acetone and benzene. DSC measurements were conducted at a heating rate of 10 °C/min using TA Instruments Q1000 and Q2000 calorimeters calibrated with ultrapure indium. Infrared spectra were recorded on a Vertex 70 FT-IR spectrometer (Bruker Optics) equipped with a liquid nitrogen-cooled HgCdTe detector. Spectra with a 4 cm^{-1} resolution were collected in the attenuated total reflection (ATR) mode using a MIRacle single reflection accessory (Pike Technologies). Polarized Raman spectra were

recorded on a LabRAM HR800 (Horiba Scientific) spectrometer using a 514.5 nm Ar^+ laser and a 600 grooves/mm grating, providing a ~5 cm^{-1} resolution. Spectra were acquired with the incident and scattered light polarized parallel (ZZ) or perpendicular (XX) to a bundle of aligned fibers.

WAXD measurements were carried out using a Bruker AXS diffractometer (Siemens Kristalloflex 780 generator) operated at 40 kV and 40 mA, using the Cu Kα (0.1542 nm) radiation collimated by a graphite monochromator and a 0.5 mm pinhole. The diffraction patterns were recorded by a HI-STAR area detector. The incident X-ray beam was perpendicular to a vertically aligned bundle of fibers. A scattering background was subtracted for display purposes, but the orientation function was calculated using the uncorrected data. To observe the phase transitions, the samples were sealed in aluminum pans and temperature was controlled by an STC 200 controller and a LN2-SYS liquid nitrogen cooling system (Instec). Higher resolution powder diffraction patterns were recorded to determine the unit cell parameters using a Bruker AXS D8 Advance powder diffractometer with an increment of 0.0167º from 10º to 45º. The cocrystallized sample or the electrospun fibers were grounded into a fine powder to obtain a smooth sample surface.

6.5 Results and discussion

6.5.1 Composition and phase diagram of the PEO-thiourea complex

Thiourea complexes with PEO with various M_w were first prepared by the cocrystallization method. The DSC thermograms in Fig. 6.1 reveal two endothermic peaks in all cases. The first melting event appears at 59, 90 and 110 ºC for PEO with M_w of 400, 1000 and 400 000 g/mol, respectively, much lower than the melting temperature of pure thiourea (178 ºC) but higher than that measured for the corresponding pure polymers (12, 33 and 65 ºC, respectively). This peak confirms the formation of a crystalline PEO-thiourea complex for all these polymers. The evolution of the melting temperature for the complexes can be explained by a decrease of the entropy of fusion as M_w increases. As a matter of fact, a similar trend is

observed for PEO-urea α complexes prepared by cocrystallization using the same series of PEO (not shown). The second melting endotherm in the thermograms of Fig. 6.1, which always appears at ca. 160-170 ºC, is due to the melting of thiourea crystals. Its presence can result from co-precipitated thiourea crystals in the original samples and/or from an incongruent melting of the complex to generate a liquid phase and crystalline thiourea. The presence of this additional peak makes the determination of the complex stoichiometry by cocrystallization less straightforward and probably explains the extremely wide range of EO:thiourea molar ratios found in the literature.[5-8]

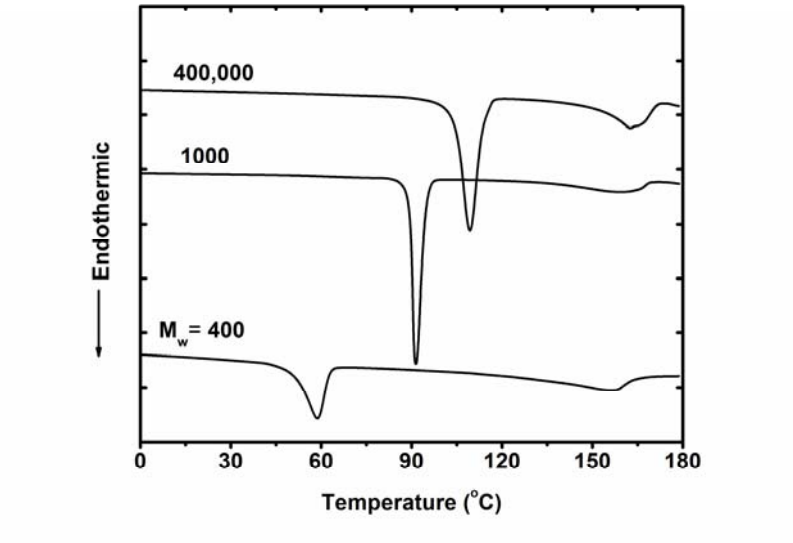

Figure 6.1. DSC thermograms recorded for cocrystallized PEO-thiourea complexes with PEO M_w of 400, 1000 and 400,000 g/mol.

To confirm the complex formation and ascertain the occurrence of an incongruent melting, WAXD patterns were recorded at room temperature, 125 ºC, and 170 ºC. Fig. 6.2 shows that the PEO-thiourea complex is highly crystalline at room temperature. Its WAXD pattern is characterized by a series of diffraction peaks that are not present in either pure PEO or thiourea, in particular those at 17.1, 19.9, 21.1, and 27.1º. When heated to 125 ºC, above the melting point of the complex, all these peaks disappear and the characteristic reflections of uncomplexed

thiourea appear, along with an amorphous halo. This confirms that the PEO-thiourea complex melts incongruently to form crystalline thiourea and a peritectic liquid phase. Since the newly formed thiourea melts at ca. 160-170 ºC, as noted in Fig. 6.1, the WAXD profile at 170 ºC only consists of a diffuse amorphous halo. It is interesting to note that an incongruent melting was also observed for the pure PEO-urea β complex, with the difference that the peritectic reaction lead to the formation of the crystalline α complex rather than of pure urea.[17] The melting temperature of the complex is much lower than that of the host molecule in both cases, suggesting that the structure of the PEO-thiourea complex may be closer to that of the layered PEO-urea β complex than to that of the channel-forming α complex.

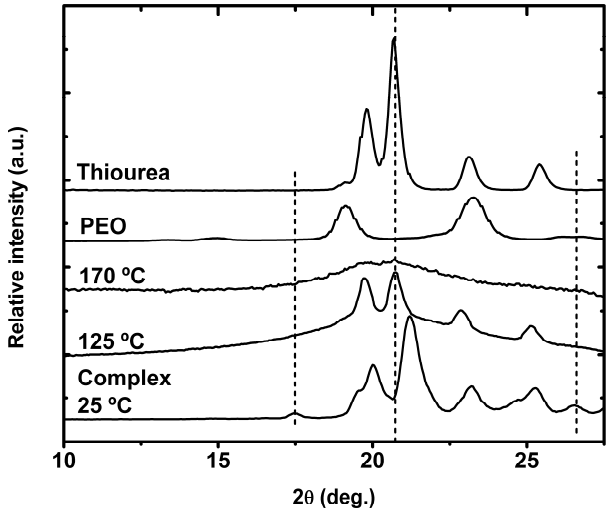

Figure 6.2. WAXD profiles of the PEO-thiourea complex at 25, 125, 170 ºC compared with those of pure PEO and thiourea at 25 ºC.

In order to determine the stoichiometry of the PEO-thiourea complex, electrospun fibers were prepared from solutions with various molar ratios and were characterized by DSC and WAXD. Fig. 6.3A shows that the melting peak of the complex (~110 ºC) gradually grows in intensity (ΔH) when the thiourea molar fraction decreases from 1 to 0.4. Meanwhile, the melting peak for thiourea decreases both in ΔH and temperature. These DSC results are reinforced by the

WAXD patterns of Fig. 6.4 in which the diffraction peaks of the complex, such as those at 17.1 and 27.1º, gradually increase at the expense of those of thiourea (which appear to be shifting because of the strong overlap) when decreasing the thiourea molar fraction to 0.4. A PEO melting peak starts appearing in the DSC thermograms when the thiourea molar fraction decreases below 0.36, indicating that the complex stoichiometry has been exceeded. The stoichiometry can be determined more precisely by plotting the melting enthalpy of the complex against the thiourea molar fraction. Fig. 6.3B shows that it reaches a maximum value of ~99 J/g for a molar fraction of 0.38 ± 0.02. Considering the experimental uncertainty, this corresponds to a PEO:thiourea molar ratio of 3:2, exactly the same as the one found for the layer-structured PEO-urea β complex.[16] Thermogravimetric analysis of samples prepared by cocrystallization showed that the stoichiometry is independent of the polymer molecular weight between 400 and 400 000 g/mol. The value determined here is in good agreement with 1:0.7 stoichiometry suggested by Tarnrutskii et al.[7]

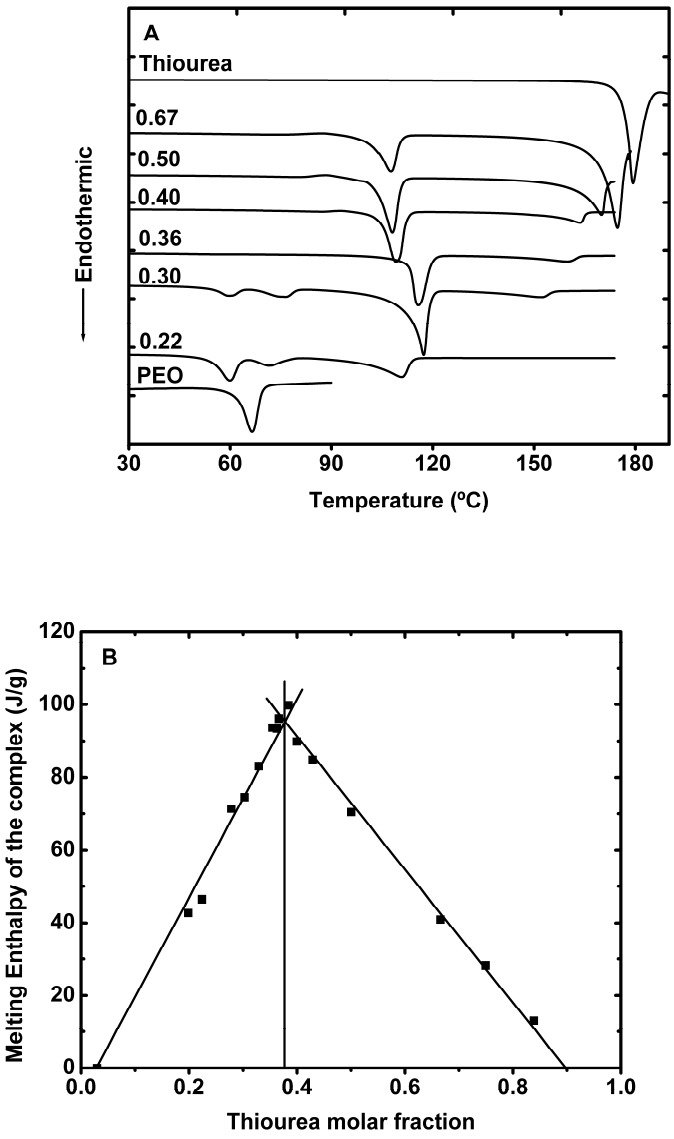

Figure 6.3. A) DSC thermograms and B) melting enthalpy of the PEO-thiourea complex as a function of the thiourea molar fraction.

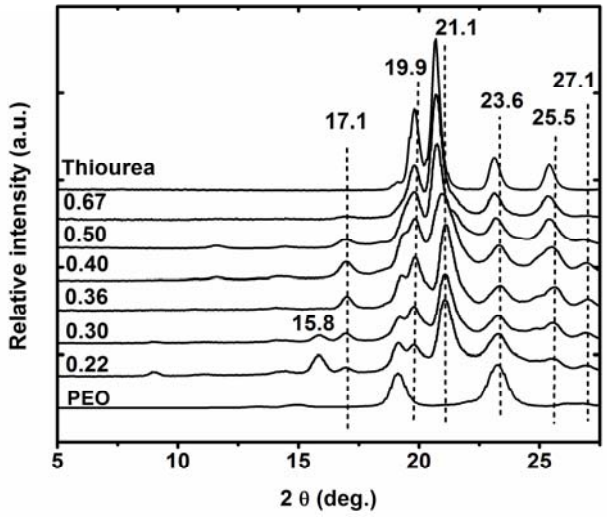

Figure 6.4. WAXD profiles of electrospun fibers prepared with various thiourea molar fractions.

It is now possible to draw a phase diagram for the PEO-thiourea binary system based on the DSC thermograms and on temperature-controlled WAXD and FT-IR measurements to identify the nature of the phases. As shown in Fig. 6.5, the diagram is characteristic of a peritectic system and is rather similar to those of the PEO-p-nitrophenol and PEO-hydroquinone systems.[18] The PEO-thiourea complex melts incongruently to produce solid thiourea and a liquid phase. Thiourea then melts over a rather broad range of temperatures below its melting temperature in the pure state, which suggests miscibility in the liquid state. While complete miscibility is difficult to prove due to partial degradation, IR spectra recorded at 170 °C suggest that H-bonds still exist between PEO and thiourea.

Two additional interesting observations can be made: first, the melting temperature of the complex increases by about 6 ºC in samples with a small excess of PEO, although the opposite could have been expected since the entropy in the liquid phase should be larger due to the presence of additional liquid PEO. A similar observation was also made for the PEO-urea β complex.[17] In both cases, this is likely due to a relative decrease of the enthalpy of the exotherm due to recrystallization of thiourea (or the α PEO-urea complex). Indeed, the presence of excess

PEO limits the recrystallization of the pure host molecule since they can form a miscible liquid phase at that temperature. Because the crystallization exotherm is overlapped with the melting endotherm, the resulting effect is an apparent shift of the melting peak to higher temperatures. A second intriguing observation is the presence of a weak endothermic peak at ca. 75 ºC when the thiourea molar fraction is below 0.36. In such a case, the WAXD patterns of Fig. 6.4 features two additional peaks at 9.0 and 15.8º, suggesting the formation of a second complex highly enriched in PEO. To our knowledge, the existence of a second PEO-thiourea complex has never been reported and will be the object of future work. This complex is shown as open circles in the phase diagram since its nature and thermodynamic stability are unknown.

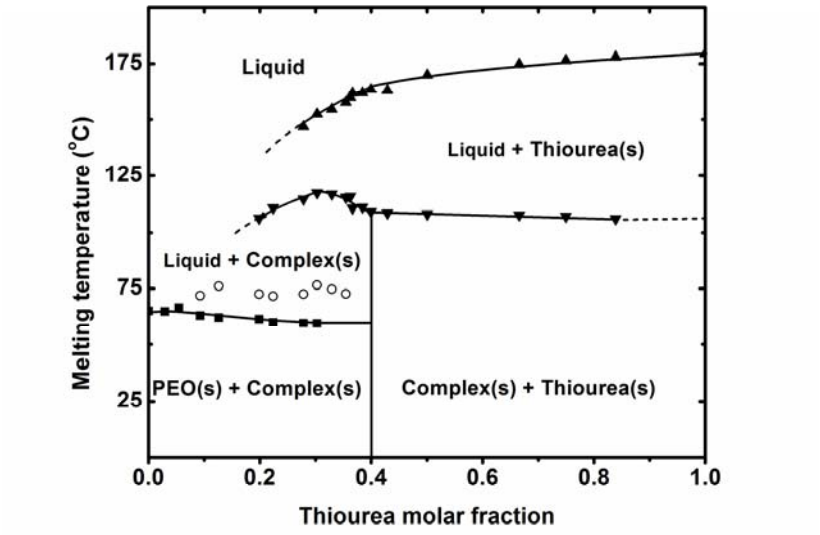

Figure 6.5. Phase diagram of the PEO-thiourea binary system.

6.5.2 Structure of the PEO-thiourea complex

The preparation of macroscopic single crystals of the PEO-thiourea complex is not straightforward, even with low-M_w PEO, and was not successful using saturated thiourea solutions in methanol, ethanol, isopropanol and benzene. In a previous work, the crystal lattice parameters of the PEO-urea β complex could be determined from the analysis of the powder and

fiber diffraction patterns of electrospun fibers because they were highly crystalline and showed a large molecular orientation.[16] In order to determine the unit cell parameters of the complex, a powder diffraction pattern was first recorded with an instrument providing a higher 2θ resolution. Based on the analysis of the data from Fig. 6.6, it is proposed that the complex possesses a monoclinic crystal structure with a = 9.15 Å, b = 18.88 Å, c = 8.25 Å and β = 92.4º. Table 1 summarizes the suggested assignment for the most intense diffraction peaks.

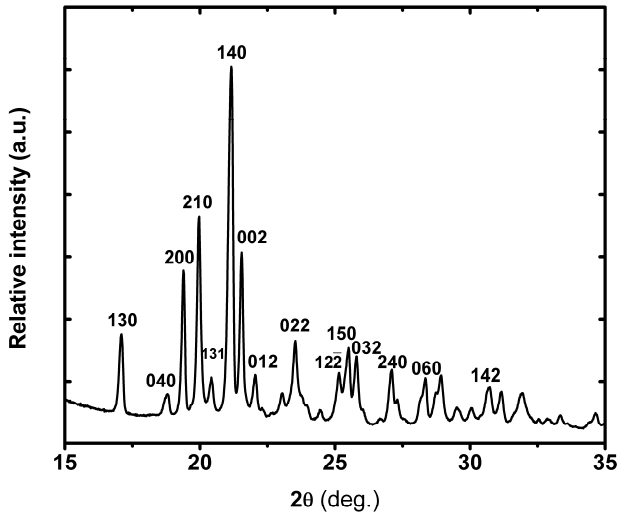

Figure 6.6. High resolution WAXD pattern of the PEO-thiourea complex.

Two-dimensional fiber diffraction patterns were also recorded to determine the orientation level in the PEO-thiourea electrospun fibers and to help confirming the unit cell parameters and plane attributions. Fig. 6.7 shows that all crystalline planes present a highly inhomogeneous azimuthal intensity distribution. The two azimuthal profiles, obtained by integrating the most intense peaks at 2θ = 19.9 and 21.1°, show narrow peaks with full widths at half height of 13º. Because of this strongly anisotropic distribution of the crystals in the fibers, it is possible to support the crystalline plane assignments by comparing σ, the calculated angle between the normal direction to a given hkl plane and the c axis, with the experimentally measured azimuthal angle, φ_{max}, between the plane normal and the fiber axis. As can be noted in

Table 6.1 the calculated angles are in very good agreement with the experimentally observed values and therefore support the proposed unit cell parameters.

Table 6.1. Crystal plane attribution for the PEO-thiourea complex based on a monoclinic unit cell with *a* = 9.15 Å, *b* = 18.88 Å, *c* = 8.25 Å and β=92.4º.

2θ peak	17.1	18.8	19.5	19.9	21.1	21.6	23.6	25.5
Plane attribution	130	040	200	210	140	002	022	150
σ (°)†	90	90	90	90	90	0	23.6	90
φ_{max} (°)†	90	90	90	90	90	0	20	90

† σ is the calculated angle between the normal of an hkl plane and the *c* axis, while φ_{max} is the measured maximum of the azimuthal angle.

It should be noted that the strong anisotropy observed in Fig. 6.7 is an interesting result in itself since molecular orientation has a large impact on many physical properties, for instance on the elastic modulus. Assuming uniaxial symmetry along the fiber direction, it is possible to quantify the orientation by calculating the orientation function, $<P_2(\cos\varphi)>_c$, as:

$$< P_2(\cos\varphi) >_c = \frac{2}{3\cos^2\sigma - 1}\frac{3 < \cos^2\varphi > -1}{2}$$

where σ is the angle between the normal to an hkl plane and the *c* axis, and the brackets indicate a mean value over the distribution of orientation. The $<\cos^2\varphi>$ value was determined as:

$$< \cos^2\varphi >= \frac{\int_0^{\pi} I(\varphi)\cos^2\varphi\sin\varphi d\varphi}{\int_0^{\pi} I(\varphi)\sin\varphi d\varphi}$$

An average $\langle P_2(\cos\varphi)\rangle_c$ value of 0.76 was obtained for the fibers of the PEO-thiourea complex. This orientation is amongst the largest values reported for electrospun fibers and is similar to values obtained for electrospun fibers of PEO and its urea complexes.[15,16,19] The combination of high crystallinity and large molecular orientation of these fibers could make them potentially useful as organic reinforcing agents in composites.

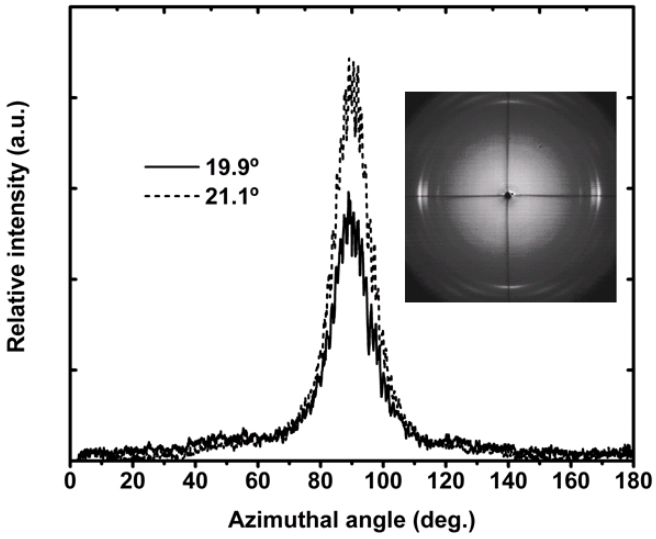

Figure 6.7. Two-dimensional WAXD pattern of the electrospun PEO-thiourea complex fibers (inset) and azimuthal profiles for the peaks at 2θ = 19.9 and 21.1º.

Considering that the lattice dimensions yield a volume of 1.4247 nm^3 and that the PEO:thiourea molar ratio is 3:2, the unit cell must contain 12 PEO repeat units and 8 thiourea molecules. Indeed, this leads to a calculated density of 1.325 g/cm^3, very close to the experimental value of 1.307 g/cm^3. The slight difference can be attributed to the presence of a small amount of amorphous material in the sample. This is consistent with the WAXD patterns of Fig. 6.2, in which only a very weak amorphous halo could be discerned at room temperature, as well as with the presence of a weak glass transition (located between -10 and 10 °C) in the first heating scan for the complex. It is noteworthy that the stoichiometry and cell parameters suggested here for the PEO-thiourea complex are very close to those of the PEO-urea β complex,

which is orthorhombic with a = 19.07 Å, b = 8.62 Å and c = 7.73 Å and also contains 12 PEO repeat units and 8 small molecules.[16] This suggests once more that they share a similar molecular structure.

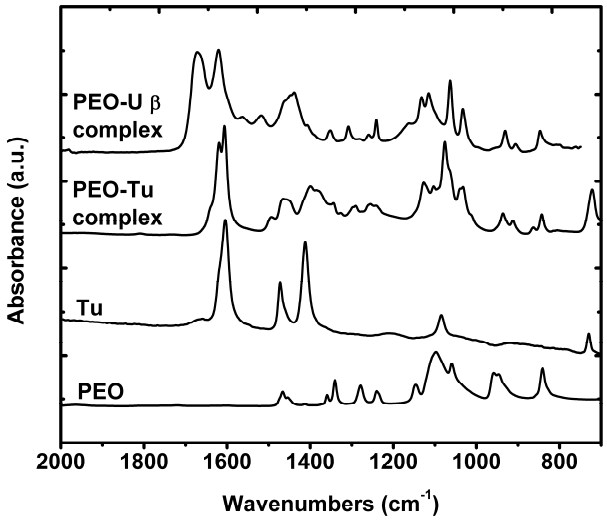

Figure 6.8. Infrared spectra of pure PEO and thiourea, and of the PEO-thiourea and PEO-urea β complexes.

Infrared spectra of the two complexes and of the pure compounds were recorded to validate this hypothesis. Fig. 6.8 clearly shows that the spectrum of the PEO-thiourea complex is not a linear sum of those of pure components. It also confirms the good purity of the complex since intense bands associated with pure PEO and thiourea (e.g., 961 and 1412 cm^{-1}, respectively) are practically absent. The conformation of crystalline PEO is a 7_2 helix with trans-gauche-trans (TGT) O-C-C-O sequences.[20] Its spectrum is characterized by the splitting of the CH_2 wagging (1359 and 1341 cm^{-1}) and CH_2 rocking (959 and 947 cm^{-1}) modes. In contrast, the PEO-thiourea complex spectrum only contains a single wagging band at 1344 cm^{-1} and its CH_2 rocking vibrations, while still split, are significantly red shifted to 936 and 912 cm^{-1}. This is rather similar to the spectrum of the PEO-urea β complex, which also features a single wagging band at 1351 cm^{-1} and rocking bands shifted to 931 and 906 cm^{-1}. In addition, a new band appears around 1300 cm^{-1} for both complexes, at 1290 cm^{-1} for the thiourea complex and at 1308 cm^{-1} for the urea β

complex. This is reminiscent of the 1301 cm^{-1} band observed in stretched PEO and ascribed to a trans conformation of the C-C bonds.[21] These results therefore indicate a significant modification of the torsion angle around the C-C bond in the complexes as compared to the gauche conformation in pure PEO.

The C-O-C stretching region is also quite different for the complex and pure PEO, indicating the formation of new hydrogen bonds between thiourea and the ether oxygen of PEO. In particular, the intense and highly overlapped C-O-C stretching band at 1098 cm^{-1} separates in two bands at 1103 and 1076/1064 cm^{-1} in the complex. Overlap with the thiourea band at 1081 cm^{-1}, which also shifts in the complex, makes a precise assignment difficult, but it is remarkable that the shoulder at 1064 cm^{-1} appears at exactly the same position as in the PEO-urea β complex, for which there is no overlap with urea in this spectral range. In contrast, this band appears at 1080 cm^{-1} in the PEO-urea α complex and could be used to distinguish between the channel and layered complexes.[25] The thiourea bands also show significant differences due to the formation of a new H-bonding network. For instance, the NH_2 bending modes at 1618 and 1602 cm^{-1} become sharper and appear at 1619 and 1607 cm^{-1} with a shoulder at 1640 cm^{-1} and the isolated C=S stretching vibration shifts from 729 cm^{-1} in thiourea to 725 cm^{-1} in the complex. A similar combination of blue shift of the NH_2 bending and red shift of the urea carbonyl stretching band was also observed in the PEO-urea β complex.[24]

Based on the unit cell dimensions and the infrared spectra, we suggest that the PEO-thiourea complex adopts a layered structure in which 4 PEO chains are located in the corners of the *ab* plane and extend for 3 repeat units along the *c* axis. These two PEO layers are separated in the longest direction (*b*) by an intercalated layer of 8 thiourea molecules. To validate this hypothesis, polarized Raman spectra of aligned fiber bundles were recorded to determine the direction of the PEO chains and thiourea molecules in the complex. Fig. 6.9 shows that the CH_2 rocking band at 845 cm^{-1} is parallel to the fiber direction, as observed for fibers of pure PEO,[19] confirming that the PEO chains are oriented along the *c* axis. Considering that the *c* axis dimension is 8.25 Å, the repeat distance of each of the three PEO repeat units must be 2.75 Å, extremely close to the value for pure PEO (2.78 Å)[20] and slightly larger than that in the PEO-urea

β complex (2.57 Å)[16]. The similarity with pure PEO appears coincidental since the infrared spectra revealed distorted torsion angles. Fig. 6.9 also shows a very strong parallel orientation for the C=S stretching band at 725 cm^{-1} and a perpendicular alignment for the N-C-N asymmetric stretching band at 1447 cm^{-1}. These results indicate that the C_2 rotation axis of thiourea is mostly parallel to the *c* axis. In its pure state, thiourea forms ribbon-like structures linked by centrosymmetric H-bonds[22] in which the two hydrogen bonds on any given sulfur atom come from two different neighboring molecules.[23] It is likely that a ribbon structure is also formed in the present case, although the details are not available in the absence of an X-ray crystalline structure.

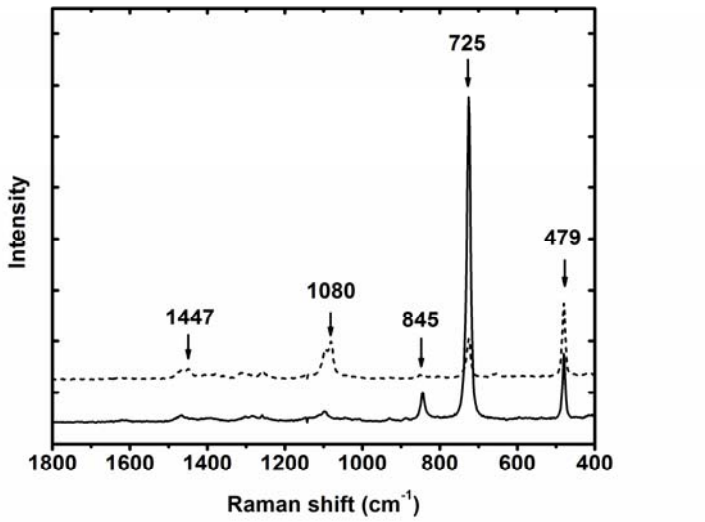

Figure 6.9. Polarized Raman spectra of the PEO-thiourea complex fibers prepared by electrospinning. The spectra with solid and broken lines were measured with the incident and scattered radiation polarized parallel and perpendicular to the fiber direction, respectively.

The proposed layered structure is consistent with the DSC results which reveal that the melting temperatures increases in the order of PEO (65 ºC), PEO-urea β complex (89 ºC), PEO-thiourea complex (110 ºC) and PEO-urea α complex (143 ºC). The higher melting temperature for the complexes as compared to pure PEO is due to the formation of strong intermolecular hydrogen bonds, as compared to only van der Waals forces in pure PEO.[16] The melting

temperature is higher (21 ºC) for the PEO-thiourea complex than for the PEO-urea β complex in spite of their similar structures. This can be explained by the larger dipole moment of thiourea as compared with urea, which also leads to a higher melting point in the pure compounds (178 vs. 135 ºC, respectively).[24] Both complexes melt at lower temperatures than the pure host molecule because the adjacent PEO layers prevent the formation of a continuous hydrogen bonding network. In contrast, the PEO-urea α complex does form a continuous network of hydrogen bonds (since PEO is included in the urea channels) and therefore presents the highest melting temperature.[10] Competing entropic effects influence the melting point of the complex in addition to this enthalpic contribution: the mixing entropy between the two components in the liquid phase is expected to reduce the melting point below that of pure urea, but the melting entropy of polymer chains is lower than that of small molecules. The latter effect appears to dominate, leading to a higher melting temperature for the PEO-urea α complex than for pure urea. It should be noted that the situation is reversed when low-M_w PEO is used for complexation (not shown) because both the melting and mixing entropies become larger for smaller polymer chains, leading to a melting temperature below that of the pure host molecule.

In contrast with urea, which can form both a channel and a layered complex with PEO, the results of this work show that thiourea can only form a layered complex with PEO (the putative PEO-rich second complex would not contain enough thiourea to form channels). This is likely because the diameter of a PEO helix is too small to generate stable interactions with a thiourea channel. A structure that includes extra thiourea molecules inside the channel, as in the PEO-urea α complex, is not forming either. It is possible that the branched analogue of PEO, poly(propylene oxide), might be able to form a channel-like inclusion complex with thiourea since it does form a pseudo-polyrotaxane with the similarly sized β-CD but not with the smaller α-CD.[11,12,18]

6.6 Conclusions

Pure samples of the PEO-thiourea complex were prepared by electrospinning and characterized by DSC, WAXD, infrared spectroscopy and Raman scattering. It was demonstrated

that the stoichiometry of the complex is 12 PEO repeat units for 8 thiourea molecules, as opposed to conflicting literature reports. A phase diagram was determined and shows that the complex melts incongruently to form thiourea crystals and a liquid phase. Powder X-ray diffraction results suggest that the unit cell is monoclinic with a = 9.15 Å, b = 18.88 Å, c = 8.25 Å and β = 92.35º. The stoichiometry, unit cell parameters and vibrational spectra all point to a molecular structure very close to that of the PEO-urea β complex. Therefore, the PEO-thiourea complex may be described in terms of a layered structure in which 4 PEO chains are located in the corners of the *ab* plane and are separated along the *b* axis by 8 thiourea molecules forming an intercalated ribbon-like layer with their C_2 axis aligned along the *c* axis. This layered structure, in contrast with the more usual channel host/guest structure, explains the relative transition temperature observed in the PEO-urea and PEO-thiourea phase diagrams.

6.7 Acknowledgements

The financial support of the Natural Sciences and Engineering Research Council of Canada (NSERC) is acknowledged. HA also thanks NSERC for a graduate scholarship. The authors thank T. Lefèvre, T. Maris and S. Essiembre for their assistance and Prof. M. Pézolet for providing access to his Raman spectrometer.

6.8 References

1. Ohya, Y.; Takamido, S.; Nagahama, K.; Ouchi, T.; Ooya, T.; Katoono, R.; Yui, N. *Macromolecules* **2007,** 40, 6441; Rekharsky, M.; Inoue, Y. *J. Am. Chem. Soc.* **2000,** 122, 4418.
2. Brown, J.F.; White, D.M. *J. Am. Chem. Soc.* **1960,** 82, 5671; Chatani, Y.; Kuwata, S. *Macromolecules* **1975,** 8, 12; Chatani, Y.; Nakatani, S. *Macromolecules* **1972,** 5, 597.
3. Harris, K.D.M. *Chem. Soc. Rev.* **1997,** 26, 279; Hollingsworth, M.D.; Harris, K.D.M., *Comprehensive Supramolecular Chemistry*. Elsevier Science Ltd.: Oxford, 1996; Vol. 6, p 177.
4. Li, J.; Ni, X.; Zhou, Z.; Leong, K.W. *J. Am. Chem. Soc.* **2003,** 125, 1788; Rusa, C.C.; Luca, C.; Tonelli, A.E. *Macromolecules* **2001,** 34, 1318; Sabadini, E.; Gosgrove, T. *Langmuir* **2003,** 19, 9680.
5. Bailey, F.E., Jr.; France, H.G. *Am. Chem. Soc. Div. Polym. Chem. Preprints* **1960,** 1, 194.
6. Bailey, F.E., Jr.; France, H.G. *J. Polym. Sci.* **1961,** 49, 397.
7. Tarnrutskii, M.M.; Shkol'nikova, L.S.; Lorei, A.K.; Dindoin, V.I.; Zykova, L.I. *Vysokomolekulyarnye Soedineniya, Seriya B: Kratkie Soobshcheniya* **1975,** 17, 817.
8. Campo, A.; Fretti, J.; Vasanthan, N. *Polymer* **2008,** 49, 374.
9. Tadokoro, H.; Yoshihara, T.; Chatani, Y.; Murahashi, S. *J. Polym. Sci. B* **1964,** 2, 363.
10. Chenite, A.; Brisse, F. *Macromolecules* **1991,** 24, (9), 2221.
11. Bogdanov, B.; Mikhailov, M.; Uzov, K.; Gavrailova, G. *J. Polym. Sci. B: Polym. Phys.* **1994,** 32, 387; Bogdanov, B.; Michailov, M.; Uzov, C.; Gavrailova, G. *Makromol. Chem.* **1994,** 195, 2227; Suehiro, K.; Nagano, Y. *Makromol. Chem.* **1983,** 184, 669.
12. Ye, H.M.; Peng, M.; Xu, J.; Guo, B.H.; Chen, Q.; Yun, T.L.; Ma, H. *Polymer* **2007,** 48, 7364.
13. Harada, A.; Li, J.; Kamachi, M. *Nature* **1992,** 356, 325.
14. Harada, A.; Li, J.; Kamachi, M. *Nature* **1994,** 370, 126.
15. Liu, Y.; Pellerin, C. *Macromolecules* **2006,** 39, (26), 8886.
16. Liu, Y.; Antaya, H.; Pellerin, C. *J. Polym. Sci. Part B: Polym. Phys.* **2008,** 46, (18), 1903.
17. Liu, Y.; Pellerin, C. *Polymer* **2009,** 50, (12), 2601.
18. Paternostre, L.; Damman, P.; Dosière, M. *Polymer* **1998,** 39, 4579.

19. Kakade, M.V.; Givens, S.; Gardner, K.; Lee, K.H.; Chase, D.B.; Rabolt, J.F. *J. Am. Chem. Soc.* **2007,** 129, (10), 2777.
20. Tadokoro, H.; Yoshihara, T.; Tahara, S.; Murahashi, S. *Makromol. Chem.* **1964,** 73, 109.
21. Takahashi, Y.; Sumita, I.; Tadokoro, H. *J. Polym. Sci. Polym. Phys. Ed.* **1973,** 11, 2113; Tashiro, K.; Tadokoro, H. *Rep. Prog. Polym. Phys. Jpn.* **1978,** XXI, 417.
22. Truter, M.R. *Acta Cryst.* **1967,** 22, 556.
23. Masunov, A.; Dannenberg, J.J. *J. Phys. Chem. A* **1999,** 103, 178; Masunov, A.; Dannenberg, J.J. *J. Phys. Chem. B* **2000,** 104, 806.
24. Kumlera, W.D.; Fohlen, G. *J. Am. Chem. Soc.* **1942,** 64, (8), 1944.

Chapter 7 : Conclusions & Perspectives

7.1 Conclusions

Highly aligned and oriented PEO-urea inclusion complex (IC) nanofibers of the α form were prepared for the first time using the electrospinning method. The results showed that the fibers consist of pure and highly crystalline IC with little or no residual free urea or PEO. The IC structure in the fibers appears to be identical to that in the bulk sample, and is in agreement with the reported model in which all PEO chains and one third of the urea molecules are found inside the self-assembled channels formed by two thirds of the urea molecules. The infrared spectroscopy results suggest that, in contrast with the trans-gauche-trans conformation adopted by pure crystalline PEO around its O-C-C-O bonds, the polymer may present a number of gauche C-O linkages and an approximately TGG conformation to fit in the narrow urea channels. As initially predicted, the molecular orientation of the PEO-urea-IC fibers is very large along the fiber axis direction, with WAXD orientation functions larger than 0.85.

In conventional self-assembled host-guest structures, the urea and thiourea complexes are treated as incommensurate (nonstoichiometric). One feature of the incommensurate structure of urea ICs is that the activation barrier to diffusion along the channel should be very low because of the relatively weak interactions between host channels and guest molecules.[1] But in the PEO-urea α complex, a commensurate (stoichiometric) relationship is obtained. This mainly originates from the self-assembly of urea and PEO molecules through strong hydrogen bonds formed between the oxygen ether of PEO and the N-H groups of urea molecules. According to Tonelli's calculation, the conventional TGT conformation of PEO can not be included in the urea channels, but all trans PEO could be included.[2] He also expected that the PEO chains in the urea channels would be more extended than in pure PEO. But in fact, the PEO chains are not

only included in the urea channels but also are more compacted. The chain repeat distance observed in the PEO-urea α complex is 2.31Å, much smaller than the repeat distance found in pure, crystalline PEO (2.78Å). This reduction is consistent with the observation of more gauche C-O conformation in the PEO-urea α complex. Since this new conformation is stabilized by the strong hydrogen bonds, we can expect that with the increase of carbon numbers in polyethers $[(CH_2)_n\text{-}O\text{-}]_x$, the influence of hydrogen bonds will decrease. The compounds would therefore prefer to form incommensurate complexes with urea and the conformation of the polyethers in the urea channels would be similar to that of pure, crystalline polyethers.

The influence of strong interactions between host and guest molecules on the conformations of polymer chains has been found in other systems. For example, two more conformations of PEO chains are proposed by Tadokoro et al. for the PEO-$HgCl_2$ complex: one is zigzag form I with a TTTTGT conformation and the other is zigzag form II with a $TGGTG^-G^-$ conformation.[3,4] Another less common form of pure PEO is the all trans planar zigzag conformation (TTT), observed by stretching PEO films two-fold.[5] But once the stretching force is released, the conformation comes back to the conventional TGT sequences. More gauche C-O conformation could be kept within the PEO-urea complex. Therefore, we conclude that the unusual conformation of PEO chains might be stabilized by the strong interaction between host and guest molecules, which is large enough to compensate the energy difference between different conformations.

The influence of extensional flow during the electrospinning process on the conformation of PEO chains has also been studied by Kim et al. They found that conformational changes were dominantly affected by the presence of Au nanoparticles rather than by electrospinning itself.[6] According to our research on electrospining of pure PEO and PEO-urea α complex, we found that the crystalline structure and conformation of PEO chains remained the same before and after electrospinning (Table

Table 7.1. Infrared absorption frequencies of PEO, the assignments of each peak and the type of dominant conformation or dichroism in amorphous and crystalline PEO and in its complexes with urea.

Absorption peak (cm^{-1})				Assignments of absorption	Types of dominant Dichroism
PEO		PEO-urea complexes			
Melt	Bulk	form β	form α		
	1359		1359	CH_2 wagging and C-C stretching	⊥ (t)
1350		1351			⊥ (g)
	1341		1341		∥ (g)
1324		1308			⊥ (t)
1295	1279	1259	1275	CH_2 twisting	⊥ (t)
1250	1241	1240	1246		∥ (g)
	959	905	944	CH_2 rocking	∥ (t)
946	947	930	954		⊥ (g)

∥ and ⊥ refer to the vibration directions parallel and perpendicular to the fiber direction, respectively.

g and t refer to the gauche and trans conformations of C-C bonds, they represent helical TGT and all trans TTT conformation for PEO chains, respectively.

7.1). The relative ratio changes of CH_2 wagging bands at 1341/1359 cm^{-1}, CH_2 twisting bands at 1241/1279 cm^{-1} for the pure PEO, which was ascribed to the change of conformation by some researchers,[7,8] in fact mainly come from the different dichroic properties. It is also found that the CH_2 wagging and CH_2 twisting bands for the PEO

chains in α form have similar dichroic properties as pure PEO. But CH_2 rocking bands appearing at 947/959 cm^{-1} for pure PEO and at 910/935 cm^{-1} for PEO-urea α complex have quite different dichroic properties. Since the PEO chain directions are the same in both cases, therefore this might indicate different conformations about C-O bonds. As indicated above, we think that there are more gauche C-O conformations in PEO-urea α complex than in pure PEO. Similar effects have been observed on polymer blends of PEO/PVC, PEO/PMMA and some PEO/solvent systems. Therefore we suggest that the electrospinning process only orients the PEO chain in the parallel direction rather than changing the conformation from helical to all trans as reported by some authors.[6]

The PEO-urea β complex has been prepared by melt-quenching of the PEO-urea α complex and has been found to convert back to the α form when heated to 90 ºC. During the research, we found that even at temperatures lower than 90 ºC, the β-to-α conversion also occurs. It took days for the transition to complete at 60 ºC, but took weeks at room temperature. Unfortunately, this observation was simultaneously made by another research group[9] who published it while we were completing our kinetic experiments. The β complex obtained by all others through melt-quenching of the α complex are in fact mixtures of β complex with urea.[9-14] As a result, the composition and crystalline structure of the β complex was unknown. Here, the electrospinning method was used to prepare the "metastable" PEO-urea β complex. The PEO:urea stoichiometric ratio was determined to be 3:2 and the crystal belongs to the orthorhombic system with a = 1.907 nm, b = 0.862 nm, and c = 0.773 nm. In contrast to the conventional channel structures formed by host-guest molecules, the PEO-urea β complex was found to form an alternate layer structure. The PEO chains direction is the same as the fiber direction and the carbonyl (C=O) stretching direction of urea molecule is perpendicular to the fiber direction. Hydrogen bonds exist both within the ribbon-like urea layers (N-H-N) as well as between urea and PEO layers (N-H-O). As a result, the melting point of the PEO-urea β complex is 53 ºC lower than that of the PEO-urea α complex, which forms three-dimensional hydrogen network by urea molecules. However, the melting point of the PEO-urea β complex is 25 ºC higher than that of pure PEO, which only has weak Van de Waals force between PEO chains.

The melt-quenched mixture of the PEO-urea β form and urea can experience a kinetic solid-solid phase transition back to the α form at temperatures lower than the T_m of β form (89 ºC) or a melt- recrystallization process above the T_m of β form.[15] When the annealing temperature is lower than the T_m of the β form, such as at 60 ºC, most infrared bands of the β complex, including those at 1351 and 1308 cm^{-1} and the C-O-C stretch at 1064 cm^{-1}, disappear almost completely in less than 15 min and are replaced by bands of the α complex. In contrast, the 1675 cm^{-1} band from urea molecules continues blue shifting and only stabilizes at 1691 cm^{-1} after almost three days of annealing. This result indicates that while the local scale conformational changes occur rapidly in a few minutes, the overall phase transition process is actually two orders of magnitude slower than previously thought. This conclusion has been further confirmed by the results obtained from WAXD. As a result, the 1691 cm^{-1} infrared band can be used as an indicator of the large scale crystalline modifications as observed through X-ray diffraction, Thus, the solid-solid β-to-α transition is a kinetic process and it is the altered conformation of PEO chains that brought the change of the whole crystalline structure.

In addition to different transition rates, we also observed that the orientation direction of the newly-formed α crystal depends on temperature. When the temperature is higher than the T_m of β form, the PEO chains melt and lose their original crystalline directionality. They then re-crystallize into α form by combining with crystalline urea. As a result, the PEO chain direction in α crystal becomes the same as the c axis direction of the initial crystalline urea. In contrast, when the temperature is lower than T_m of the β form, the PEO chains remain in a crystalline environment gradually convert to the more energy-stable α form by a solid-solid transition. The PEO chain direction does not change and it is the urea molecules that go around form β to produce the form α crystals. This assumption still needs further confirmation by more experiments.

In contrast to the mixtures with urea, pure PEO-urea β form, prepared by electrospinning, is thermodynamically stable up to its melting temperature. There is not significant phase transition observed when the temperature is lower than the on-set melting temperature of it. The melting of PEO-urea β form is incongruent and leads to

the formation of the crystalline α complex and liquid PEO. A phase diagram is drawn over the complete composition range and allows interpreting the formation of various out-of equilibrium mixtures observed experimentally.

In addition to the PEO-urea β and α complexes, PEO-thiourea complex was also prepared via electrospinning method. PEO-thiourea was thought to form a channel-like complex as in the PEO-urea α complex and some other host-guest system with various stoichiometry in literature.[16-18] But the stoichiometric composition of PEO:thiourea complex obtained here is 3:2, a ratio that is much less than required for the formation of conventional channel structured complexes but the same as in the layer-structured PEO-urea β form. The melting temperature of this complex is 116 ºC, much lower than that of crystalline thiourea (180 ºC). Therefore, the unconventional layer-structure is thought to form as well within the PEO-thiourea complex. Just as in the PEO-urea β form, alternate PEO and thiourea layers are connected by hydrogen bonds. This layer-structured thiourea complex is stable and will recrystallize into thiourea after melting. The crystalline structure of the PEO-thiourea complex is suggested to be monoclinic with a = 9.15 Å, b = 18.88 Å and c = 8.25 Å and β = 92.35º. The thiourea molecules take a ribbon-like arrangement, as the urea does in the PEO-urea β form. But the C=S stretching direction of thiourea is parallel to the fiber direction rather than perpendicular as in the β form. As in the PEO-urea β form, the CH_2 rocking band appeared at a much lower wavenumbers, which might indicate more gauche C-O conformation in the thiourea complex.

7.2 Perspectives

Highly aligned and oriented PEO-urea and PEO-thiourea complexes have been obtained here either from suspension or from solution. Since the former is especially interesting, from what we know, it is one of the few suspensions used successfully to prepare electrospun nanofibers.[19,20] It might be used to prepare highly oriented, aligned nanofibers with other colloidal systems and increase the application field of the

electrospinning method. For instance, PEO and α-cyclodextrin have been found to form complexes which either precipitate (low PEO M_w) or form a gel (high PEO M_w) formation when mixed in water. For the low M_w PEG, it is impossible to prepare electrospun fibers by themselves. However, Uyar et al. recently used high M_w PEO as a carrier to prepare cyclodextrin polyseudorataxane nanofibers and found that PEG- α-cyclodextrin can be electrospun into nanofibers without destruction of the inclusion complex and its channel structure.[21] But as for the high M_w PEO- α-cyclodextrin complex, it is still impossible to prepare electrospun nanofibers. The main reason is the gel-like formation and the difficulty in releasing the water during the conventional electrospinning process. To solve this problem, some agents, such as urea and NaOH could be added to weaken the hydrogen bonds formed among PEO, CD and water, or to adjust the pH value and temperature to facilitate electrospinning process.

As for the origin of molecular orientation during the electrospinning process, it is still not so clear. It has been attributed to the unstable whipping process, the influence of polar solvent and the stretching during take-up on the rotator. To clarify the effects at different stages, on-site observation is necessary to check the elecrrospinning process. For instance, FT-IR might be used to do the measurement on the Taylor cone, the whipping fibers, and the fibers collected on the rotating disk. The conformation of PEO is TGT at conventional state, but is TTT after stretching and will come back to TGT after the stretching is released. Therefore, it might be possible to determine the stretching level by comparing different conformation compositions.

We also found that the polymer complexes can be crystallized directly in an oriented from. Such orientation from crystallization has been observed in both spin-coated and melt-recrystallized samples. As shown in Figure 2.2, the melt-quenched PEO-urea form α displayed inhomogeneous arc intensity in the 2D WAXD graph, which means that the crystals are oriented at least within the X-ray beam size. As to the origin and the mechanism of the orientation, we speculate that it could be attributed to the crystallization process. The molar ratio of PEO and urea is 4:9 in the α complex. And, due to the strong intermolecular hydrogen bonds between PEO and urea, the two

molecules are miscible in the melt state. During the cooling process of the PEO-urea α complex, urea crystallize first at about 90 ºC to form a tetragonal network connected by hydrogen bonds among neighboring urea molecules. Since the crystalline urea contains no PEO molecules, the uncrystallized PEO may be accommodated either in the melt surrounding the urea growing spherulites or it may be contained as uncrystallized matter within the spherulites. In fact, we think the uncrystallized PEO must be incorporated within the urea spherulites for the following two reasons. First, because of the abundance of urea molecules in form α, strong hydrogen bonds formed between uncrystallized PEO and hydrogen-network of urea are still pervasive even after the formation of urea spherulites. In other words, completely non-hydrogen bonded PEO chains never exist in the melt-cooling process of form α. Therefore, uncrystallized PEO is intimately connected with urea and will not be expelled out of it. Second, the urea spherulites grow up to full or nearly full impingement, demonstrating that there is little or no building up of non-crystallized PEO beyond the urea growing front. As a result, the noncrystalline PEO is contained within the urea spherulite, such that the composition is the same throughout the whole area, no matter whether it is within or outside the crystalline urea growing body.

When temperature is decreased further to 65 ºC, the molten PEO and few urea molecules embedded within the urea spherulites crystallize to the β form. Given the conventional thickness of lamellar is in the order of 10 nm, thus the crystallization of β form within the urea spherulites is within the nanoconfined environments and it is known that the phase transition of these materials in the nanoconfined environment may differ from those in the bulk.[22-25] As shown in Figure 2.4, the c axis of β form is oriented perpendicular with the c axis of urea molecules. It is though that the crystal orientation is not determined by the primary nucleation but dominated by the crystal growth step. And the β form will take the orientation that provides the most effective growth to achieve the maximum crystallinity within the nanoconfined structure. It follows from the observation that the PEO chains in β form have a tendency to assume perpendicular orientation to the surface of urea crystal plane. All these hyphthesis need more experiments to support.

In addition to PEO-urea β complex, PEO has been found to form metastable β complexes with p-nitropheno, and resorcinol.[26,27] These β complexes are extremely unstable and will convert to more stable α complex in the end. As a result, their composition and crystalline structure are not well determined. Just like the PEO-urea β complex, those metastable β complexes might be prepared by electrospinning method and their composition and crystalline structure might be determined.

The layer-structured PEO-urea β complex and PEO-thiourea complex have not been observed or reported before. Just as the conventional channel-structured urea complex could be used to prepare less-branched polymers, these layer-structured urea and thiourea complexes might be used as templates to prepare two-dimensional compounds from three-dimensional ones. The selectivity of urea and thiourea molecules based on the diameter of guest molecules might also be used in separation. For instance, PEO and poly(propylene oxide) (PPO) have been found to form inclusion complexes with α and β cyclodextrins, respectively. According to the channel diameters, we assume that thiourea might form a channel structured complex with PPO, but urea can not include a single PPO chain inside if the diameter of the channel is the same as in its conventional channel structure (5.5 Å).They even might be used to separate chiral polymers, such as poly(L-lactide) (PLLA) and poly(D-lactide) (PDLA). Ohya et al. have found that α-CD formed an IC with PLLA whereas the IC formation efficiency of PDLA, the enantiomer of PLLA, was extremely low with α-CD.[28] Tonelli has calculated that the optical active and stereoregular PLLA could be incorporated in the narrow channels its IC (5.5 Å) with urea in the extended, nearly planar zigzag, all-trans conformation. But regularly alternating poly(L,D-lactide) (PLDLA) chains were not able to fit in cylinders with diameter less than 7.5 Å.[29] Thus, we might expect urea IC with PLLA but not PDLA and PDLA might form IC with thiourea.

PEO has been found to form inclusion complexes with urea, α-CD and some other small molecules, such as p-nitrophenol,[26,30] resorcinol,[27] 2-methyl resorcinol (MRES),[31] hydroquinone,[32,33] mercuric chloride,[3,4] sodium thiocyanate,[34] sodium iodide,[35] lithium iodide[36] and p-dihalogenobenzenes.[37,38] For weak Van der Waals

interactions, such as PEO-p-dihalogenobenzenes complexes, the conformation of PEO molecules is nearly identical to that found for pure PEO.[37] However, strong electrostatic interaction, such as in the PEO-$HgCl_2$ complex, induces dramatic modification of the PEO chain conformation. Two more models of PEO chain with $HgCl_2$ complex are proposed by Tadokoro et al.[3,4]: one is zigzag I with a TTTTGT conformation and the other is zigzag II with a $TGGTG^-G^-$ conformation. The zigzag form I (TTTTGT) has also been taken as the main conformation of PEO in the complexes with LiV_3O_8[39] and $CdPS_3$ preintercalated with hydrated alkali cations.[40] For the hydrogen bonds between the oxygen ether of PEO chains and the O-H or N-H groups of guest molecules, it is more complex and different conformations have been suggested for the PEO chain. More work need to be done to further clarify the influence of intermolecular forces on the crystalline structure and conformation of PEO chains in these complex systems.

Another interesting project is to study the conformation of coalesced polymer chains after removing the host molecules. Tonelli et al.[41,42] have researched the coalesced polymer chains after removing of cyclodextrin columns. They found that the conformation changes of polymer chains brought in by the complexation with cyclodextrin could be maintained after the removing of the host molecules. They also found, when immiscible polymers are included as guests in the narrow channels of the inclusion complexes formed with cyclodextrins and then washed with hot water to remove the host CD lattice, that intimately mixed blends of the polymers are obtained. In contrast, during our research on the PEO-α-CD and PEO-urea complexes, the coalesced PEO still keep the TGT conformation as in pure PEO after removing of host molecules in the aqueous solution. This is attributed to the similar solubility of polymer chains and host molecules. If we choose another polymer, such as PLLA or polycaprolactone, which have different solubility properties from PEO, the putative altered conformation in the complexes might be maintained.[29] It is worthwhile to do further research on two immiscible polymers that can form complexes with urea or thiourea molecules, and the electrospinning method could be used to facilitate the miscibility of polymer blends.

As shown in Chapter 2 (Figure 2.9), high M_w PEO chains are not fully covered with α-CD even when an excess of α-CD is used for complexation. But as for PEO-urea α complex, the PEO chains are fully covered with urea. This could be attributed to the different formation process for the PEO-urea and PEO- α CD complexes. The threading process of CD around the polymer chains is slow and there is large resistance to pass through the whole polymer chain, especially for high molecular weight polymers. Based on this, we suggest preparing a block-complex composed of two different host structures. As indicated in Figure 7.1, the polymer chains might be complexed with two different hosts, thus the conformation of the same polymer chains would be different. For example, the part covered by CD might take TTT conformation but the other part covered by urea might take a 4_1 helical conformation as suggested by Chenite and Brisse.[43] The dynamic properties of a single polymer chain might be different and the two host structures could be modified by chemical or physical methods, which might have the potential application in the building up of nano devices.

.

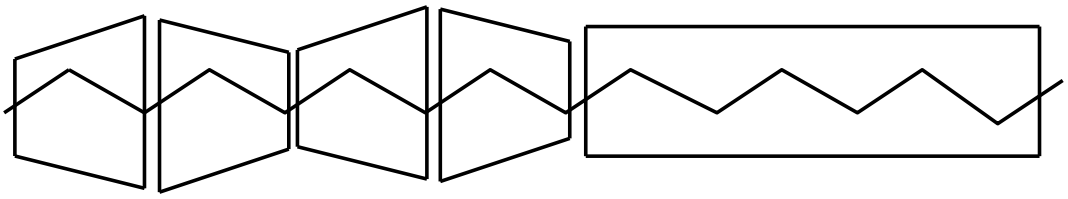

Figure 7.1 Scheme of block-complexes composed of PEO chains and CD and urea guest molecules.

In both channel-structured and layer-structured host-guest complexes, the long chain guest molecules are well organized and arranged. As a result the crystallinity increased significantly compared with uncomplexed guest molecules. It might even provide a way to prepare crystalline structure out of those polymers that can not form well-organized structures under conventional conditions, such as PMMA and PS. Within the confined channels or layers, the dynamic properties of polymer chains might be

completely different from the uncomplexed ones. It might provide more information on the intermolecular or intramolecular interactions among the host-guest molecules.

7.3 References

1. Marti-Rujas, J.; Desmedt, A.; Harris, K. D. M.; Guillaume, F. *J. Am. Chem. Soc.* **2004**, 126, 11124.
2. Tonelli, A. E. *Macromolecules* **1990**, 23, 3134.
3. Iwamoto, R.; Saito, Y.; Ishihara, H.; Tadokoro, H. *J. Polym. Sci. Part A-2* **1968**, 6, 1509.
4. Yokoyama, M.; Ishihara, H.; Iwamoto, R.; Tadokoro, H. *Macromolecules* **1969**, 2, 184.
5. Takahashi, Y.; Sumita, I.; Tadokoro, H. *J. Polym. Sci. Polym. Phy. Ed.* **1973**, 11, 2113.
6. Kim, G.-M.; Wutzler, A.; Radusch, H.-J.; Michler, G. H.; Simon, P.; Sperling, R. A.; Parak, W. J. *Chem. Mater.* **2005**, 17, 4949.
7. Marcos, J. I.; Orlandi, E.; Zerbi, G. *Polymer* **1990**, 31, 1899.
8. Straka, J.; Schmidt, P.; Dybal, J.; Schneider, B.; Spevacek, J. *Polymer* **1995**, 36, 1147.
9. Ye, H. M.; Peng, M.; Xu, J.; Guo, B. H.; Chen, Q.; Yun, T. L.; Ma, H. *Polymer* **2007**, 48, 7364.
10. Tadokoro, H.; Yoshihara, T.; Chatani, Y.; Murahashi, S. *J. Polym. Sci. B* **1964**, 2, 363.
11. Bogdanov, B.; Uzov, C.; Gavrailova, G. *Acta Polym.* **1994**, 45, 381.
12. Bogdanov, B.; Mikhailov, M.; Uzov, K.; Gavrailova, G. *Angew. Makromol. Chem.* **1992**, 195, 165.
13. Bogdanov, B.; Mikhailov, M.; Uzov, K.; Gavrailova, G. *J. Polym. Sci. Part B: Polym. Phys.* **1994**, 32, 387.
14. Bogdanov, B.; Michailov, M.; Uzov, C.; Gavrailova, G. *Makromol. Chem.* **1994**, 195, 2227.
15. Liu, Y.; Pellerin, C. *Polymer* **2009**, 50, 2601.
16. Bailey, F. E., Jr.; France, H. G. *J. Polym. Sci.* **1961**, 49, 397.

17. Tarnrutskii, M. M.; Shkol'nikova, L. S.; Lorei, A. K.; Dindoin, V. I.; Zykova, L. I. *Vysokomolekulyarnye Soedineniya, Seriya B: Kratkie Soobshcheniya* **1975**, 17, 817.
18. Campo, A.; Fretti, J.; Vasanthan, N. *Polymer* **2008**, 49, 374.
19. Matthews, J. A.; Wnek, G. E.; Simpson, D. G.; Bowlin, G. L. *Biomacromolecules* **2002**, 3, 232.
20. Liu, Y.; Pellerin, C. *Macromolecules* **2006**, 39, 8886.
21. Uyar, T.; Kingshott, P.; Besenbacher, F. *Angew. Chem. Int. Ed.* **2008**, 47, 9108.
22. Zhu, L.; Cheng, S. Z. D.; Calhoun, B. H.; Ge, Q.; Quirk, R. P.; Thomas, E. L.; Hsiao, B. S.; Yeh, F.; Lotz, B. *Polymer* **2001**, 42, 5829.
23. Giannelis, E. P.; Krishnamoorti, R.; Manias, E. *Adv. Polym. Sci.* **1999**, 138, 107.
24. Woo, E.; Huh, J.; Jeong, Y. G.; Shin, K. *Phys. Rev. Lett.* **2007**, 98, 136103.
25. Hsiao, M.-S.; Chen, W. Y.; Zheng, J. X.; Horn, R. M. V.; Quirk, R. P.; Ivanov, D. A.; Thomas, E. L.; Lotz, B.; Cheng, S. Z. D. *Macromolecules* **2008**, 41, 4794.
26. Point, J. J.; Damman, P. *Macromolecules* **1992**, 25, 1184.
27. Delaite, E.; Point, J. J.; Damman, P.; Dosière, M. *Macromolecules* **1992**, 25, 4768.
28. Ohya, Y.; Takamido, S.; Nagahama, K.; Ouchi, T.; Ooya, T.; Katoono, R.; Yui, N. *Macromolecules* **2007**, 40, 6441.
29. Tonelli, A. E. *Macromolecules* **1992**, 25, 3581.
30. Damman, P.; Point, J. J. *Macromolecules* **1993**, 26, 1722.
31. Paternostre, L.; Damman, P.; Dosière, M. *Macromolecules* **1999**, 32, 153.
32. Paternostre, L.; Damman, P.; Dosière, M. *Polymer* **1998**, 39, 4579.
33. Paternostre, L.; Damman, P.; Dosière, M. *J. Polym. Sci. Part B: Polym. Phys.* **1999**, 37, 1197.
34. Chatani, Y.; Fujii, Y.; Takayanagi, T.; Homma, A. *Polymer* **1990**, 31, 2238.
35. Chatani, Y.; Okamura, S. *Polymer* **1987**, 28, 1815.
36. Borodin, O.; Smith, G. D. *Macromolecules* **1998**, 31, 8396.
37. Point, J. J.; Jasse, B.; Dosiere, M. *J. Phys. Chem.* **1986**, 90, 3273.
38. Point, J. J.; Damman, P. *Macromolecules* **1991**, 24, 2019.
39. Yang, G.; Hou, W.; Sun, Z.; Yan, Q. *J. Mater. Chem.* **2005**, 15, 1369.

40. Jeevanandam, P.; Vasudevan, S. *Chem. Mater.* **1998**, 10, 1276.

41. Rusa, C. C.; Tonelli, A. E. *Macromolecules* **2000**, 33, 5321.

42. Wei, M.; Tonelli, A. E. *Macromolecules* **2001**, 34, 4061.

43. Chenite, A.; Brisse, F. *Macromolecules* **1991**, 24, 2221.